Cell Journal (Yakhteh)

Guide for Authors

Aims and Scope: The "Cell Journal (Yakhteh)" is a peer review and monthly English publication of Royan Institute of Iran. The aim of the journal is to disseminate information by publishing the most recent scientific research studies based on medical and developmental biology including cell therapy and regenerative medicine, stem cell biology reproductive medicine, medical genetics, immunology, oncology, clinical biochemistry, neuroscience, and tissue engineering. **Cell J**, has been certified by the Ministry of Culture and Islamic Guidance since 1999 and accredited as a scientific and research journal by HBI (Health and Biomedical Information) Journal Accreditation Commission since 2000 which is an open access journal. **This journal holds the membership of the Committee on Publication Ethics (COPE).**

1. Types of articles

The articles in the field of Cellular and Molecular can be considered for publications in **Cell J.** These articles are as below:

A. Original articles

Original articles are scientific reports of the original research studies. The article consists of English Abstract (structured), Introduction, Materials and Methods, Results, Discussion, Conclusion, Acknowledgements, Author's Contributions, and References **(Up to 40).**

B. Review articles

Review articles are the articles written by well experienced authors and those who have excellence in the related fields. The corresponding author of the review article must be one of the authors of at least three published articles appearing in the references. The review article consists of English Abstract (unstructured), Introduction, Conclusion, Author's Contributions, and References **(Up to 90).**

C. Systematic Reviews

Systematic reviews are a type of literature review that collect and critically analyzes multiple research studies or papers. The Systematic reviews consist of English Abstract (unstructured), Introduction, Materials and Methods, Results, Discussion, Conclusion, Acknowledgements, Author's Contributions, and References **(Up to 90).**

D. Short communications

Short communications are articles containing new findings. Submissions should be brief reports of ongoing researches. The short communication consists of English Abstract (unstructured), the body of the manuscript (should not hold heading or subheading), Acknowledgements, Author's Contributions, and References **(Up to 30).**

E. Case reports

Case reports are short discussions of a case or case series with unique features not previously described which make an important teaching point or scientific observation. They may describe novel techniques or use equipment, or new information on diseases of importance. It consists of English Abstracts (Unstructured), Introduction, Case Report, Discussion, Acknowledgements, Author's Contributions, and References **(Up to 30).**

F. Editorial

Editorials are articles should be written in relevant and new data of journals' filed by either the editor in chief or the editorial board.

G. Imaging in biology

Images in biology should focus on a single case with an interesting illustration such as a photograph, histological specimen or investigation. Color images are welcomed. The text should be brief and informative.

H. Letter to the editors

Letter to the editors are in response to previously published **Cell J** articles, and may also include interesting cases that do not meet the requirement of being truly exceptional, as well as other brief technical or clinical notes of general interest.

I. Debate

Debates are articles which show a discussion of the positive and negative view of the author concerning all aspect of the issue relevant to scientific research.

2. Submission process

It is recommended to see the guidelines for reporting different kinds of manuscripts. This guide explains how to prepare the

manuscript for submission. Before submitting, we suggest authors to familiarize themselves with **Cell J** format and content by reading the journal via the website (www.celljournal.com). The corresponding author ensures that all authors are included in the author list and agree with its order, and they must be aware of the manuscript submission.

A. Author contributions statements

It is essential for authors to include a statement of responsibility in the manuscript that specifies all the authors' contributions. This participation must include: Conceptualization, Methodology, Software, Validation, Formal analysis, Investigation, Resources, Data Curation, Writing - Original Draft, Writing - Review & Editing, Visualization, Supervision, Project administration, and Funding acquisition. Authors who do not meet the above criteria should be acknowledged in the Acknowledgments section.

B. Cover letter and copyright

Each manuscript should be accompanied by a cover letter, signed by all authors specifying the following statement: "The manuscript has been seen and approved by all authors and is not under active consideration for publication. It has neither been accepted for publication nor published in another journal fully or partially (except in abstract form). **Also, no manuscript would be accepted in case it has been pre-printed or submitted to other websites.** I hereby assign the copyright of the enclosed manuscript to **Cell J.**" The corresponding author must confirm the proof of the manuscript before online publishing. It is needed to suggest three peer reviewers in the field of their manuscript.

C. Manuscript preparation

Authors whose first language is not English encouraged to consult a native English speaker in order to confirm his manuscripts to American or British (not a mixture) English usage and grammar. It is necessary to mention that we will check the plagiarism of your manuscript by iThenticate Software. The manuscript should be prepared in accordance with the "International Committee of Medical Journal Editors (ICMJE)". Please send your manuscript in two formats word and PDF (including: title, name of all the authors with their degree, abstract, full text, references, tables and figures) and also send tables and figures separately in the site. The abstract and text pages should have consecutive line numbers in the left margin beginning with the title page and continuing through the last page of the written text. Each abbreviation must be defined in the abstract and text when they are mentioned for the first time. Avoid using abbreviation in the title. Please use the international and standard abbreviations and symbols

It should be added that an essential step toward the integration and linking of scientific information reported in published literature is using standardized nomenclature in all fields of science and medicine. Species names must be italicized (*e.g., Homo sapiens*) and also the full genus and species written out in full, both in the title of the manuscript and at the first mention of an organism in a paper.

It is necessary to mention that genes, mutations, genotypes, and alleles must be indicated in italics. Please use the recommended name by consulting the appropriate genetic nomenclature database, e.g., HUGO for human genes. In another words; if it is a human gene, you must write all the letters in capital and italic (*e.g., OCT4, c-MYC*). If not, only write the first letter in capital and italic (*e.g., Oct4, c-Myc*). **In addition, protein designations are the same as the gene symbol but are not italicized.**

Of note, Cell J will only consider publishing genetic association study papers that are novel and statistically robust. Authors are advised to adhere to the recommendations outlined in the STREGA statement (http://www.strega-statement.org). The following criteria must be met for all submissions:

1. Hardy-Weinberg Equilibrium (HWE) calculations must be carried out and reported along with the P-values if applicable [see Namipashaki et al. 2015 (Cell J, Vol 17, N 2, Pages: 187-192) for a discussion].

2. Linkage disequilibrium (LD) structure between SNPs (if multiple SNPs are reported) must be presented.

3. Appropriate multiple testing correction (if multiple independent SNPs are reported) must be included.

Submissions that fail to meet the above criteria will be rejected before being sent out for review.

Each of the following manuscript components should begin in the following sequence:

Authors' names and order of them must be carefully considered (full name(s), highest awarded academic degree(s), email(s), and institutional affiliation(s) of all the authors in English. Also, you must send mobile number and full postal address of the corresponding author).

Changes to Authorship such as addition, deletion or rearrangement of author names must be made only before the manuscript has been accepted in the case of approving by the journal editor. In this case, the corresponding author must explain the reason of changing and confirm them (which has been signed by all authors of the manuscript). If the manuscript has already been published in an online issue, an erratum is needed. Please contact us via info@celljournal.org in case of any changes (corrections, retractions, erratum, etc.).

Title is providing the full title of the research (do not use abbreviations in title).

Running title is providing a maximum of 7 words (no more than 50 characters).

Abstract must include Objective, Materials and Methods, Results, and Conclusion (no more than 300 words).

Keywords, three to five, must be supplied by the authors at the foot of the abstract chosen from the Medical Subject Heading (MeSH). Therefore; they must be specific and relevant to the paper.

The following components should be identified after the abstract:

Introduction: The Introduction should provide a brief background to the subject of the paper, explain the importance of the study, and state a precise study question or purpose.

Materials and Methods: It includes the exact methods or observations of experiments. If an apparatus is used, its manufacturer's

name and address should be stipulated in parenthesis. If the method is established, give reference but if the method is new, give enough information so that another author can perform it. If a drug is used, its generic name, dose, and route of administration must be given. Standard units of measurements and chemical symbols of elements do not need to be defined.

Statistical analysis: Type of study and statistical methods should be mentioned and specified by any general computer program used.

Ethical considerations*:* Please state that informed consent was obtained from all human adult participants and from the parents or legal guardians of minors and include the name of the appropriate institutional review board that approved the project. It is necessary to indicate in the text that the maintenance and care of experimental animals complies with National Institutes of Health guidelines for the humane use of laboratory animals, or those of your Institute or agency.

Clinical trial registration: All of the Clinical Trials performing in Iran must be registered in Iranian Registry of Clinical Trials (www.irct.ir). The clinical trials performed abroad, could be considered for publication if they register in a registration site approved by WHO or www.clinicaltrials.gov. If you are reporting phase II or phase III randomized controlled trials, you must refer to the CONSORT Statement for recommendations to facilitate the complete and transparent reporting of trial findings. Reports that do not conform to the CONSORT guidelines may need to be revised before peer-reviewing.

Results: They must be presented in the form of text, tables, and figures. Take care that the text does not repeat data that are presented in tables and/or figures. Only emphasize and summarize the essential features of the main results. Tables and figures must be numbered consecutively as appeared in the text and should be organized in separate pages at the end of the manuscript while their location should be mentioned in the main text.

Tables and figures: If the result of your manuscript is too short, it is better to use the text instead of tables & figures. Tables should have a short descriptive heading above them and also any footnotes. Figure's caption should contain a brief title for the whole figure and continue with a short explanation of each part and also the symbols used (no more than 100 words). All figures must be prepared based on cell journal's guideline in color (no more than 6 Figures and Tables) and also in TIF format with 300 DPI resolution.

Of Note: Please put the tables & figures of the result in the results section not any other section of the manuscript.

Supplementary materials would be published on the online version of the journal. This material is important to the understanding and interpretation of the report and should not repeat material within the print article. The amount of supplementary material should be limited. Supplementary material should be original and not previously published and will undergo editorial and peer review with the main manuscript. Also, they must be cited in the manuscript text in parentheses, in a similar way as when citing a figure or a table. Provide a caption for each supplementary material submitted.

Discussion: It should emphasize the present findings and the variations or similarities with other researches done by other researchers. The detailed results should not be repeated in the discussion again. It must emphasize the new and important aspects of the study.

Conclusion: It emphasizes the new and important aspects of the study. All conclusions are justified by the results of the study.

Acknowledgements: This part includes a statement thanking those who contributed substantially with work relevant to the study but does not have authorship criteria. It includes those who provided technical help, writing assistance and name of departments that provided only general support. You must mention financial support in the study. Otherwise; write this sentence "There is no financial support in this study".

Conflict of interest: Any conflict of interest (financial or otherwise) and sources of financial support must be listed in the Acknowledgements. It includes providers of supplies and services from a commercial organization. Any commercial affiliation must be disclosed, regardless of providing the funding or not.

Of Note: If you have already any patent related to the subject of your manuscript, or you are going to apply for such a patent, it must be mentioned in this part.

References: The references must be written based on the Vancouver style. Thus the references are cited numerically in the text and listed in the bibliography by the order of their appearance. The titles of journals must be abbreviated according to the style used in the list of Journals Indexed in PubMed. Write surname and initials of all authors when there are six or less. In the case of seven or more authors, the names of the first six authors followed by "et al." must be listed. You can download Endnote file for Journal references style: endnote file

The reference of information must be based on the following order:

Article:

Surname(s) and first letter of name &middle name(s) of author(s) .Manuscript title. Journal title (abbr).publication date (year); Volume & Issue: Page number.

Example: Manicardi GC, Bianchi PG, Pantano S, Azzoni P, Bizzaro D, Bianchi U, et al. Presence of endogenous nicks in DNA of ejaculated human spermatozoa and its relationship to chromomycin A3 accessibility. Biol Reprod. 1995; 52(4): 864-867.

Book:

Surname(s) and first letter of name & middle name(s) of author(s).Book title. Edition. Publication place: publisher name; publication date (year); Page number.

Example: Edelman CL, Mandle CL. Health promotion throughout the lifespan. 2nd ed. ST Louis: Mosby; 1998; 145-163.

Chapter of book:

Surname(s) and first letter of name & middle name(s) of author(s).Chapter title. In: Surname(s) and first letter of name & middle name(s) of editor(s), editors. Book title. Edition. Publication place: publisher name; publication date (year); Page number.

Example: Phillips SJ, Whisnant JP. Hypertension and stroke. In: Laragh JH, Brenner BM, editors. Hypertension: pathophysiology, diagnosis, and management. 2nd ed. New York: Raven Press; 1995; 465-478.

Abstract book:

Example: Amini rad O.The antioxidant effect of pomegranate juice on sperm parameters and fertility potential in mice. Cell J. 2008;10 Suppl 1:38.

Thesis:

Name of author. Thesis title. Degree. City name. University. Publication date (year).

Example: Eftekhari Yazdi P. Comparison of fragment removal and co-culture with Vero cell monolayers on development of human fragmented embryos. Presented for the Ph.D., Tehran. Tarbiyat Modarres University. 2004.

Internet references

Article:

Example: Jahanshahi A, Mirnajafi-Zadeh J, Javan M, Mohammad-Zadeh M, Rohani M. Effect of low-frequency stimulation on adenosineA1 and A2A receptors gene expression in dentate gyrus of perforant path kindled rats. Cell J. 2008; 10 (2): 87-92. Available from: http://www.celljournal.org. (20 Oct 2008).

Book:

Example: Anderson SC, Poulsen KB. Anderson's electronic atlas of hematology.[CD-ROM]. Philadelphia: Lippincott Williams & Wilkins; 2002.

D. Proofs are sent by email as PDF files and should be checked and returned within 72 hours of receipt. It is the authors' responsibility to check that all the text and data as contained in the page proofs are correct and suitable for publication. **We are requested to pay particular attention to author's names and affiliations as it is essential that these details be accurate when the article is published.**

E. Pay for publication: Publishing an article in **Cell J** requires Article Processing Charges (APC) that will be billed to the submitting author following the acceptance of an article for publication. For more information please see www.celljournal.org.

F. Ethics of scientific publication: Manuscripts that have been published elsewhere with the same intellectual material will refer to duplicate publication. If authors have used their own previously published work or work that is currently under review, as the basis for a submitted manuscript, they are required to cite the previous work and indicate how their submitted manuscript offers novel contributions beyond those of the previous work. Research and publication misconduct is considered a serious breach of ethics.

The Journal systematically employs iThenticate, plagiarism detection and prevention software designed to ensure the originality of written work before publication. Plagiarism of text from a previously published manuscript by the same or another author is a serious publication offence. Some parts of text may be used, only where the source of the quoted material is clearly acknowledged.

3. General information

A. You can send your manuscript via online submission system which is available on our website. If the manuscript is not prepared according to the format of **Cell J**, it will be returned to authors.

B. The order of article appearance in the Journal is not demonstrating the scientific characters of the authors.

C. Cell J has authority to accept or reject the manuscript.

D. Corresponding authors should send the manuscripts via the Online Manuscript Submission System. All submissions will be evaluated by the associated editor in order to check scope and novelty. If the manuscript suits the journal criteria, the associated editor would select the single-blind peer-reviewers. The reviewers of the manuscript must not share information about the review with anyone without permission of the editors and authors. If three reviewers pass their judgments on the manuscript, it will be presented to the associated editor of **Cell J**. In the case of having a favorable judgment on the manuscript, reviewers' comments will be presented to the corresponding author (the identification of the reviewers will not be revealed). After receiving the revision, the associated editor would choose the final reviewer among the previous ones. The final decision will be taken by editor-in-chief based on the final reviewer's comments. The review process takes between 2 to 4 months in **Cell J**. The executive member of journal will contact the corresponding author directly within 3-4 weeks by email. If authors do not receive any reply from journal office after the specified time, they can contact the journal office. Finally, the executive manager will respond promptly to authors' request.

After receiving the acceptance letter, the abstract of the paper would be published electronically. The paper will be in a queue to be published in one Cell J. At last, the corresponding author should verify a proof copy of the paper in order to be published.

The Final Checklist

The authors must ensure that before submitting the manuscript for publication, they have to consider the following parts:

1. The first page of manuscript should contain title, name of the author/coauthors, their academic qualifications, designation & institutions they are affiliated with, mailing address for future correspondence, email address, phone, and fax number.

2. Text of manuscript and References prepared as stated in the "guide for authors" section.

3. Tables should be on a separate page. Figures must be sent in color and also in JPEG (Jpg) format.

4. Cover Letter should be uploaded with the signature of all authors.

5. An ethical committee letter should be inserted at the end of the cover letter.

The Editor-in-Chief: Ahmad Hosseini, Ph.D.

Cell Journal *(Yakhteh)*

P.O. Box: 16635-148, Iran

Tel/Fax: + 98-21-22510895

Emails: info@celljournal.org

journals@celljournal.org

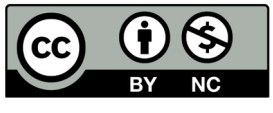

Dr. Saeed Kazemi Ashtiani

IN THE NAME OF GOD

Gone But not Forgotten

In the memory of the late Director of Royan Institute, Founder of Stem Cells Research in Iran and Chairman of ***Cell Journal*** *(Yakhteh)*. May he rest in peace.

PUBLISHED & SPONSORED BY:
Publication of Royan Institute (ACECR)

Indexed in:
1. Thomson Reuters (ISI)
2. PubMed
3. PubMed Central (PMC)
4. National Library Medicine (NLM)
5. Biosis Preview
6. Index Medicus for the Eastern Mediterranean Region (IMEMR)
7. Regional Information Center for Sciences and Technology (RICeST)
8. Index Copernicus International
9. Cambridge Scientific Abstract (CSA)
10. EMBASE
11. Scopus
12. Cinahl Database
13. Google Scholar
14. Chemical Abstract Service (CAS)
15. Proquest
16. Directory of Open Access Journals (DOAJ)
17. Open Academic Journals Index (OAJI)
18. Directory of Research Journals Indexing (DRJI)
19. Scientific Information Database (SID)
20. Iranmedex
21. Islamic World Science Citation Center (ISC)
22. Magiran
23. Science Library Index
24. Biological Abstracts
25. Essential Science Indicators
26. EuroPub

Editorial Office Address (Dr. Ahmad Hosseini):
Royan Institute, P.O.Box: 16635-148,
Tehran, Iran
Tel & Fax: (+9821)22510895
Website: www.celljournal.org
Emails: info@celljournal.org
journals@celljournal.org

Printing Company:
Naghshe e Johar Co.
No. 103, Fajr alley, Tehranpars Street,
Tehran, Iran.

Cell Journal(Yakhteh), Vol 25, No 4, April 2023, Serial Number: 111, Pages: 217-286

CONTENTS

Original Articles

• The Effect of Amniotic Membrane Extracted Eye Drop on Repairing The Corneal Epithelial in Patients after Trans-Epithelial Photorefractive Keratectomy: A Randomized Controlled Trial

Alireza Ranaei, Ahmad Chavoshi, Hossein Aghamollaei, Mostafa Naderi, Ali Agha Alishiri, Khosrow Jadidi **217**

• Understanding The Regulatory Role of USP32 and SHMT2 in The Progression of Gastric Cancer

Jun Li, Yafei Bo, Bo Ding, Lei Wang **222**

• Establishment of A Three-Dimensional Culture Condition for The U266 Cell Line Based on Peripheral Blood Plasma-Derived Fibrin Gels

Mahshid Jomehpour, Mohammadmahdi Khosravi, Mehrnaz Janfada, Saeid Abroun, Sadaf Vahdat..... **229**

• Comparative Epigenetic Analysis of Imprinting Genes Involved in Fertility, in Cryopreserved Human Sperms with Rapid Freezing versus Vitrification Methods

Nahid Khosronezhad, Vahideh Hassanzadeh. Maryam Hezavehei, Abdolhossein Shahverdi, Maryam Shahhoseini **238**

• 3,5,3'-Triiodo-L-Thyronine Regulates Actin Cytoskeleton Dynamic in The Differentiated PC-12 Cells during Hypoxia through An αvβ3 Integrin

Tamar Barbakadze, Elisabed Kvergelidze, Judit Bátor, József Szeberényi, D.Sc.3, David Mikeladze **247**

• Fabrication of Cell-Laden AME-Loaded Collagen-Based Hydrogel Promotes Fibroblast Proliferation and Wound Healing *In Vitro*

Mohammad Azimi Alamouty, Niloufar Shayan Asl, Abdollah Safari, Marzieh Ebrahimi, Hamed Daemi **255**

• Down-Regulation of CEND1 Expression Contributes to The Progression and Temozolomide Resistance of Glioma

Zhou Houjun, Bai Peng **264**

• Effect of Deep Brain Stimulation in The Ventral Tegmental Area on Neuronal Activity in Local and Remote Brain Regions in Kindled Mice

Parisa Esmaeili Tazangi, Faisal Alosaimi, Fatemeh Bakhtiarzadeh, Amir Shojaei, Ali Jahanshahi, Javad Mirnajafi-Zadeh **273**

• Front page of Cell Journal(Yakhteh): Figure 4 A2, Page: 277

Cell J
Cell Journal(Yakhteh)
Homepage: https://www.celljournal.org/
Original Article
Vol 25, No 4, April 2023, Pages: 217-221

The Effect of Amniotic Membrane Extracted Eye Drop on Repairing The Corneal Epithelial in Patients after Trans-Epithelial Photorefractive Keratectomy: A Randomized Controlled Trial

Alireza Ranaei, M.D.[1, 2], Ahmad Chavoshi, M.D.[1, 2], Hossein Aghamollaei, Ph.D.[2], Mostafa Naderi, M.D.[2], Ali Agha Alishiri, M.D.[2], Khosrow Jadidi, M.D.[2*]

1. Student Research Committee, Baqiyatallah University of Medical Sciences, Tehran, Iran
2. Chemical Injures Research Center, Systems Biology and Poisonings Institute, Baqiyatallah University of Medical Sciences, Tehran, Iran

Abstract

Objective: Recent studies imply extensive applications for the human amniotic membrane (hAM) and its extract in medicine and ophthalmology. The content of hAM meets many requirements in eye surgeries, such as refractive surgery as the most important and commonly used method for treating the dramatically increasing refractive errors. However, they are associated with complications such as corneal haziness and corneal ulcer. This study was designed to evaluate the impact of amniotic membrane extracted eye drop (AMEED) on Trans-PRK surgery complications.

Materials and Methods: This randomized controlled trial was performed during two years (July 1, 2019-September 1, 2020). Thirty-two patients (64 eyes), including 17 females and 15 males, aged 20 to 50 years (mean age of 29.59 ± 6.51) with spherical equivalent between -5 to -1.5 underwent Trans Epithelial Photorefractive Keratectomy (Trans-PRK) surgery. One eye was selected per case (case group) and the other eye was considered as control. Randomization was done using the random allocation rule. The case group was treated with AMEED, and the artificial tear drop every 4 hours. The control eyes received artificial tear drops instilled every 4 hours. The evaluation continued for three days after the Trans-PRK surgery.

Results: A significant decrease in CED size was found in the AMEED group on the second day after surgery (P=0.046). Also, this group had a substantial reduction in pain, hyperemia, and haziness.

Conclusion: This study showed that AMEED drop can increase the healing rate of corneal epithelial lesions after Trans-PRK surgery and reduce the early and late complications of Trans-PRK surgery. Researchers and Ophthalmologists should consider AMEED as a selection in patients with persistent corneal epithelial defects and patients who have difficulty in corneal epithelial healing. We understood AMEED has a different effect on the cornea after surgery; therefore, the researcher must know AMEED's exact ingredients and help expand AMEED uses (registration number: TCTR20230306001).

Keywords: Amnion, Photorefractive Keratectomy, Refractive Surgical Procedures, Wound Healing

Citation: **Ranaei A, Chavoshi A, Aghamollaei H, Naderi M, Agha Alishiri A, Jadidi Kh. The effect of amniotic membrane extracted eye drop on repairing the corneal epithelial in patients after trans-epithelial photorefractive Keratectomy: a randomized controlled trial. 2022; 25(3): 217-221. doi: 10.22074/CELLJ.2022.8165.**

Introduction

Recent studies have shown that the human amniotic membrane (hAM) and its extract have many potentials in medicine and ophthalmology applications because of their unique content (1, 2). The hAM includes growth factors, collagens (I, III, IV, and V), lamina, and cytokines with anti-inflammatory (3), anti-scaring, anti-apoptotic, anti-angiogenic (4), and anti-fibrotic properties (1). In the literature, a standard method has been described that produces an amniotic membrane extract for making the amniotic membrane extracted eye drop (AMEED) with the same properties as the amniotic membrane. According to the relevant reports, AMEED increases *in vitro* limbal stem cells and corneal epithelial repair in rabbits (5) and horses (6) after injury. No complications have been reported for AMEED yet (5, 7).

On the other hand, refractive error is the most common cause of vision problems globally. According to a statement issued by the World Health Organization, myopia as a refractive disorder will affect half of the world's population by 2050 (8, 9). One way to eliminate the refractive conditions is surgery, which can be performed through various methods, including photorefractive keratectomy (PRK), Trans-PRK, laser subepithelial keratomileusis (LASEK), and laser in situ keratomileuses (LASIK). All these methods can also be used to correct the corneal curvature. In the Trans-PRK modality, which is a less invasive method compared to PRK, the patients suffer from two types of post-surgery complications: early and late complications. Early complications include CEDs, eye pain, conjunctival

Received: 07/August/2021, Revised: 20/December/2021, Accepted: 11/January/2022
***Corresponding Address: P.O.Box: 1698749511, Chemical Injures Research Center, Systems Biology and Poisonings Institute, Baqiyatallah University of Medical Sciences, Tehran, Iran**
Email: kh.jadidi.1401@gmail.com

Royan Institute
Cell Journal (Yakhteh)

injection or hyperemia, tearing, and photophobia. Late complications include visual acuity decrease and corneal haziness, which reaches its peak within 1 to 2 months after surgery and then gradually disappears within 6 to 12 months, which can delay reaching the patient's final vision (10, 11).

Accordingly, a triple-blinded historical randomized controlled trial was designed to evaluate the impact of AMEED on the CEDs, conjunctival injection, eye pain, corneal haziness, and visual acuity after Trans-PRK surgery.

Materials and Methods

Ethical considerations

The study was considered by the Baqiyatallah Ethics Committee (IR.BMSU.BAQ.REC.1399.032) and Thai clinical trials registry (TCTR20230306001) all patients who agreed to undergo trans-PRK surgery signed an informed consent to be entered into this clinical trial. The study was performed following the principles of the Helsinki Declaration.

Intervention

This randomized controlled trial was carried out in the Baqiyatallah Hospital between 2019 and 2020 on patients aged 20 to 50 years who attended the ophthalmology clinic for refractory problems. They were included in the study if they had a range of spherical equivalent between -5 to -1.5, measured by an auto-refractometer and the approval of trial lenses. The patients with a history of using topical ophthalmic drugs in the past three months, eye surgery at any time, and use of drugs that affect the tear condition (blood pressure medication, rheumatism medication, antipsychotic medication, etc.) were excluded from the study. Additionally, the patients with a history of any eye diseases other than refractive disorders, diabetes history, drug allergy, rheumatic disease, or any other systemic disease, and anisometric eyes were excluded from the study. During the Trans-PRK surgery (SCHWIND AMARIS 1050RS) on each patient, one eye was selected as the case, and the fellow eye was considered as the control using a random allocation rule for randomization. Contact lenses and routine medications were used in patients after Trans-PRK surgery. The case group was treated with AMEED (Lifecell Pharmaceuticals, Inc. Iran) every four hours and artificial tear drop every four hours (conventional treatment with AMEED) up to three days post-surgery. In the control eyes (fellow eyes), artificial teardrop (conventional treatment) was instilled every four hours within the same duration. The cornea was examined daily in both groups until the complete epithelial repair. The patients' eyes were stained with fluorescein, and a photo of the stained part (the same part of the epithelial defect) was taken with a photo slit device. The size of the defect in the picture was determined by ImageJ version 1.2 software, and then it was augmented by manual refinement. Patients after corneal epithelial healing were re-examined in the first, third, and sixth months after surgery.

It should be noted that both groups of patients have received routine and standard treatments. Regular medications included chloramphenicol 0.5% ophthalmic drop (Sina Darou Laboratories, Inc. Iran), Betamethasone (Darou Pakhsh Pharmaceutical Manufacturing Company, Iran), artificial tears (Iranian Parenteral & Pharmaceutical Co. Iran), Fluorometholone (Sina Darou Laboratories, Inc. Iran), and Liposic ophthalmic gel (Bausch and Lomb, Inc. UK) for both groups.

All measurements were performed using a Haag-Streit Slit lamp (BQ 900, Haag-Streit, Koeniz, Switzerland) with a standard zoom of sixteen. We evaluated the conjunctival injection grading using the Efron system (Fig.1) (12) and measured the corneal haziness according to the standard evaluation (Table 1) (13). The pain measurement was also based on a 0-10 Likert scale.

Statistical analysis

The collected data were analyzed by SPSS software version 16 (IBM, Chicago). We used Mann-Whitney U and Kendall correlation tests. $P<0.05$ was considered statistically significant, and data was depicted by mean ± standard deviation (95% confidential interval).

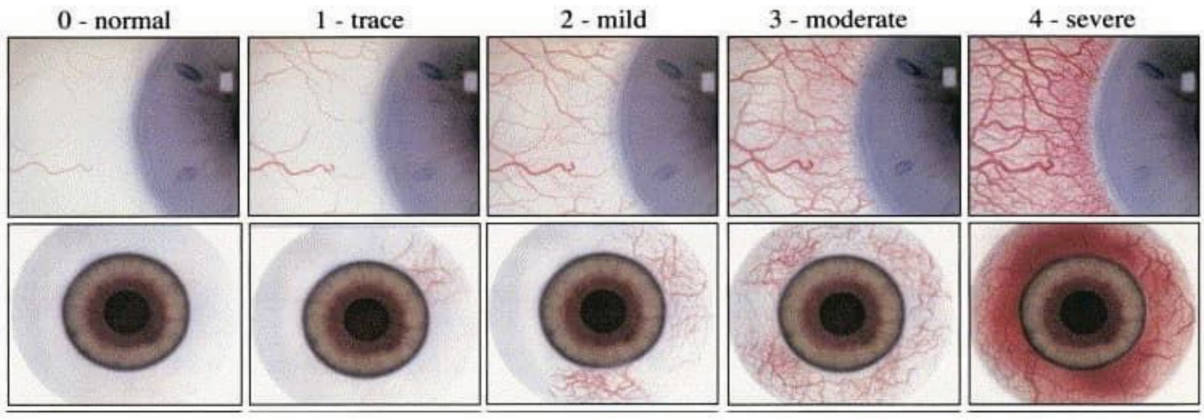

Fig.1: Conjunctival Injection Grading in Efron system. Efron system was used for injection grading in this study.

Table 1: Corneal haziness grading according to standard evaluation

Grade	Characteristics
Grade 0	No corneal haze
Grade 1	Iris details visible
Grade 2	Pupillary margin visible, iris details not visible
Grade 3	Pupillary margin not visible
Grade 4	Corneal totally opaque

The standard evaluation was used for corneal haziness grading in this study.

Results

This study evaluated 32 patients (64 eyes), including 17 females and 15 males, with a mean age of 29.59 ± 13.02 years at the time of Trans-PRK surgery. After three days post-surgery, all CEDs disappeared from the cornea in both groups. On the second day after surgery, corneal epithelial defect in AMEED and control groups was 2.42 mm^2 and 3.84 mm^2, respectively, showing a significant difference (P=0.046, Table 2).

Table 2: CED Size in myopic patients after TRANS-PRK surgery in AMEED and control group (fellow eye)

Groups	AMEDD	Control
Size on surgery day (mm^2)	46.82 ± 3.70	46.52 ± 6.02
Size first day after surgery (mm^2)	14.77 ± 12.64	17.34 ± 12.36
Size second day after surgery (mm^2)	2.42 ± 6.28	3.84 ± 4.76*
Size third day after surgery (mm^2)	0.18 ± 2.08	0.08 ± 0.98

Data are presented as mean ± SD. *; P<0.05, Mann-Whitney U.

Moreover, the conjunctival injection was markedly more reduced in the AMEED group on the second (P=0.019) and third days (P=0.004) after surgery (Table 3). Three months after surgery, the haziness was significantly lower in the AMEED group (P=0.040, Table 4). As expected, the corneal haziness in each follow-up had a significant negative correlation with the visual acuity. Spearman correlation test between visual acuity and haziness for first, third, and sixth month post-surgery in all patients was R1=-0.49 (P<0.001), R3=-0.57 (P<0.001), and R6=-0.75 (P<0.001), respectively.

Table 3: Injection in myopic patients after TRANS-PRK surgery in AMEED and control group (fellow eye)

Groups	AMEED	Control
Pain first day after surgery	3.65 ± 3.02	3.87 ± 4.16
Pain second day after surgery	1.15 ± 2.10	1.43 ± 2.58
Pain third day after surgery	0.03 ± 0.34	0.31 ± 0.84*
Injection first day after surgery	2.09 ± 1.70	2.40 ± 1.66
Injection second day after surgery	0.96 ± 1.28	1.37 ± 1.30*
Injection third day after surgery	0.09 ± 0.58	0.40 ± 0.98*

Data are presented as mean ± SD. *P<0.05, Mann-Whitney U.

Table 4: Haziness and visual acuity (Late complication) in myopic patients after TRANS-PRK surgery in AMEED and control group (fellow eye)

Groups	AMEED	Control
Haziness after 1 month	0.40 ± 0.88	0.46 ± 1.00
Haziness after 3 months	0.12 ± 0.66	0.34 ± 0.96*
Haziness after 6 months	0.06 ± 0.48	0.06 ± 0.48
Visual acuity baseline	0.77 ± 0.60	0.76 ± 0.64
Visual acuity after 1 month	0.02 ± 0.06	0.02 ± 0.06
Visual acuity after 3 months	0.00 ± 0.02	0.00 ± 0.02
Visual acuity after 6 months	0.0000 ± 00	0.0000 ± 00

Data are presented as mean ± SD. *P<0.05, Mann-Whitney U.

Discussion

Refractive errors, especially myopia, are dramatically increasing worldwide (14, 15). Refractive surgery is a popular method of solving this problem. PRK and TRANS-PRK surgery are surface ablation methods for epithelial removal. Trans-PRK is a less invasive method and can control the size of the corneal epithelial defect (16-18). As long as CEDs exist on the cornea's surface, they can be the beginning of many other problems (19). The most notable consequence is corneal ulcers due to epithelial progression in inflammatory processes (20). Therefore, one of the most critical measurements to prevent postoperative complications after refractive surgery is the faster resolution of epithelial defects. The triple-blind placebo-controlled RCT used in this study assessed the effects of AMEED in postoperative TRANS-PRK surgery complications compared to the control group (fellow eyes) and showed faster epithelial healing without clinically relevant side effects.

The present study's findings showed that on the surgery day and the first day after surgery, the CED size was similar in both groups. On the second day after surgery, the CED size was significantly smaller in the AMEED group than in the controls. On the third day after surgery in both groups, CED disappeared. Considering that literature suggests time as one of the most influential factors, in the present study, in the AMEED-received eyes, CEDs healed faster; however, on the third day, all CEDs disappeared due to 24 hours crossing. This rapid healing rate could be because of the mostly young age of subjects (mean age was 29.59 years) and the absence of any ocular disease other than a refractive error in all cases. In a review by Murri et al. (7), the efficacy of AMEED for the acceleration of the corneal epithelial defect was investigated, and it was shown that it is potentially valuable for the ocular surface disorder. Another study by Sabater-Cruz et al. (21) used AMEED for the wound healing delay group and dry eye disease group for the long term. The

study demonstrated that AMEED could heal persistent epithelial defects, dry eye disease, and corneal ulcers without any adverse effects. Also, a survey by Kordić et al. (22) depicted that AMEED was successfully applied for persistent epithelial defect in two patients (two drops per hour), which is consistent with the present result.

In the studied patients, the reported pain as a post-surgical early complication on the first and second day after surgery was similar between AMEED and control eyes. On the third day after the operation, the pain significantly reduced in AMEED groups. The conjunctival injection was markedly less on the second and third days after surgery. Similarly, a case series study on the chemical burn showed that amniotic membrane extract significantly reduced pain and inflammation (23). These results indicate that AMEED has an ameliorative effect on the post-surgical early complications.

Furthermore, a significant difference was observed in the haziness as a late complication three months after surgery between the AMEED and control groups. Accordingly, we hypothesized that time has a vital role in haziness results since that in the first-month follow-up, AMEED and control groups were quite similar in haziness, while after six months, haziness was recovered entirely. We concluded that in the first month the time has not been enough to make differences.

Therefore, for a more reliable evaluation, performing the same procedure in a population of older adults with short interval consideration is suggested. Moreover, considering less than 24 hours intervals of the last CED sizing examination time would probably reveal different results. A permeable study demonstrated the dose-dependent efficacy of AMEED (5). Therefore, applying AMEED at a higher dose (with intervals less than every 4 hours) is expected to confer more difference between test and control eyes.

Conclusion

This study shows that AMEED can increase the healing rate of corneal epithelial lesions after Trans-PRK surgery and reduce the early and late complications of Trans-PRK surgery. Further studies can approve this medication for reducing Trans-PRK complications. Conducting other studies for evaluation of AMEED for treatment of patients with persistent corneal epithelial defects and patients who have difficulty in corneal epithelial healing is also suggested. Considering the variety of ingredients present in this extract, finding the active ingredient that delivers the greatest effect on improving epithelial defects will be of interest.

Acknowledgments

We would like to thank the staff of Baqiyatallah Hospital Ophthalmology Clinic for their support. There is no financial support and conflict of interest in this study.

Authors' Contributions

A.R., Kh.J., A.Ch.; Concept and design. A.R., A.Ch., H.A., A.A.A., M.N.; Data acquisition and drafting the manuscript. A.R., A.Ch., H.A., A.A.A., M.N., K.J.; Data analysis and final approval of the manuscript. K.J.; Critical revising of the manuscript. All authors read and approved the final manuscript.

References

1. Plumer C. The use of amniotic membrane transplantation for ocular surface reconstruction: a review and series of 58 equine clinical cases (2002-2008). Vet Ophthalmol. 2009; 12(1): 17-24.
2. Baradaran Rafii A, Ebrahimi M, Shayan N, Shahabi K, Shams M. In-vivo cultivation of limbal stem cells for ocular surface reconstruction. Bina J Ophthalmol. 2015; 20(3): 255-263.
3. Litwiniuk M, Grzela T. Amniotic membrane: new concepts for an old dressing. Wound Repair Regen. 2014; 22(4): 451-456.
4. Malhotra C, Jain AK. Human amniotic membrane transplantation: different modalities of its use in ophthalmology. World J Transplant. 2014; 4(2): 111.
5. Shayan Asl N, Nejat F, Mohammadi P, Nekoukar A, Hesam S, Ebrahimi M, et al. Amniotic membrane extract eye drop promotes limbal stem cell proliferation and corneal epithelium healing. Cell J. 2019; 20(4): 459-468.
6. Lyons VN, Townsend WM, Moore GE, Liang S. Commercial amniotic membrane extract for treatment of corneal ulcers in adult horses. Equine Vet J. 2021; 53(6): 1268-1276.
7. Murri MS, Moshirfar M, Birdsong OC, Ronquillo YC, Ding Y, Hoopes PC. Amniotic membrane extract and eye drops: a review of literature and clinical application. Clin Ophthalmol. 2018; 12: 1105-1112.
8. Giloyan A, Khachadourian V, Petrosyan V, Harutyunyan T. Prevalence and determinants of uncorrected refractive error among a socially vulnerable older adult population living in Armenia. Public Health. 2021; 190: 30-36.
9. Evangelos P, Chrisi K. Prevalence and distribution of refractive errors among adults in Athens-Greece (urban area). Opth Clin Ther. 2020; 4(2): 3-8.
10. Adib-Moghaddam S, Soleyman-Jahi S, Sanjari Moghaddam A, Hoorshad N, Tefagh G, Haydar AA, et al. Efficacy and safety of transepithelial photorefractive keratectomy. J Cataract Refract Surg. 2018; 44(10): 1267-1279.
11. Hassan Mohammad H, Mohamed Tag El-Din AE-M, S Al-Sheikh M. Postoperative corneal haze after transepithelial photorefractive keratectomy (trans prk) versus conventional photorefractive keratectomy (prk). AIMJ. 2020; 49(3): 979-986.
12. Efron N, Morgan PB, Katsara SS. Validation of grading scales for contact lens complications. Ophthalmic Physiol Opt. 2001; 21(1): 17-29.
13. Tandon R, Gupta N, Kalaivani M, Sharma N, Titiyal JS, Vajpayee RB. Amniotic membrane transplantation as an adjunct to medical therapy in acute ocular burns. Br J Ophthalmol. 2011; 95(2): 199-204.
14. Holden BA, Fricke TR, Wilson DA, Jong M, Naidoo KS, Sankaridurg P, et al. Global prevalence of myopia and high myopia and temporal trends from 2000 through 2050. Ophthalmology. 2016; 123(5): 1036-1042.
15. Varadarajan AV, Poplin R, Blumer K, Angermueller C, Ledsam J, Chopra R, et al. Deep learning for predicting refractive error from retinal fundus images. Invest Ophthalmol Vis Sci. 2018; 59(7): 2861-2868.
16. Kundu G, D'Souza S, Lalgudi VG, Arora V, Chhabra A, Deshpande K, et al. Photorefractive keratectomy (PRK) prediction, examination, treatment, follow-up, evaluation, chronic treatment (PERFECT) protocol - a new algorithmic approach for managing post PRK haze. Indian J Ophthalmol. 2020; 68(12): 2950-2955.
17. Zarei-Ghanavati S, Shandiz JH, Abrishami M, Karimpour M. Comparison of mechanical debridement and trans-epithelial myopic photorefractive keratectomy: a contralateral eye study. J Curr Ophthalmol. 2019; 31(2): 135-141.

18. Sanchez-Avila RM, Uribe-Badillo EE, Sanz JF-V, Muruzabal F, Jurado N, Alfonso-Bartolozzi B, et al. Plasma rich in growth factors versus Mitomycin C in photorefractive keratectomy. Medicine (Baltimore). 2021; 100(3): e24139.
19. Shah MN, Misra M, Wihelmus KR, Koch DD. Diffuse lamellar keratitis associated with epithelial defects after laser in situ keratomileusis. J Cataract Refract Surg. 2000; 26(9): 1312-1318.
20. Fini ME, Cook JR, Mohan R. Proteolytic mechanisms in corneal ulceration and repair. Arch Dermatol Res. 1998; 290(1): S12-S23.
21. Sabater-Cruz N, Figueras-Roca M, Ferrán-Fuertes M, Agustí E, Martínez-Conesa EM, Pérez-Rodríguez ML, et al. Amniotic membrane extract eye drops for ocular surface diseases: use and clinical outcome in real-world practice. Int Ophthalmol. 2021; 41(9): 2973-2979.
22. Kordić R, Popović Suić S, Jandroković S, Kalauz M, Kuzman T, Škegro I, et al. Application of the amniotic membrane extract (AMX) for the persistent epithelial defect (PED) of the cornea. Coll Antropol. 2013; 37 Suppl 1: 161-164.
23. Sheha H, Liang L, Hashem H, Ramzy M, ZaKi A. Amniotic membrane extract for acute ocular chemical burns. Tech Ophthalmol. 2010; 8(4): 146-150.

Cell J
Cell Journal(Yakhteh)
Homepage: https://www.celljournal.org/
Original Article
Vol 25, No 4, April 2023, Pages: 222-228

Understanding The Regulatory Role of USP32 and SHMT2 in The Progression of Gastric Cancer

Jun Li, M.D.[1], Yafei Bo, M.D.[2], Bo Ding, M.D.[1], Lei Wang, M.D.[1]*

1. Department of Gastrointestinal Surgery, General Hospital of Ningxia Medical University, Yinchuan, Ningxia, China
2. Department of Emergency, General Hospital of Ningxia Medical University, Yinchuan, Ningxia, China

Abstract

Objective: Gastric cancer is the fifth most common neoplasm and the fourth reason for mortality globally. Incidence rates are highly variable and dependent on risk factors, epidemiologic and carcinogenesis patterns. Previous studies reported that *Helicobacter pylori* (*H. pylori*) infection is one the strongest known risk factor for gastric cancer. USP32 is a deubiquitinating enzyme identified as a potential factor associated with tumor progression and a key player in cancer development. On the other hand, SHMT2 is involved in serine-glycine metabolism to support cancer cell proliferation. Both USP32 and SHMT2 are reported to be upregulated in many cancer types, including gastric cancer, but its complete mechanism is not fully explored yet. The present study explored possible mechanism of action of USP32 and SHMT2 in the progression of gastric cancer.

Materials and Methods: In this experimental study, Capsaicin (0.3 g/kg/day) and *H. pylori* infection combination was used to successfully initiate gastric cancer conditions in mice. It was followed by 40 and 70 days of treatment to establish initial and advanced conditions of gastric cancer.

Results: Histopathology confirmed formation of signet ring cell and initiation of cellular proliferation in the initial gastric cancer. More proliferative cells were also observed. In addition, tissue hardening was confirmed in the advanced stage of gastric cancer. USP32 and SHMT2 showed progressive upregulated expression, as gastric cancer progress. Immunohistologically, it showed signals in abnormal cells and high-intensity signals in the advanced stage of cancer. In USP32 silenced tissue, expression of *SHMT2* was completely blocked and reverted cancer development as evident with less abnormal cell in initial gastric cancer. Reduction of SHMT2 level to one-fourth was observed in the advanced gastric cancer stages of USP32 silenced tissue.

Conclusion: USP32 had a direct role in regulating SHMT2 expression, which attracted therapeutic target for future treatment.

Keywords: Cancer, Gastric Cancer, *H. pylori*, SHMT2, USP32

Citation: **Li J, Bo Y, Ding B, Wang L. Understanding the regulatory role of USP32 and SHMT2 in the progression of gastric cancer. Cell J. 2023; 25(4): 222-228. doi: 10.22074/CELLJ.2022.557384.1046.**

Introduction

Gastric cancer is a condition of malignant tumour originated from gastric mucosa layer. Each year, more than 1 million people are newly developing gastric cancer, as the 3rd most leading form of cancer that results in death (1, 2). Another important fact behind the gastric cancer is that 70% of cases are reported from developing countries whereby China alone is reported with more than 50% of cases (3). Although there is some advancement happening in the treatment procedure, prognosis of gastric cancer in the early stage is still poor that makes the overall 5 years survival rate less than 20-30% (4). In the present scenario, it is essential to identify a new prognostic marker to identify gastric cancer in its early stage and to design new therapies, to improve 5 year survival rate (5).

Ubiquitin-specific protease 32 (USP32) is recognized as a new member of the ubiquitin-specific proteases subfamily. It alters protein stability and localization, thereby regulating their activity in different pathological stages of many human diseases, like cancer (6-8). So far, it has been reported that USP32 was over-expressed in lung and breast cancers, enhancing cellular proliferation and tissue metastasis (9). Recent knock-down studies with USP32 represented significant reduction of gastric cancer cell proliferation and cellular migrations both *in vitro* and *in vivo* (10). However, very little is known about the regulating effect of USP32 on other key proteins to promote gastric cancer.

Serine hydroxymethyltransferase-2 (SHMT2) is a key enzyme presented within the mitochondria. It is involved in the conversation of serine to glycine (11, 12). SHMT2 was highly expressed in many cancer cells like brain, colorectal,

Received: 10/June/2022, Revised: 03/November/2022, Accepted: 24/December/2022
***Corresponding Address: Department of Gastrointestinal Surgery, General Hospital of Ningxia Medical University, Yinchuan, Ningxia, China**
Email: wanglei1182@sina.com

Royan Institute
Cell Journal (Yakhteh)

bladder and kidney, which enhanced (7) their proliferative ability (13, 14). SHMT2 enhanced serine catabolism and thereby supported cancer growth by increasing nucleotide synthesis (12), mitochondrial translation (15), redox balance (16), methylation of DNA and histone protein (12) and by suppression of retrotransposon activation (17). Higher expression of SHMT2 was recently reported in gastric, colon and esophageal cancers (18). Therefore, this needs to extensively studied in different stages of gastric cancer along with the other key linked protein. The present investigation explored relationship of USP32 with SHMT2 protein in progression of gastric cancer.

Materials and Methods

The experimental study was ethically approved by General Hospital of Ningxia Medical University, Ningxia, China (EXC/20180819).

Mice model and experimental design

Two-months-old male mice of strain C57-BL/6J-219 with an average weight of 20-22 g were purchased from Vital River Laboratory (Ningxia, China). The mice were free from Helicobacter spp., Salmonella spp and Citrobacter rodentium. They were maintained in laboratory environment with ambient temperature of 24ºC, humidity of 55-60% and light/dark cycle for every 12 hours interval. The mice were fed with a regular diet containing sterilized commercial pellets obtained from Beijing HFK Bioscience (China) and provided with sterilized water ad libitum. All of the experimental procedures, followed here, were performed after getting the institutional ethical committee approval and they were in accordance with the recent guidelines. The mice were randomly divided into three groups: negative control (NC) group, initial stage gastric cancer group and advanced stage gastric cancer group (n=10 for each group). After one week of the acclimation period, the mice were administrated capsaicin (0.3 g/kg/day) in dietary food for two weeks before *H. pylori* infection and the capsaicin administration was continued throughout the experiment, as described earlier (19). From the 3rd week of capsaicin injection, each mouse was administered a suspension of the *H. pylori* SS1 strain containing 10^8 CFUs/ml by gavage, three times per week. Additionally, for effective *H. pylori* colonization, pantoprazole (25 mg/kg) was administrated three times per week by gavage method to lower gastric acidity. The experimental procedure was continued: one group of animals was euthanized at the end of 40 weeks and the other groups were euthanized at 70 weeks. For control purpose, the mice were left untreated and euthanized at the end of 70 weeks. After euthanizing the mice, the stomach was excised out and the gastric tumour was microscopically dissected for further experiments.

Histological procedure

The dissected gastric cancer tissue with size of 3-5 mm was carefully transferred to 10% formalin solution and kept for 48 hours at room temperature. The tissues was washed with tap water and subjected to dehydration step using an increased concentration of ethanol (70-100%). The dehydrated tissue was transferred to xylene for the tissue clearing step and it was finally embedded with wax. Using microtome, 6 µm thin sectioning of the block containing tissues was done and the ribbon was placed on the glass slides. The glass slides containing the sections were dewaxed, dehydrated and stained with haematoxylin and eosin. The slides were finally mounted using DPX mounting solution (Sigma Aldrich, Germany) and examined under EVOS® FL Cell Imaging System (Thermo Fisher Scientific, USA).

Immunohistochemistry

The wax-embedded tissue was set up in the microtome and allowed for 5 µm uniform sectioning. After dewaxing and rehydration, the sections were subjected to antigen retrieval step using heat-induced method in which the slides were boiled for 10 minutes in 10 mM sodium citrate buffer (pH=6.0). The slides were pre-incubated with 5% bovine serum albumin (BSA, Thermo Fisher Scientific, USA) in 1X TBST for 1 hour prior to primary antibody incubation for background minimization. The primary antibodies anti-USP32 (ab251903, 1:800; Abcam, USA), anti-SHMT2 (12762, 1:1000; Cell Signaling Technology, USA) and anti-β actin (sc-47778, 1:1000; Santa Cruz, USA) were diluted in 5% BSA solution and overlaid with tissue samples. They were then incubated in 4ºC for 4 hours. The slides were washed with 1X TBST for three times to remove non-specific binding of antibody. Next, they were further incubated with HRP conjugated secondary antibody (ab97051, 1:1000; Abcam, USA) for 2 hours in room temperature. After washing, the slides were completely drain out and incubated with the HRP (Bio Rad, India) substrate solution of DAB (3,3´-Diaminobenzidine; Bio Rad, India) for 15 minutes in dark environment at 37ºC. After washing, the slides were counter stained with haematoxylin for 5 minutes and the sections were mounted using DPX solution. The slides were examined under EVOS® FL Cell Imaging System (Thermo Fisher Scientific, USA).

siRNA against *USP32*

For *USP32* silencing purposes, commercially available siRNA against *USP32* 5´-GACCUGUGGACUCUCAUAUTT-3´ (si-USP32-homo-386) was purchased from Gene Pharma, China along with the NC 5′-UUCUCCGAACGUGUCACGUdTdT-3´ (si-NC) (10). The siRNA samples were dissolved in water to achieve final concentration of 0.6 µg/µl. It was next mixed with 0.5 µl of 50 nM Lipofectamine 2000 prior to injection to improve transfection efficiency. Injection of siRNA was performed through the tail vein exactly before

one month of mice scarification.

RNA isolation and quantitative reverse transcription polymerase chain reaction

Total RNA was isolated from tissues using Trizol reagent (Invirogen, USA) as per the standard protocol. Synthesis of complementary DNA (cDNA) was performed using RevertAid First strand cDNA synthesis kit (Thermo Fisher Scientific, USA). For evaluating the relative transcript levels of different genes, quantitative reverse transcription polymerase chain reaction (qRT-PCR) was performed with the help of SYBR Green RT-PCR kit (Takara Shuzo Co. Ltd, Japan). The thermo-cycling was performed on the Quant Studio 5.0 Real-Time PCR system (Applied Biosystems, USA). Quantitative assessment of mRNA expression levels was made using the $2^{-\Delta\Delta Ct}$ method. *GAPDH* was used as an endogenous expression controls. Sequences of the qRT-PCR primers used were:

USP32-

F: 5′-GGCTGCTCGTGATATGCTGTTC-3′
R: 5′-GTTTCTGGGCTGACACCTTGC-3′

SHMT2-

F: 5′-AGTCTATGCCCTATAAGCTCAACCC-3′
R: 5′-GCCGGAAAAGTCGAGCAGT-3′

GADPH-
F: 5′-CATCTCTGCCCCCTCTGCTGA-3′
R: 5′-GGATGACCTTGCCCACAGCCT-3′.

$2^{-\Delta\Delta Ct}$ method was used for estimating the relative expression levels.

Western blotting

The dissected gastric cancer tissue samples were crushed with 2X samples buffer using a pre-cooled mortar and pestle. The cell lysate was heated in a boiling water bath for 10 minutes and later cooled. The concentration of protein samples were determined using Bradford method. The equal quantity of protein samples (70 µg/well) were loaded in the 10% sodium dodecyl sulfate–polyacrylamide gel electrophoresis (SDS-PAGE) and separated at 100V for 4 hours. The separated proteins in the gel were transferred to the PVDF membrane effectively using the semi-dry method. To minimize the background signals, the PVDF membrane was incubated with blocking solution containing 5% BSA solution in 1X TBST buffer for 2 hours at 37ºC. The membrane was then incubated with primary antibodies like, anti-USP32 (ab190184, 1:800; Abcam, USA), anti-SHMT2 (12762, 1:1000; Cell Signaling Technology) or anti-β actin (sc-47778, 1:1000; Santa Cruz, USA) for 4 hours at 4ºC. After terminating incubation, the membrane was washed with 1X PBS for three times, each time containing 10 minutes each. Finally, the blot was incubated with the secondary antibodies (ab205718, 1:5000 or ab205720, 1:15000; Abcam, USA) and further developed with Pierce™ DAB Substrate Kit (Thermo Fisher Scientific, USA). The band intensity developed in the membrane was documented using gel documentation system and analysed using ImageJ software.

Statistical analysis

For achieving statistical significance, the experiments were repeated for at least three or more times and the obtained results were denoted in mean ± SD. Student's t test and ANOVA using posthoc Tukey's t test were used to estimate significance of the statistical difference between two/among many data points. The obtained results were considered as statistically significant when the $P<0.005$.

Results

Induction of initial and advanced stages of gastric cancer

In the control gastric tissue, the cells were normal without any abnormal variations and the cells were packed in regular interval (Fig.1A). In initial stage of gastric cancer, tissue showed histological variations like formation of signet ring cell along with initiation of more proliferative cells which disturb the normal arche structure of gastric tissue arrangement (Fig.1B). In the advanced stage of gastric cancer, there were complete change of normal gastric tissue structure with more proliferative cells which were ultimately resulted in more cellular density and tissue hardening (Fig.1C). In *USP32* silenced tissue, the histopathological observation in initial gastric cancer stage revealed no signet ring cell formation and reduced proliferative nature of cells were also seen (Fig.1D). Similarly, in *USP32* silenced tissue, the histopathological observation in advanced gastric cancer stage revealed no tissue hardening and highly reduced proliferative nature of cells (Fig.1E).

USP32 and SHMT2 showed elevated expression as gastric cancer progress

Following the confirmation of initial and advanced stages of gastric cancer, expression of USP32 and SHMT2 were analyzed upon the progression of gastric cancer, as shown in Figure 2. In the control gastric tissue, expression of USP32 was difficult to locate within the tissue layer (Fig.2A). However, in initial tumour tissue, expression of USP32 was substantially upregulated within the abnormal cells (Fig.2B). As the cancerous condition progresses, expression of USP32 showed strong signals throughout the tissue layer (Fig.2C). Similarly, SHMT2 expression levels were examined in the control gastric tissue (Fig.2D). SHMT2 showed progressive overexpression with respect to cancer stages (Fig.2D-F). Expression of SHMT2 was localized to abnormal cells in the initial stage of gastric cancer (Fig.2E). However, expression of SHMT2 was widespread (with high intensity signals) throughout the tissue in advanced stage of gastric cancer (Fig.2F).

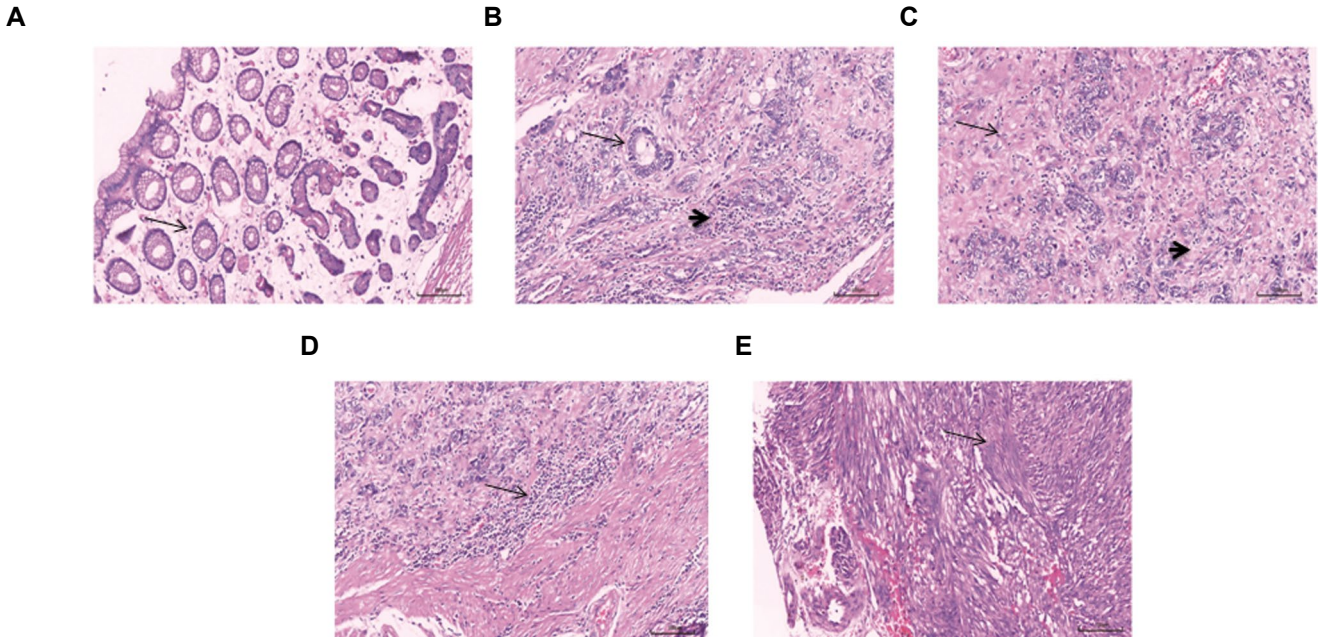

Fig.1: Histopathogy of gastric cancer progression. **A.** The control gastric tissue shows uniformly distributed cellular arrangement. **B.** Initial gastric cancer tissue showing signet ring cell (arrow) and proliferative cells (arrow head). **C.** Advanced stage of gastric cancer tissue with more proliferative cells (arrow) with tissue hardening (arrow head). **D.** *USP32* silenced the initial gastric cancer tissue without signet ring cell with less proliferative cells (arrow). **E.** *USP32* silenced advanced gastric cancer tissue without tissue hardening and with moderate proliferative cells (arrow) (scale bar: 50 µm).

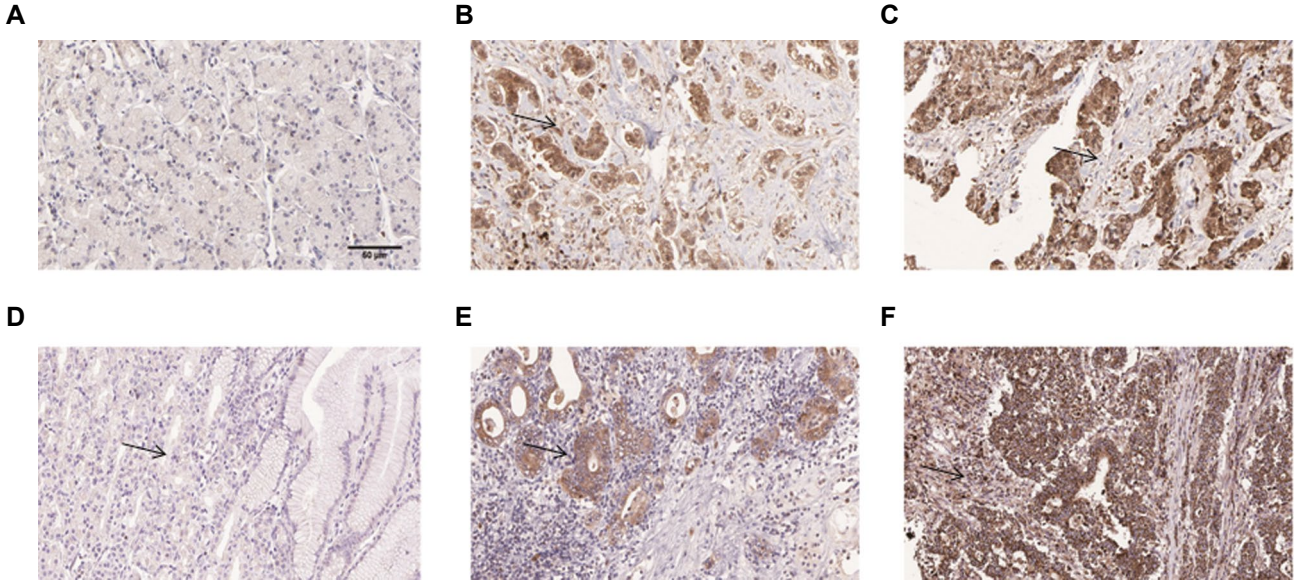

Fig.2: USP32 and SHMT2 expression analyses using immunohistochemistry. **A.** Control gastric tissue showing less signals for USP32. **B.** Progressive signal for USP32 observed in the initial gastric cancer tissue (arrow). **C.** Abundant and intense signal for USP32 observed in advanced stage gastric cancer (arrow). **D.** SHMT2 signal are very limited in the control gastric tissue (arrow). **E.** SHMT2 shows upregulated expression in initial gastric cancer tissue (arrow). **F.** Overexpression of SHMT2 was observed in the advanced stage of gastric cancer tissue (arrow) (scale bar: 50 µm).

USP32 silencing diminishes the *SHMT2* expression in the both initial and advanced stages of gastric cancer

To understand role of USP32 in regulating *SHMT2* expression, gene silencing experiments were performed. siRNA against *USP32* was found to completely block expression of *USP32* in the control tissue (Fig.3A) and it substantially reduced *USP32* expression in the initial gastric cancer tissue (Fig.3B). Additionally, downregulated expression of *USP32* was observed in the advanced stage of gastric cancer following siRNA injection against *USP32* (Fig.3C). Alteration of *SHMT2* expression, following *USP32* silencing was also investigated and it was observed that expression of *SHMT2* was completely downregulated in the control and initial stages of gastric cancer (Fig.3D, E). *USP32* silencing in advanced stage gastric cancer, reduced expression of *SHMT2* to a moderate level (Fig.3F).

USP32 specifically alters *SHMT2* expression

Following immunohistochemistry, western blot and

qRT-PCR experiments were performed to observe expression levels of USP32 and SHMT2 in the initial and advanced stages of gastric cancer. As shown in Figure 4A and B, expression level of USP32 was increased progressively in the initial and advanced stages of gastric cancer compared to the control tissue. Similarly, expression of SHMT2 showed progressive increase in the initial and advanced stages of gastric cancer compared to the control tissue. Silencing *USP32*, reduced expression of SHMT2 in the both initial and advanced stages of gastric cancer compared to the control tissue. Similarly, *SHMT2* silencing drastically reduced expression of *USP47* (almost not able to detect) in the control tissue and initial stage gastric cancer tissue. In the advanced stage, expression of USP47 was reduced compared to the non-silenced tissue. As shown in Figure 4C, similar results, as obtained in western blotting, were obtained by qRT-PCR.

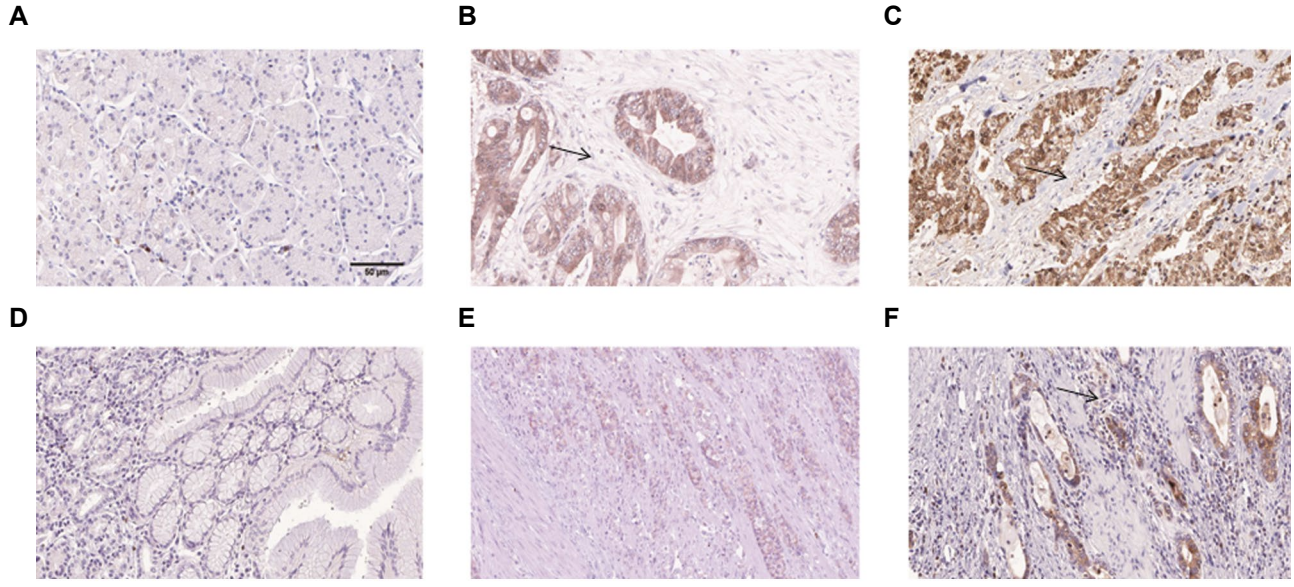

Fig.3: *USP32* silencing and *SHMT2* suppression. **A.** *USP32* silenced the gastric control tissue without *USP32* signal. **B.** *USP32* silenced in the initial gastric cancer tissue show limited expression of *USP32* (arrow). **C.** *USP32* silenced in the advanced stage gastric cancer tissue with moderate *USP32* expression (arrow). **D.** *USP32* silenced in the control gastric tissue without *SHMT2* expression. **E.** *USP32* silenced in the initial gastric cancer tissue show no *SHMT2* expression. **F.** *USP32* silenced in the advanced stage gastric cancer tissue with moderate *SHMT2* expression (arrow) (scale bar: 50 µm).

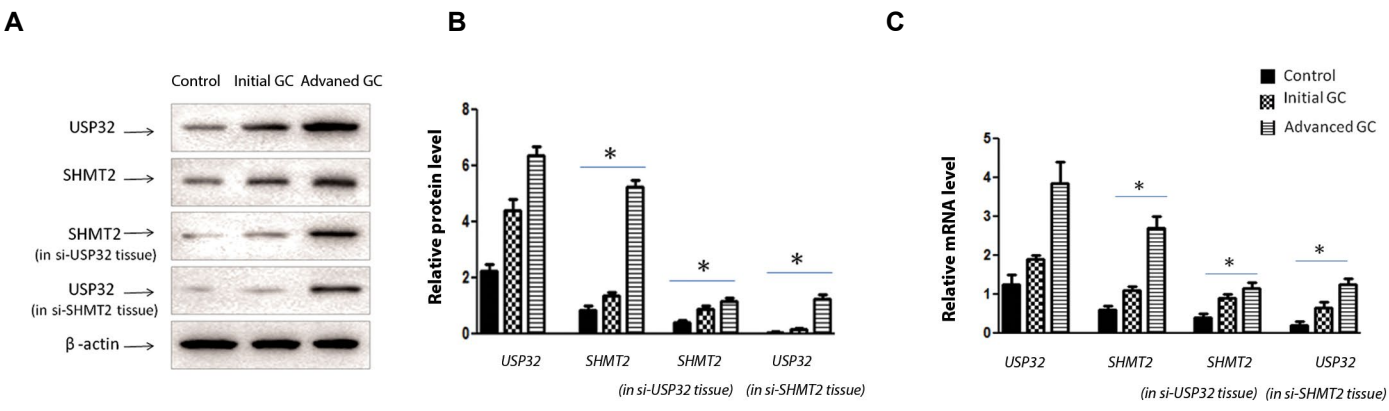

Fig.4: Expression analysis of USP47 and SHMT2. **A**, **B.** Protein expression level of USP32 was significantly and progressively increased in initial and advanced stages of gastric cancer than control tissue. Similarly, SHMT2 shows slight expression in the control tissue but its expression was significantly and progressively increased in the initial and advanced stages of gastric cancer. In *USP32* silenced tissue, expression of SHMT2 was drastically reduced in the control and initial gastric cancer tissues. However, in the advanced gastric cancer stage, the *USP32* silenced tissue showed significantly reduced expression of SHMT2 compared to the non-silenced tissue. Similarly, in the *SHMT2* silenced tissue, expression of USP47 was drastically reduced (almost not able to detect any band) in the control and initial stage gastric cancer tissue. However, in the advanced gastric cancer stage, *SHMT2* silenced tissue showed significantly reduced expression of USP47 compared to the non-silenced tissue. **C.** Quantitative reverse transcription polymerase chain reaction (qRT-PCR) analysis: mRNA expression level of *USP32* was significantly and progressively increased in the initial and advanced stages of gastric cancer than the control tissue. Similarly, *SHMT2* shows lower mRNA expression in the control tissue, but its expression was significantly and progressively increased in the initial and advanced stages of gastric cancer. In the *USP32* silenced tissue, mRNA expression of *SHMT2* was reduced in the control and initial gastric cancer tissues. However, in the advanced gastric cancer stage, *USP32* silenced tissue showed significantly reduced mRNA expression of *SHMT2* compared to non-silenced tissue. Similarly, in the *SHMT2* silenced tissue, mRNA expression of *USP47* was reduced in the control and initial stage gastric cancer tissue. However, in the advanced gastric cancer stage, the *SHMT2* silenced tissue showed significantly reduced mRNA expression of *USP47* compared to the non-silenced tissue. $2^{-\Delta\Delta Ct}$ method was used for estimating the relative expression levels. All of the experiments were performed thrice and (*) shows P<0.005.

Discussion

Combination of capsaicin and *H. pylori* infections contribute to developing gastric inflammation and finally gastric cancer. The synergy of capsaicin and *H. pylori* combination is able to induce gastric tumorigenesis by inducing inflammatory-related proteins and cytokines (19). Treated mice for 40 weeks showed signet ring cells, which are the sign of tumour initiation (20). In the initial gastric stage, the cells started to proliferate more, which was evident in tumour initiation (21). Following 70 weeks of treatment procedure, more proliferative cells were observed throughout the tissue layer. Along with this, tissue hardness were observed. These were due to the changes in extracellular matrix protein, as a consequent of extensive changes in cellular morphology (22). *USP32* silencing experiment was fascinating, as it reduced level of proliferative cells in the initial and advanced stages of gastric cancer. From the result, it is proposed that *USP32* silencing can inhibit progression of gastric cancer. It may also have a possible control over cellular migration and invasion, although this needs to be investigated. Earlier, similar type of link has been found between USP32 and SMAD Family Member 2 (SMAD2), in the development and progression of gastric cancer (10).

USP32 showed a progressive upregulated expression in the initial and advanced stages of gastric cancer, and careful examination showed that in the initial stage gastric cancer, its expression was restricted within the abnormal cells. USP32 may promote key cancer-related proteins through deubiquitinating in abnormal cells, which may promote cell migration (23), regulate stemness or be involved in epithelial-mesenchymal transition (24). Signal intensity for USP32 was high in the advanced stage of gastric cancer which may represent it strongly regulated different gastric cancer-related proteins as the cancer progresses. Usually, SHMT2 is highly expressed in mitochondria, while it is also detected in cytoplasm and nucleus (25). After reprogramming normal cell to gastric cancer cell, elevated serine/glycine metabolism is essential for cellular proliferation (26). With this evidence, the progressive upregulated expression of SHMT2 was observed with more cytoplasmic and nuclear expression.

In *USP32* silenced initial gastric cancer, SHMT2 expression was completely diminished. This implied its control over USP32. The expression of SHMT2 was also reduced in the *USP32* silenced advanced stage of gastric cancer. It implied its tight regulation even in the advanced stage. SHMT2 overexpression frequently occurs in the advanced grade of glioma condition and it has a role in cellular proliferation and invasion (18). Therefore, suppression its activity by inhibiting USP32 can hinder the root of SHMT2 activation and it may be used as a future therapeutic target.

Conclusion

Our findings provided a new insight into expression and function of USP32 in gastric cancer. USP32 was found to regulate SHMT2 expression in initial and advanced stages of gastric cancer and vice versa. Targeting USP32 and SHMT2 might be the potential therapeutic strategy for gastric cancer.

Acknowledgements

Department of Gastrointestinal Surgery, General Hospital of Ningxia Medical University (Ningxia, China) is acknowledged for providing research support. There is no financial support and conflict of interest in this study.

Authors' Contributions

J.L.; Conception and design of the manuscript. Y.B.; Data acquisition or data analysis and interpretation. B.D.; Performs experimental work and drafting the manuscript. L.W.; Final approval of the manuscript, statistical analysis and supervision. All authors read and approved the final manuscript.

References

1. Global Burden of Disease Cancer Collaboration; Fitzmaurice C, Abate D, Abbasi N, Abbastabar H, Abd-Allah F, et al. Global, regional, and national cancer incidence, mortality, years of life lost, years lived with disability, and disability-adjusted life-years for 29 cancer groups, 1990 to 2017: a systematic analysis for the global burden of disease study. JAMA Oncol. 2019; 5(12): 1749-1768.
2. Thrift AP, El-Serag HB. Burden of gastric cancer. Clin Gastroenterol Hepatol. 2020; 18(3): 534-542.
3. Qinghai Z, Yanying W, Yunfang C, Xukui Z, Xiaoqiao Z. Effect of interleukin-17A and interleukin-17F gene polymorphisms on the risk of gastric cancer in a Chinese population. Gene. 2014; 537(2): 328-332.
4. Tahara T, Shibata T, Nakamura M, Yamashita H, Yoshioka D, Okubo M, et al. Association between IL-17A, -17F and MIF polymorphisms predispose to CpG island hyper-methylation in gastric cancer. Int J Mol Med. 2010; 25(3): 471-477.
5. Lee H, Kim WJ, Kang HG, Jang JH, Choi IJ, Chun KH, et al. Upregulation of LAMB1 via ERK/c-Jun axis promotes gastric cancer growth and motility. Int J Mol Sci. 2021; 22(2): 626.
6. Aksentijevich I, Zhou Q. NF-κB pathway in autoinflammatory diseases: dysregulation of protein modifications by ubiquitin defines a new category of autoinflammatory diseases. Front Immunol. 2017; 8: 399.
7. Chen S, Chen X, Li Z, Mao J, Jiang W, Zhu Z, et al. Identification of ubiquitin-specific protease 32 as an oncogene in glioblastoma and the underlying mechanisms. Sci Rep. 2022; 12(1): 6445.
8. Chandrasekaran AP, Kaushal K, Park CH, Kim KS, Ramakrishna S. USP32 confers cancer cell resistance to YM155 via promoting ER-associated degradation of solute carrier protein SLC35F2. Theranostics. 2021; 11(20): 9752-9771.
9. Hu W, Wei H, Li K, Li P, Lin J, Feng R. Downregulation of USP32 inhibits cell proliferation, migration and invasion in human small cell lung cancer. Cell Prolif. 2017; 50(4): e12343.
10. Dou N, Hu Q, Li L, Wu Q, Li Y, Gao Y. USP32 promotes tumorigenesis and chemoresistance in gastric carcinoma via upregulation of SMAD2. Int J Biol Sci. 2020; 16(9): 1648-1657.
11. Wang Q, Tian J, Li X, Liu X, Zheng T, Zhao Y, et al. Upregulation of endothelial DKK1 (Dickkopf 1) promotes the development of pulmonary hypertension through the Sp1 (Specificity Protein 1)/SHMT2 (Serine Hydroxymethyltransferase 2) pathway. Hypertension. 2022; 79(5): 960-973.
12. Maddocks OD, Labuschagne CF, Adams PD, Vousden KH. Serine metabolism supports the methionine cycle and DNA/RNA methylation through de novo ATP synthesis in cancer cells. Mol Cell. 2016; 61(2): 210-221.
13. Xie SY, Shi DB, Ouyang Y, Lin F, Chen XY, Jiang TC, et al. SHMT2 promotes tumor growth through VEGF and MAPK signaling pathway in breast cancer. Am J Cancer Res. 2022; 12(7): 3405-3421.
14. Shi H, Fang X, Li Y, Zhang Y. High expression of serine Hydroxy-

methyltransferase 2 indicates poor prognosis of gastric cancer patients. Med Sci Monit. 2019; 25: 7430-7438.
15. Morscher RJ, Ducker GS, Li SH, Mayer JA, Gitai Z, Sperl W, et al. Mitochondrial translation requires folate-dependent tRNA methylation. Nature. 2018; 554(7690): 128-132.
16. Ye J, Fan J, Venneti S, Wan YW, Pawel BR, Zhang J, et al. Serine catabolism regulates mitochondrial redox control during hypoxia. Cancer Discov. 2014; 4(12): 1406-1417.
17. Kottakis F, Nicolay BN, Roumane A, Karnik R, Gu H, Nagle JM, et al. LKB1 loss links serine metabolism to DNA methylation and tumorigenesis. Nature. 2016; 539(7629): 390-395.
18. Liu Y, Yin C, Deng MM, Wang Q, He XQ, Li MT, et al. High expression of SHMT2 is correlated with tumor progression and predicts poor prognosis in gastrointestinal tumors. Eur Rev Med Pharmacol Sci. 2019; 23(21): 9379-9392.
19. Aziz F, Xin M, Gao Y, Chakroborty A, Khan I, Monts J, et al. Induction and prevention of gastric cancer with combined helicobacter pylori and capsaicin administration and DFMO treatment, respectively. Cancers (Basel). 2020; 12(4): 816.
20. Pernot S, Voron T, Perkins G, Lagorce-Pages C, Berger A, Taieb J. Signet-ring cell carcinoma of the stomach: Impact on prognosis and specific therapeutic challenge. World J Gastroenterol. 2015; 21(40): 11428-11438.
21. Zavros Y. Initiation and maintenance of gastric cancer: a focus on CD44 variant isoforms and cancer stem cells. Cell Mol Gastroenterol Hepatol. 2017; 4(1): 55-63.
22. Ebata T, Mitsui Y, Sugimoto W, Maeda M, Araki K, Machiyama H, et al. Substrate stiffness influences doxorubicin-induced p53 activation via ROCK2 expression. Biomed Res Int. 2017; 2017: 5158961.
23. Cai J, Li M, Wang X, Li L, Li Q, Hou Z, et al. USP37 promotes lung cancer cell migration by stabilizing snail protein via deubiquitination. Front Genet. 2020; 10: 1324.
24. Qin T, Li B, Feng X, Fan S, Liu L, Liu D, et al. Abnormally elevated USP37 expression in breast cancer stem cells regulates stemness, epithelial-mesenchymal transition and cisplatin sensitivity. J Exp Clin Cancer Res. 2018; 37(1): 287.
25. Anderson DD, Stover PJ. SHMT1 and SHMT2 are functionally redundant in nuclear de novo thymidylate biosynthesis. PLoS One. 2009; 4(6): e5839.
26. Kim D, Fiske BP, Birsoy K, Freinkman E, Kami K, Possemato RL, et al. SHMT2 drives glioma cell survival in ischaemia but imposes a dependence on glycine clearance. Nature. 2015; 520(7547): 363-367.

Cell J
Cell Journal(Yakhteh)
Homepage: https://www.celljournal.org/
Original Article
Vol 25, No 4, April 2023, Pages: 229-237

Establishment of A Three-Dimensional Culture Condition for The U266 Cell Line Based on Peripheral Blood Plasma-Derived Fibrin Gels

Mahshid Jomehpour, M.Sc.[1#], Mohammadmahdi Khosravi, M.Sc.[1#], Mehrnaz Janfada, M.Sc.[1#], Saeid Abroun, Ph.D.[1], Sadaf Vahdat, Ph.D.[2*]

1. Department of Hematology, Faculty of Medical Sciences, Tarbiat Modares University, Tehran, Iran
2. Applied Cell Sciences Division, Department of Hematology, Faculty of Medical Sciences, Tarbiat Modares University, Tehran, Iran

Abstract

Objective: The study of pathophysiology as well as cellular and molecular aspects of diseases, especially cancer, requires appropriate disease models. *In vitro* three-dimensional (3D) structures attracted more attention to recapitulate diseases rather than *in vitro* two-dimensional (2D) cell culture conditions because they generated more similar physiological and structural properties. Accordingly, in the case of multiple myeloma (MM), the generation of 3D structures has attracted a lot of attention. However, the availability and cost of most of these structures can restrict their use. Therefore, in this study, we aimed to generate an affordable and suitable 3D culture condition for the U266 MM cell line.

Materials and Methods: In this experimental study, peripheral blood-derived plasma was used to generate fibrin gels for the culture of U266 cells. Moreover, different factors affecting the formation and stability of gels were evaluated. Furthermore, the proliferation rate and cell distribution of cultured U266 cells in fibrin gels were assessed.

Results: The optimal calcium chloride and tranexamic acid concentrations were 1 mg/ml and 5 mg/ml for gel formation and stability, respectively. Moreover, the usage of frozen plasma samples did not significantly affect gel formation and stability, which makes it possible to generate reproducible and available culture conditions. Furthermore, U266 cells could distribute and proliferate inside the gel.

Conclusion: This available and simple fibrin gel-based 3D structure can be used for the culture of U266 MM cells in a condition similar to the disease microenvironment.

Keywords: Blood Plasma, Fibrin, Multiple Myeloma, Three-Dimensional Culture

Citation: **Jomehpour M, Khosravi M, Janfada M, Abroun S, Vahdat S. Establishment of a three-dimensional culture condition for the U266 cell line based on peripheral blood plasma-derived fibrin gels. Cell J. 2023; 25(4): 229-237. doi: 10.22074/CELLJ.2023.562849.1138.**

Introduction

Multiple myeloma (MM) is one of the most common type of blood cancer worldwide after lymphoma (1). MM is slightly more common in men, and the average age at diagnosis is 65 years. The overall five-year survival rate for patients with MM is 56% (2). Despite the recent introduction of various drugs and treatment strategies for MM (2), relapses occur in most patients (3), and MM remains predominantly incurable (4). Therefore, it is required to study the mechanisms involved in MM pathogenesis and evaluate the effectiveness of novel drugs in a more similar condition to the MM microenvironment.

Most myeloma research is conducted *in vitro* due to the lack of suitable animal models that accurately mimic the disease (5). In this regard, various cell lines, such as OPM-2, MM.1s, RPMI-8226 and U266, have been grown in two-dimensional (2D) cell culture systems and used for drug screening and disease research. Among them, U266 is a well-known and frequently-utilized myeloma cell line (6) that expresses IL-6, a crucial component for the maintenance and proliferation of myeloma cells (7, 8).

Although accessibility, simplicity and low cost have made 2D cell culture one of the most widely used culture conditions, this type of cell culture has numerous limitations. Some examples of limitations are the inability to simulate the natural microenvironment of cells, three-dimensional (3D) cell-cell and cell-matrix interactions in tissue or tumor mass, tumor heterogeneity and 3D aspects of the tissues and tumors, including oxygen and nutrient gradients (9); therefore, fabrication of various kinds of tissue- or tumor-like 3D structures has been developed and introduced in recent years. The fabrication of fibrin gels using the plasma fraction of bone marrow (BM) aspirate is an important example of the development

Received: 02/October/2022, Revised: 30/January/2023, Accepted: 14/February/2023
 # These authors equally contributed to this work.
***Corresponding Address: P.O.Box: 14115-111, Applied Cell Sciences Division, Department of Hematology, Faculty of Medical Sciences, Tarbiat Modares University, Tehran, Iran**
Email: s_vahdat@modares.ac.ir

Royan Institute
Cell Journal (Yakhteh)

of 3D structures for BM tissue (1, 10). Fibrin gels as natural substrates would be safe and suitable matrices for a wide range of cell-based applications (11), with less inflammatory response induction and acceptable cell adhesion capacity, suitable for cell differentiation, and similar to the natural extracellular matrix of some types of cells in the human body (12).

One approach for the generation of fibrin gels is the use of commercial fibrin samples and a mixture of fibrinogen and thrombin, which is expensive and carries the risk of viral transmission (13). As another approach, patients' BM sample-derived plasma can be used, which appropriately could recapitulate the BM microenvironment. However, as BM aspiration for plasma derivation is a time-consuming, complicated invasive procedure, and it is not available for all research, the development of fibrin gels using an alternative to patient-derived BM plasma samples can advance this field.

In this study, it was tried to produce fibrin gels from the peripheral blood plasma samples as an alternative to BM plasma-derived gels in order to generate simple and available patient sample-independent 3D culture conditions for the U266 cell line. Moreover, the effect of plasma freezing on the generation and stability of gels was evaluated.

Materials and Methods

Study design

In this experimental study, fibrin gels derived from fresh or frozen peripheral blood plasma samples were generated in the presence of calcium chloride and tranexamic acid for the culture of U266 cells in 3D structures (Fig.1). To this end, different concentrations of calcium chloride and tranexamic acid were added to plasma samples to find the optimum concentrations for further experiments. Plasma samples in the absence of calcium chloride and tranexamic acid were used as control groups for gel formation and stability experiments, respectively. Moreover, in order to assess the proliferation rate and viability of cultured cells in the generated structures, U266 cells without gels were considered the control groups. All experiments were performed using at least three independent replicates.

Plasma derivation from peripheral blood

Plasma samples were derived from the peripheral blood of three volunteer individuals who were negative for viral contamination [human immunodeficiency virus (HIV) and hepatitis B virus (HBV)]. Each donor provided two milliliters of blood in EDTA anticoagulant. The blood plasma fraction was separated by centrifugation at 1500 rpm for 10 minutes at 22°C. In order to remove the donor-specific factors affecting the generation of gels, the separated plasma samples were pooled. A fraction of plasma was frozen at -20°C to evaluate the effect of plasma freezing on gel generation and stability.

Generation of fibrin gels

Fibrin gels were fabricated using 40 µl of freshly isolated or frozen plasma samples, calcium chloride (Cat. No.: C7902, Sigma-Aldrich, Darmstadt, Germany) (to induce gelation), and tranexamic acid (14) (Caspian Tamin Pharma.Co., Rasht, Iran) (which generates more stable fibrin gels), in a total volume of 100 µl in RPMI-1640 medium (Cat. No.: 035-51800, Gibco, USA) (1). Different concentrations of calcium chloride (1-5 mg/ml) were used to find the optimum concentration for gelation. Gel formation was examined at subsequent 15-minute intervals for two hours at 37°C. Microtubes were inverted and tapped for assessment of gelation.

Moreover, in order to increase the stability of fibrin gels, different concentrations of tranexamic acid (1-6 mg/ml) were used to determine the optimum concentration with the least amount of gel degradation over seven days. For this purpose, the percentage of weight changes of fibrin gels over seven days was considered a measure of their stability (1). Gels were placed at 37°C and 50 µl of RPMI-1640 medium was added on top of the gels to prevent them from drying.

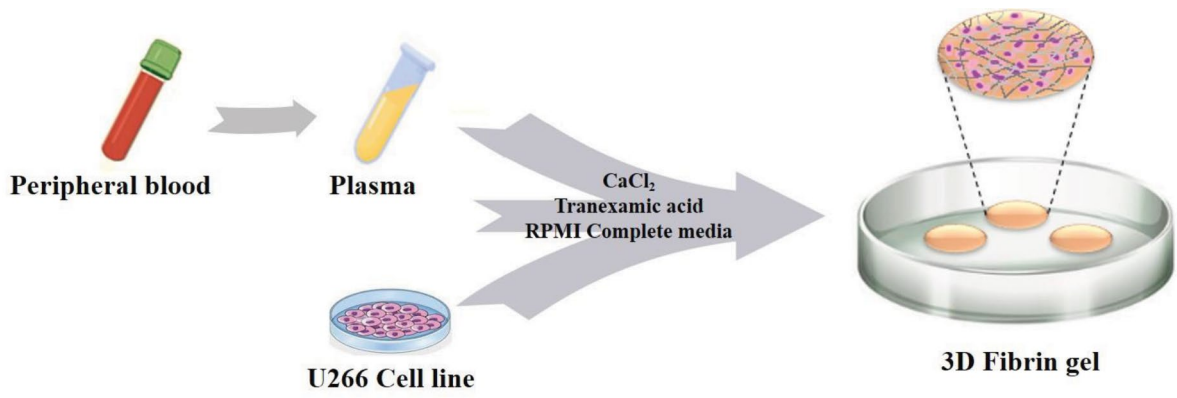

Fig.1: The schematic of our study design. A simple and cost-beneficial 3D culture condition was developed using peripheral blood-derived plasma, 1 mg/ml calcium chloride and 5 mg/ml tranexamic acid for the culture of U266 multiple myeloma cells in order to recapitulate a condition closer to the disease microenvironment.

Gel-free culture of U266 cells

The U266 MM cell line was provided from the Iranian National Center for Genetic and Biologic Resources. Cells were cultured in the complete culture medium, including RPMI-1640 medium supplemented by 1% l-glutamine, 10% fetal bovine serum (FBS, Cat. No.: BI-1201, Bioidea, Tehran, Iran) and 1% penicillin/streptomycin (Cat. No.: BI-1203, Bioidea, Tehran, Iran) at 37°C, 5% CO_2 and 95% humidity (15).

Flow cytometry

Flow cytometry was used to assess the expression of CD138 surface marker on U266 cells. Three days post-culture, U266 cells were centrifuged to remove culture medium and washed with PBS. Thereafter, 10^5 cells were incubated with CD138 antibody (Cat. No.: IQP-153F, IQ Products, Netherlands) at 4°C for 30 minutes. After two washes, CD138 expression was analyzed using flow cytometer system (BD FACSCanto II, BD Biosciences, USA). Data analysis was performed with Flowing Software 2.5.1.

MTT assay

In order to find the appropriate cell seeding count, MTT assay was performed. For this purpose, we cultured different cell seeding counts of U266 cells (10^4, 2×10^4, 3×10^4, 4×10^4, 8×10^4, 1.6×10^5) in 2D condition (without gel). One, two and three days post-culture, tetrazolium salt solution (Cat. No.: 88417, Sigma-Aldrich, Darmstadt, Germany) was added to each well of a 96-well plate and was incubated at 37°C for 3 hours. Then, the plate was centrifuged at 400 g for 5 minutes. The supernatant was removed and replaced with a dimethyl sulfoxide (DMSO) solution to solubilize the sediment. The absorbance of the solution is then quantified with an ELISA reader (Labsystems Multiskan MS, Artisan Technology Group) at 570 nm.

Culture of U266 cells within the 3D fibrin gels

In order to culture U266 cells in fibrin gels, suspended cells in complete culture media were mixed with plasma, and thereafter, calcium chloride and tranexamic acid were added to initiate gelation. Using complete culture medium, the total volume was increased to achieve the density of 3×10^4 cells per 100 µl. Then, each 100 µl of cell/gel mixture was placed in non-adherent culture plates in the form of droplet-like structures (16) and transferred to an incubator at 37°C. The complete culture medium was added to the generated droplet-like structures after gelation.

Enzymatic digestion of fibrin gels

After three days, the cultured U266 cells were isolated from fibrin gels by incubating and digesting the gels with different concentrations of collagenase type I (1, 5 and 10 mg/ml) (Cat. No.: 17100-017, Gibco, USA). For this regard, the generated droplet-like cell/gel structures were washed and digested with collagenase type I enzyme at 37°C. The enzyme was diluted after the complete digestion of gels using culture medium and removed by centrifugation at 1500 rpm for 5 minutes.

Cell viability assessment

Trypan blue staining (Cat. No.: BI-1803, Bioidea, Tehran, Iran) was used to evaluate cell proliferation and viability. For this purpose, 10 µl of the cell suspension and 10 µl of 0.4% trypan blue were mixed, and thereafter, 10 µl of the mixture was loaded on a Neubauer hemocytometer slide for examination. Cell viability was calculated as the ratio of live cells without color to all cells. Moreover, the cell expansion fold in fibrin gel was measured as the ratio of the cell count at day three of culture to the seeding cell count (17).

Histological assessment

In order to evaluate cell distribution inside the gels, fibrin gels containing U266 cells three days post-culture were fixed in 1% formaldehyde (Cat. No.: HT501128, Sigma-Aldrich, Darmstadt, Germany) for 24 hours at 4°C. Then, each of the created fibrin gels was placed in a 2% agarose solution to facilitate the cutting and embedding process. A microtome was used to section paraffin-embedded samples (5-µm thick). Finally, the sections were stained by hematoxylin and eosin (H&E) (18).

Statistical analysis

The experiments were carried out with at least three independent replications. Statistical analysis was performed by the t test method between two groups and by the ANOVA (Tukey post hoc) method between at least three groups. SPSS software (version 26, IBM, United States) was used for statistical analysis. The significance of differences between groups was assessed using the $P \leq 0.05$ significance level. In the graphs, the data is presented as mean ± standard deviation.

Ethical considerations

The procedure performed in this study was approved by the Ethics Committee of Tarbiat Modares University (IR.MODARES.REC.1399.229).

Results

Fibrin gels were generated using peripheral blood-derived plasma

To develop a 3D structure suitable for culture of the U266 cell line, fibrin gels were formed using peripheral blood plasma (Fig.1). As presented in Figure S1 (See Supplementary Online Information at www.celljournal.org), among different groups with different calcium chloride concentrations (1-5 mg/ml), gelation was observed in plasma samples incubated with 1 mg/ml and 2 mg/ml calcium chloride; however, other calcium chloride concentrations (3, 4 and 5 mg/ml) could not induce gel formation even after two hours of incubation. Therefore, concentrations of 1 mg/ml and 2 mg/ml calcium chloride were used for further experiments.

Tranexamic acid increased gel stability

To determine the optimal tranexamic acid concentration with minimum gel degradation in seven days, the

percentage of weight changes was calculated in the presence of 1 mg/ml (Fig.2A, B) or 2 mg/ml (Fig.2C, D) calcium chloride as well as different concentrations of tranexamic acid (1-6 mg/ml). As shown in Figure 2B, although degradation was observed in all generated fibrin gels containing 1 mg/ml calcium chloride over seven days, the overall degradation rate was lower in tranexamic acid-treated gels compared to gels without tranexamic acid (TX0). Moreover, gel degradations in 2-6 mg/ml tranexamic acid-treated groups were significantly less than those in the TX0 group, one day after gel formation (the P values of the differences of the TX2, TX3, TX4, TX5 and TX6 groups compared to the TX0 group were 0.02, 0.02, 0.00, 0.01 and 0.01, respectively). Additionally, degradation rates in groups with 2, 4, 5 and 6 mg/ml tranexamic acid were significantly less than in the TX1 (treated with 1 mg/ml tranexamic acid) group five days after gel formation (the P values of the differences of the TX2, TX4, TX5 and TX6 groups compared to the TX1 group were 0.03, 0.03, 0.01 and 0.02, respectively). However, as shown in Figure 2D, the degradation rates of gels generated with 2 mg/ml calcium chloride were not significantly affected and decreased in the presence of different concentrations of tranexamic acid when compared to the TX0 control group over a seven-day period.

Plasma freezing did not affect the gel stability

To evaluate the effect of plasma freezing on gel formation and stability, thawed plasma samples were used for fibrin gel formation using 1 mg/ml (Fig.3A, B) or 2 mg/ml (Fig.3C, D) calcium chloride and different concentrations of tranexamic acid (1-6 mg/ml). Two hours after mixing the mentioned items, fibrin gels were formed in all samples, showing no impact of plasma freezing on gel formation (data not shown). Thereafter, the weight changes were measured for all gels during the following seven days. As presented in Figure 3, similarly as when using fresh plasma, degradations were observed in frozen plasma-derived gels during subsequent days, and the degradation rates were decreased by utilizing tranexamic acid. Moreover, the degradation rates of gels formed by 1 mg/ml calcium chloride and 1-6 mg/ml tranexamic acid during the first three days were significantly less than those of the TX0 control group (Fig.3B) (the P values of the differences of the TX1, TX2, TX3, TX4, TX5 and TX6 groups compared to the TX0 group at day 1 were 0.01, 0.00, 0.00, 0.00, 0.00 and 0.00, respectively, at day 2 were 0.02, 0.02, 0.01, 0.00, 0.01 and 0.01, respectively and at day 3 were 0.02, 0.02, 0.00, 0.02, 0.00 and 0.01, respectively). Additionally, the degradation rates of gels formed by 3, 5 and 6 mg/ml tranexamic acid at day five were significantly less than those of the TX0 control group (Fig.3B) (the P values of the differences of the TX3, TX5 and TX6 groups compared to the TX0 group at day 5 were 0.03, 0.02 and 0.03, respectively). However, similarly as observed in fresh plasma-derived gels, the degradation rates of gels formed by 2 mg/ml calcium chloride and different concentrations of tranexamic acid were not significantly affected compared to the TX0 control group (Fig.3D).

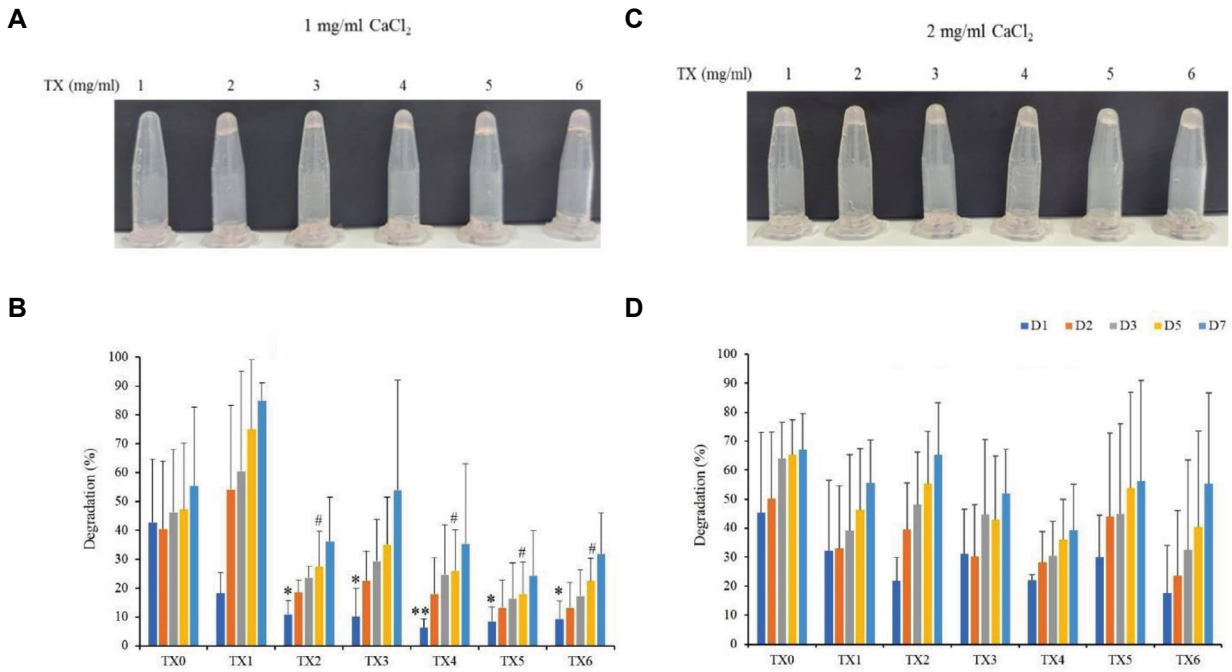

Fig.2: The effect of different concentrations of tranexamic acid on the stability of fibrin gels formed by fresh plasma and 1 or 2 mg/ml calcium chloride. **A.** Fibrin gels formed by 1 mg/ml calcium chloride and different concentrations of tranexamic acid at day five. **B.** The percentages of weight changes as a measure of gel degradation in the formed gels using different concentrations of tranexamic acid and 1 mg/ml calcium chloride during seven subsequent days. **C.** Fibrin gels formed by 2 mg/ml calcium chloride and different concentrations of tranexamic acid at day five. **D.** The percentages of weight changes as a measure of gel degradation in the formed gels using different concentrations of tranexamic acid and 2 mg/ml calcium chloride during seven subsequent days. The mean ± standard deviation is used to present all data. The statistically significant differences compared to the group without tranexamic acid (TX0) at day one and compared to the group with 1 mg/ml tranexamic acid (TX1) at day five are displayed with * and #, respectively. *, #; P<0.05 and **; P<0.01. The exact numbers of P values are presented in the text. Statistical analysis was performed by ANOVA (Tukey post hoc) method with three experimental replicates. TX stands for tranexamic acid, and D stands for day. Numbers displayed alongside TX indicate different concentrations (mg/ml) of tranexamic acid.

According to the obtained results, 1 mg/ml calcium chloride was selected as the optimum concentration for further steps. Furthermore, based on the data shown in Figure 3, the degradations of the gels formed in the presence of 3, 5 and 6 mg/ml tranexamic acid were significantly less than those of the TX0 group during five days, and the variation of gel degradation at day seven was smaller in the gels formed in the presence of 5 mg/ml tranexamic acid compared to the other groups, although the differences were not statistically significant. Therefore, the 5 mg/ml tranexamic acid concentration was selected for the next experiments. Moreover, as shown in Figure 4, the degradation percentages of gels formed by frozen plasma samples in the presence of 1 mg/ml calcium chloride and 5 mg/ml tranexamic acid were not statistically different from those of gels formed using fresh plasma samples, 1 mg/ml calcium chloride and 5 mg/ml tranexamic acid.

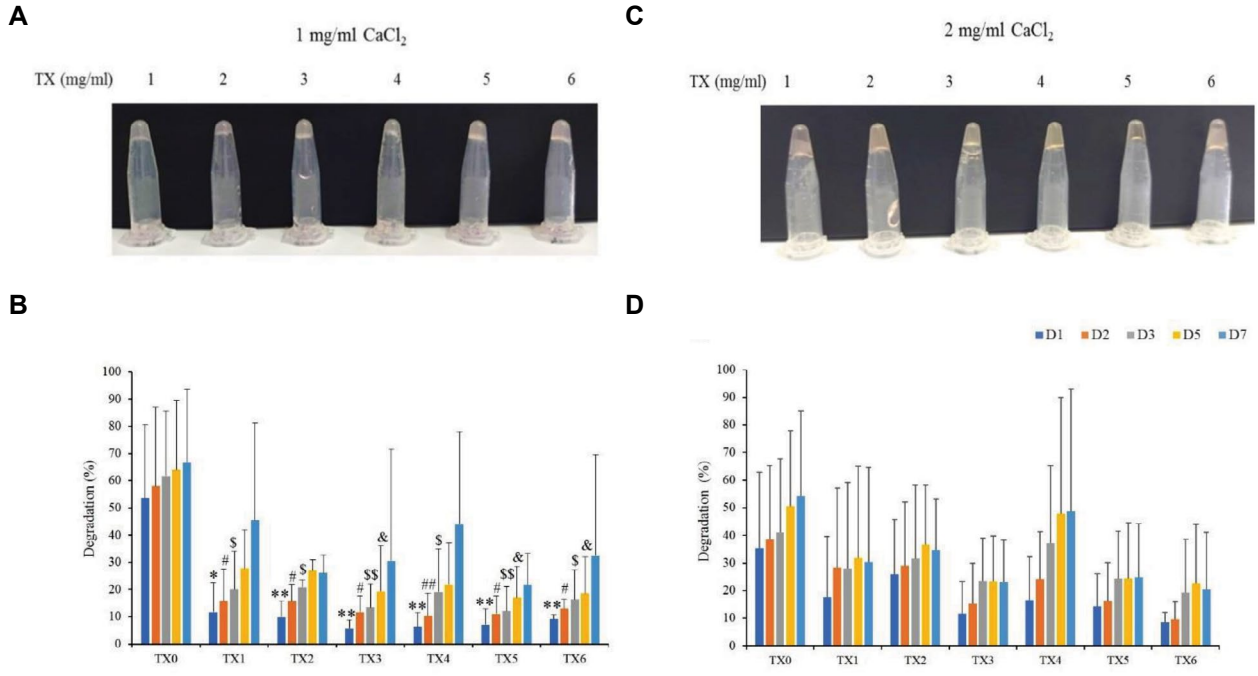

Fig.3: The effect of different concentrations of tranexamic acid on the stability of fibrin gels formed by frozen plasma and 1 or 2 mg/ml calcium chloride. **A.** Fibrin gels formed by 1 mg/ml calcium chloride and different concentrations of tranexamic acid at day five. **B.** The percentages of weight changes as a measure of gel degradation in the formed gels using different concentrations of tranexamic acid and 1 mg/ml calcium chloride during seven subsequent days. **C.** Fibrin gels formed by 2 mg/ml calcium chloride and different concentrations of tranexamic acid at day five. **D.** The percentages of weight changes as a measure of gel degradation in the formed gels using different concentrations of tranexamic acid and 2 mg/ml calcium chloride during seven subsequent days. The mean ± standard deviation is used to present all data. The statistically significant differences between groups with different concentrations of tranexamic acid compared to the gels without tranexamic acid (TX0) at days one, two, three and five are displayed with *, #, $ and &, respectively. *, #, $, &; P<0.05 and **, ##, $$; P<0.01. The exact numbers of P values are presented in the text. Statistical analysis was performed by ANOVA (Tukey post hoc) method with three experimental replicates. TX stands for tranexamic acid, and D stands for day. Numbers displayed alongside TX indicate different concentrations (mg/ml) of tranexamic acid.

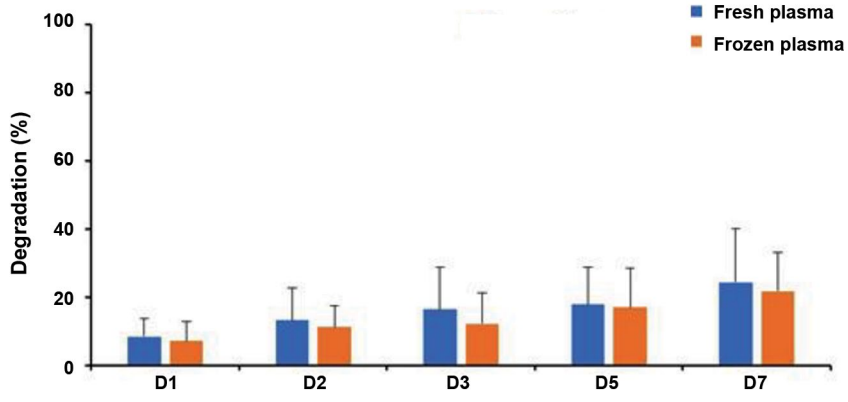

Fig.4: The degradation rates for the gels formed with fresh or frozen plasma samples in the presence of 1 mg/ml calcium chloride and 5 mg/ml tranexamic acid over the course of seven days. The data is presented in the form of mean ± standard deviation. Statistical analysis was performed by ANOVA (Tukey post hoc) method with three experimental replicates. D stands for day.

The fibrin gel-based 3D culture condition could support the culture of U266 cells

In order to evaluate the feasibility of using fibrin gels formed by peripheral blood-derived plasma samples as 3D culture structures, U266 MM cells were used. The morphology of U266 cells in the gel-free culture condition is presented in Figure 5A. As shown in Figure 5B, U266 cells were positive for the CD138 myeloma marker. When 3×10^4 U266 cells were cultured in 100 µl of complete culture media, the cell expansion fold was significantly higher than when other cell seeding densities were cultured, which was evaluated by MTT assay in gel-free cultures of U266 cells three days post-culture (Fig.5C) (the P values of differences of 3×10^4 seeding density compared to 10^4 seeding density at days 1 and 2 were 0.01 and 0.03, respectively, compared to 2×10^4 seeding density at day 1 was 0.00 and compared to 1.6×10^5 seeding density at day 3 was 0.01; however, the P values of differences of 4×10^4 seeding density compared to 10^4 and 2×10^4 seeding densities at day 1 were 0.00 and 0.00, respectively, and compared to 1.6×10^5 seeding density at day 3 was 0.01). As a result, 3×10^4 cells/100 µl was selected as the optimal cell seeding density for 3D culture of U266 within the gels (Fig.6A). Thereafter, different concentrations of collagenase type I (1 mg/ml, 5 mg/ml and 10 mg/ml) were used to isolate cultured U266 cells from the gels three days post-culture. Accordingly, although different concentrations of collagenase type I did not significantly affect the cell viabilities, the viability of isolated cells was higher after treatment with 5 mg/ml collagenase (Fig.S2, See Supplementary Online Information at www.celljournal.org) and this concentration was selected for further steps.

To evaluate the expansion fold of cultured U266 cells in fibrin gels, isolated cells from the gels were counted three days after culture. As presented in Figure 6B, the U266 expansion fold after three days of culture in fibrin gels was similar to the cultured cells in the 2D gel-free condition, and the differences in expansion folds between these two types of cell culture conditions were not statistically significant. Moreover, U266 cells were distributed through the gels, which was assessed using phase contrast imaging (Fig.6C) as well as H&E staining of sectioned paraffin-embedded gels (Fig.6D).

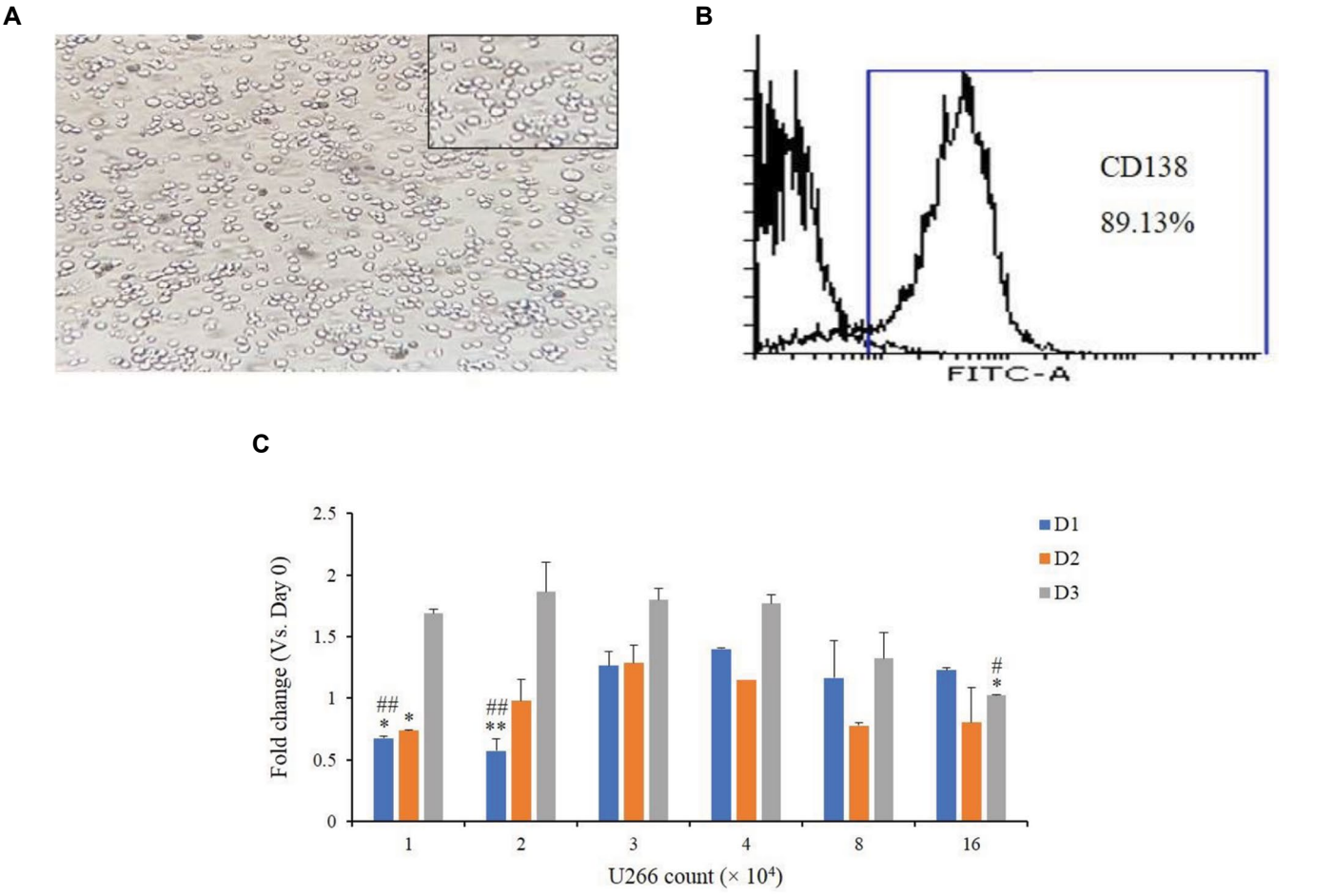

Fig.5: Gel-free culture of U266 cells. **A.** The morphology of U266 cells at day three of culture (×20). **B.** Flow cytometry analysis of CD138 marker expression on U266 cells. **C.** The effect of different seeding densities on the U266 cell fold after three days of culture versus day zero. The data is presented in the form of mean ± standard deviation. The statistically significant groups compared to the 3×10^4 and to 4×10^4 seeding density groups are presented by * and #, respectively, at the same corresponding days post-culture. *, #; P<0.05 and **, ##; P<0.01. The exact numbers of P values are presented in the text. Statistical analysis was performed by ANOVA (Tukey post hoc) method with three experimental replicates. D stands for day.

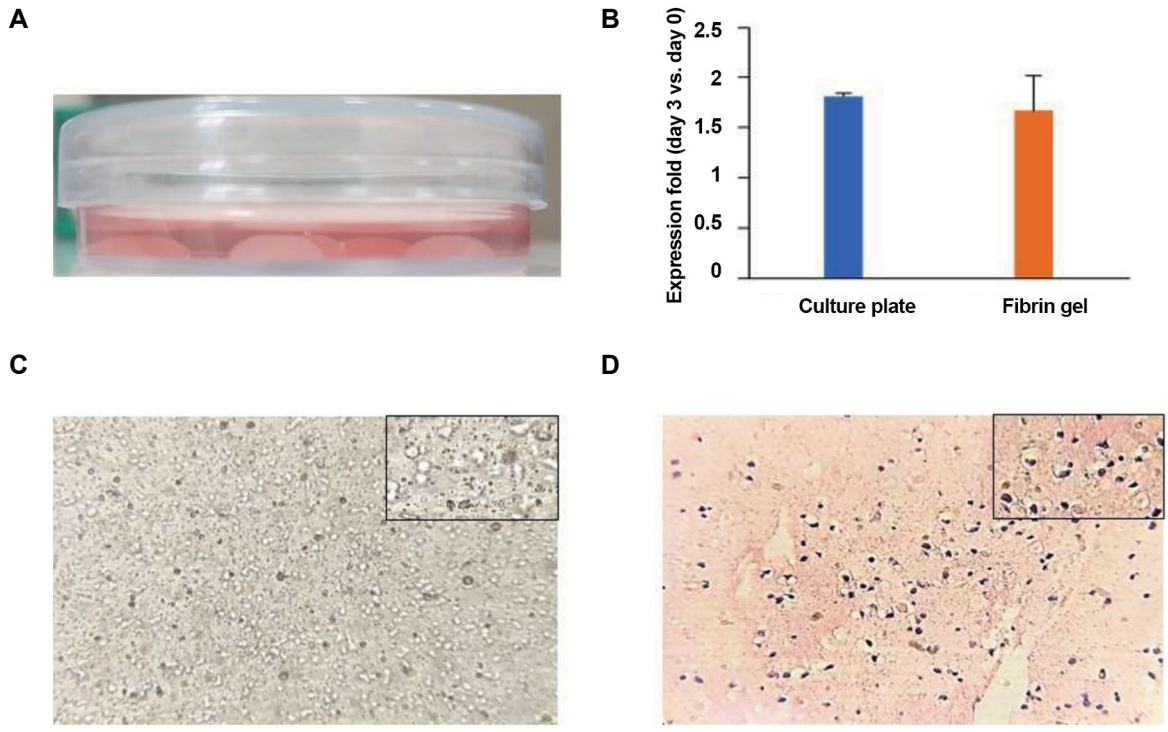

Fig.6: Culture of U266 cells within the fibrin gels. **A.** The droplets generated by the mixture of U266 cells and fibrin gel components, after gelation. **B.** Expansion fold of U266 cells at day three post-culture compared to day zero in two different culture conditions: in culture plates and in fibrin gels. Statistical analysis was performed by the t test method with three experimental replicates. **C.** Phase-contrast image of U266 cells in fibrin gels (×20). **D.** Distribution of U266 cells in fibrin gels using H&E staining (×20).

Discussion

In this study, it was tried to generate a simple, available, cost-beneficial and reproducible 3D structure for the culture of the MM cell line in order to have culture conditions more similar to the 3D BM microenvironment for further applications. In this regard, fibrin gels were generated as native substrates for the culture of the U266 cell line. Fibrin gels are widely used as cell injection substrates, cell culture plate coatings, and tissue-engineered structures (19, 20). In comparison with synthetic polymers, fibrin gel had widespread advantages such as a controllable degradation rate, non-toxic degradation products, and excellent biocompatibility. In addition, the morphology, mechanical properties, and stability of fibrin gels can be regulated by controlling precursor materials and ionic strength (21). Moreover, fibrin gels have shown high cell culture efficiency and enhanced adhesion properties (22). The fibrin-based 3D generated structures have been introduced and applied for disease modeling of various types of diseases, including MM (10, 23, 24).

Most fibrin gel-based structures for MM disease modeling have been generated using BM-derived plasma samples (1, 10, 25). However, this type of structure may be affected by patient-specific variables and is not accessible to all researchers. Therefore, we aimed to use peripheral blood plasma samples as alternatives for BM blood plasma samples. It has been shown that there is no significant difference between fibrinogen levels in fibrin clots derived from peripheral blood and BM (26). Several studies used peripheral blood plasma to generate 3D structures in order to model various diseases (1, 23, 24). On the other hand, it is possible that in the process of plasma derivation, platelets remained in the plasma fraction and affected the gel properties as well as the growth and fate of the cultured cells. It has been shown that platelets contain abundant growth factors, including platelet-derived growth factor (PDGF), transforming growth factor (TGF)-b1, insulin-like growth factor (IGF)-1, and bone morphogenetic protein (BMP)-2, and entrapped platelets can progressively release these cytokines during fibrin matrix remodeling (27). Moreover, integrin αIIbβ3 is expressed abundantly, with an estimated 80,000 copies per platelet. The integrin binds fibrinogen and other plasma proteins. Thrombin promotes the signaling processes by increasing platelets Ca^{2+} levels, activating integrins α2β1 and αIIbβ3, and exposure of phosphatidylserine. Extensive fibrin formation can also be observed on coated platelets and relies on transglutaminase (FXIII) activity and αIIbβ3 binding. It should be noted that platelets from MM patients are activated with disease progression, and MM cell lines activate platelets. Moreover, the results of xenograft MM models have shown that platelets contribute to the tumor cell engraftment of MM cell lines *in vivo* (28, 29).

In the first step, the effects of different factors, including calcium chloride concentration, tranexamic

acid concentration, and long-term plasma preservation, on gel formation and stability were evaluated. It was revealed that 1 mg/ml calcium chloride was the optimum concentration for gelation of fresh and thawed frozen plasma samples. Similarly, de la Puente et al. evaluated the effect of different concentrations (0-4 mg/ml) of calcium chloride on fibrin gel formation. They showed that 1 mg/ml calcium chloride was the best concentration with the least gelation time (1). On the other hand, we showed that different concentrations of tranexamic acid were able to stabilize fresh and frozen plasma-derived gels for seven days. However, minimum variations in gel degradation rates during seven days were seen when 5 mg/ml of tranexamic acid was used, especially in the case of frozen plasma samples (although the differences were not statistically significant at day seven). Consistently, several studies have evaluated the impact of different concentrations of tranexamic acid on the stability of fibrin gels. They showed that 4 mg/ml of tranexamic acid had the least gel degradation rate (1, 13, 30). The observed differences between optimal tranexamic acid concentrations may be attributed to batch variations and the purity of products.

In practice, the availability and reproducibility of fresh plasma samples are two challenging issues that may be overcome by the development of plasma banks (31). This required the evaluation of the impact of long-term plasma cryopreservation on gel formation and stability. It was revealed that plasma cryopreservation did not statistically affect the gelation procedure and gel degradation during the seven days. Similarly, it has been reported that freezing has little effect on fibrinogen levels (32). Moreover, the level of fibrinogen remains stable in twice-thawed and refrozen fresh frozen plasma (33). In order to more precisely evaluate the effect of plasma cryopreservation on gel properties, assessment of the concentration of plasma components such as coagulation factors before and after freezing is recommended to be considered in future studies.

In order to assess the impact of cell culture in 3D fibrin gels on the viability and proliferation of MM cells, the U266 cell line was selected. In the first step, the density of 3×10^4 cells per 100 µl was selected to be cultured in both 2D and 3D culture conditions (gel-free and inside the fibrin gel, respectively). The selected cell seeding density was in line with another study that has used this cell density for the culture of other MM cell lines in fibrin gels (1). U266 cells counted three days after culture in fibrin gels showed an expansion fold similar to cells cultured in 2D gel-free condition, indicating that the generated gel might have no toxic effects on the viability and proliferation of U266 cells. Similarly, other studies using calcium chloride and tranexamic acid for gel formation did not report any toxic effects of these two compounds on cultured cells (1, 10, 24, 25). For instance, the impact of tranexamic acid on the viability of myeloma cell lines was tested by MTT assay, and no toxic effect on cell viability was found at any of the tested concentrations (1-10 mg/ml) (1). However, a more precisely assessment of the probable toxic effects of these two compounds on U266 cells necessitates additional testing to detect any mutations and specific cell damage. On the other hand, it has been reported that after eight days of culture, the viability of conjunctiva mesenchymal stem cells-derived photoreceptor cells cultured in fibrin gel, which was composed of fibrinogen and thrombin, was enhanced compared to the cells cultured in tissue culture plates (34). Moreover, another study showed that after three days of culture, the viability of induced pluripotent stem cells cultured in fibrin gel was similar to cells cultured in tissue culture plates (35). Furthermore, the proliferation rates of U266 cells in both 2D and 3D culture conditions were similar to the reported proliferation rates of the RPMI8226 MM cell line (36).

It should be noted that more evaluations, such as apoptosis and necrosis assessments of cultured cells using flow cytometry, are required to highlight the suitability of fibrin gels for the survival and proliferation of cultured U266 cells. Moreover, our used enzymatic digestion protocol might affect the viability and the calculated expansion fold of cells cultured in fibrin gels; therefore, histological assessments of cells in 3D structures would overcome the negative effects of enzymatic digestion protocols on cells and be recommended for future studies. H&E staining exhibited the distribution of cultured U266 cells in the gel, which may increase their 3D interactions. The observed pattern of U266 cell distribution in the gel was similarly reported by other studies culturing different types of cells (13, 30, 36), which may highlight the importance of 3D culture of MM cells for the development of more physiologically relevant *in vitro* disease models (37, 38).

Conclusion

We have developed a 3D culture condition based on fibrin gels derived from peripheral blood plasma samples for the culture of the U266 MM cell line. The gels could be generated from cryopreserved plasma samples, which makes them accessible and suitable for a wide range of applications. U266 MM cells cultured in peripheral blood plasma-derived gels maintained their proliferation rate and were distributed throughout the gel. This culture system may be an appropriate substitute for BM-derived fibrin gels for 3D culture of MM cells to study the disease and drug effectiveness.

Acknowledgments

The authors would like to express their appreciation to the peripheral blood donors. This work was supported by a grant from Tarbiat Modares University and a grant from the Iran National Science Foundation (INSF) to Sadaf Vahdat with grant number 99024778. The authors have no conflict of interest.

Authors' Contributions

Ma.J., M.K., Me.J.; Contributed equally to Methodology, Formal analysis, Visualization and Writing original draft.

S.A.; Conceptualization and Study consultation, Review and Editing the manuscript. S.V.; Conceptualization and Study supervision, and Writing, Review and Editing the manuscript. All authors read and approved the final version of manuscript.

References

1. de la Puente P, Muz B, Gilson RC, Azab F, Luderer M, King J, et al. 3D tissue-engineered bone marrow as a novel model to study pathophysiology and drug resistance in multiple myeloma. Biomaterials. 2015; 73: 70-84.
2. Ignatz-Hoover JJ, Driscoll JJ. Therapeutics to harness the immune microenvironment in multiple myeloma. Cancer Drug Resistance. 2022; 5(3): 647-661.
3. Kirshner J, Thulien KJ, Martin LD, Debes Marun C, Reiman T, Belch AR, et al. A unique three-dimensional model for evaluating the impact of therapy on multiple myeloma. Blood. 2008; 112(7): 2935-2945.
4. Arhoma A, Chantry AD, Haywood-Small SL, Cross NA. SAHA-induced TRAIL-sensitisation of Multiple Myeloma cells is enhanced in 3D cell culture. Exp Cell Res. 2017; 360(2): 226-235.
5. Libouban H. The use of animal models in multiple myeloma. Morphologie. 2015; 99(325): 63-72.
6. Sarin V, Yu K, Ferguson ID, Gugliemini O, Nix MA, Hann B, et al. Evaluating the efficacy of multiple myeloma cell lines as models for patient tumors via transcriptomic correlation analysis. Leukemia. 2020; 34(10): 2754-2765.
7. Harmer D, Falank C, Reagan MR. Interleukin-6 interweaves the bone marrow microenvironment, bone loss, and multiple myeloma. Front Endocrinol (Lausanne). 2019; 9: 788.
8. Li FJ, Tsuyama N, Ishikawa H, Obata M, Abroun S, Liu S, et al. A rapid translocation of CD45RO but not CD45RA to lipid rafts in IL-6-induced proliferation in myeloma. Blood. 2005; 105(8): 3295-3302.
9. Kapałczyńska M, Kolenda T, Przybyła W, Zajączkowska M, Teresiak A, Filas V, et al. 2D and 3D cell cultures - a comparison of different types of cancer cell cultures. Arch Med Sci. 2018; 14(4): 910-919.
10. Sun J, Muz B, Alhallak K, Markovic M, Gurley S, Wang Z, et al. Targeting CD47 as a novel immunotherapy for multiple myeloma. Cancers (Basel). 2020; 12(2): 305.
11. Siedentop KH, Park JJ, Shah AN, Bhattacharyya TK, O'Grady KM. Safety and efficacy of currently available fibrin tissue adhesives. Am J Otolaryngol. 2001; 22(4): 230-235.
12. de la Puente P, Ludeña D. Cell culture in autologous fibrin scaffolds for applications in tissue engineering. Exp Cell Res. 2014; 322(1): 1-11.
13. de la Puente P, Ludeña D, Fernández A, Aranda JL, Varela G, Iglesias J. Autologous fibrin scaffolds cultured dermal fibroblasts and enriched with encapsulated bFGF for tissue engineering. J Biomed Mater Res A. 2011; 99(4) :648-654.
14. Cholewinski E, Dietrich M, Flanagan TC, Schmitz-Rode T, Jockenhoevel S. Tranexamic acid--an alternative to aprotinin in fibrin-based cardiovascular tissue engineering. Tissue Eng Part A. 2009; 15(11): 3645-3653.
15. Saba F, Soleimani M, Abroun S. New role of hypoxia in pathophysiology of multiple myeloma through miR-210. EXCLI J. 2018; 17: 647-662.
16. Saheli M, Sepantafar M, Pournasr B, Farzaneh Z, Vosough M, Piryaei A, et al. Three-dimensional liver-derived extracellular matrix hydrogel promotes liver organoids function. J Cell Biochem. 2018; 119(6): 4320-4333.
17. Vahdat S, Pahlavan S, Aghdami N, Bakhshandeh B, Baharvand H. Establishment of A protocol for in vitro culture of cardiogenic mesodermal cells derived from human embryonic stem cells. Cell J. 2019; 20(4): 496-504.
18. Vahdat S, Mousavi SA, Omrani G, Gholampour M, Sotoodehnejadnematalahi F, Ghazizadeh Z, et al. Cellular and molecular characterization of human cardiac stem cells reveals key features essential for their function and safety. Stem Cells Dev. 2015; 24(12): 1390-1404.
19. Hinsenkamp A, Kun K, Gajnut F, Majer A, Lacza Z, Hornyák I. Cell attachment capacity and compounds of fibrin membranes isolated from fresh frozen plasma and cryoprecipitate. Membranes (Basel). 2021; 11(10): 783.
20. Pal A, Tripathi K, Pathak C, Vernon BL. Plasma-based fast-gelling biohybrid gels for biomedical applications. Sci Rep. 2019; 9(1): 10881.
21. Wolberg AS. Thrombin generation and fibrin clot structure. Blood Rev. 2007; 21(3): 131-142.
22. Swartz DD, Russell JA, Andreadis ST. Engineering of fibrin-based functional and implantable small-diameter blood vessels. Am J Physiol Heart Circ Physiol. 2005; 288(3): H1451-H1460.
23. Alhallak K, de la Puente P, Jeske A, Sun J, Muz B, Rettig MP, et al. 3D tissue engineered plasma cultures support leukemic proliferation and induces drug resistance. Leuk Lymphoma. 2021; 62(10): 2457-2465.
24. Calar K, Plesselova S, Bhattacharya S, Jorgensen M, de la Puente P. Human plasma-derived 3D cultures model breast cancer treatment responses and predict clinically effective drug treatment concentrations. Cancers (Basel). 2020; 12(7): 1722.
25. Alhallak K, Jeske A, de la Puente P, Sun J, Fiala M, Azab F, et al. A pilot study of 3D tissue-engineered bone marrow culture as a tool to predict patient response to therapy in multiple myeloma. Sci Rep. 2021; 11(1): 19343.
26. Shoji T, Nakasa T, Yoshizuka M, Yamasaki T, Yasunaga Y, Adachi N, et al. Comparison of fibrin clots derived from peripheral blood and bone marrow. Connect Tissue Res. 2017; 58(2): 208-214.
27. Chien CS, Ho HO, Liang YC, Ko PH, Sheu MT, Chen CH. Incorporation of exudates of human platelet-rich fibrin gel in biodegradable fibrin scaffolds for tissue engineering of cartilage. J Biomed Mater Res B Appl Biomater. 2012; 100(4): 948-955.
28. Takagi S, Tsukamoto S, Park J, Johnson KE, Kawano Y, Moschetta M, et al. Platelets enhance multiple myeloma progression via il-1β upregulation. Clin Cancer Res. 2018 15; 24(10): 2430-2439.
29. Yan M, Jurasz P. The role of platelets in the tumor microenvironment: From solid tumors to leukemia. Biochim Biophys Acta. 2016; 1863(3): 392-400.
30. de la Puente P, Ludeña D, López M, Ramos J, Iglesias J. Differentiation within autologous fibrin scaffolds of porcine dermal cells with the mesenchymal stem cell phenotype. Exp Cell Res. 2013; 319(3): 144-152.
31. Illert WE, Butsch H, Nuber D, Howe J, Sänger W,Weidinger S. Long-term storage of fresh frozen plasma at–40 C. A Multicenter study on the stability of labile coagulation factors over a period of 3 years. Infus Ther Transfus Med. 2001; 28: 189-194.
32. Alesci S, Borggrefe M, Dempfle CE. Effect of freezing method and storage at -20 degrees C and -70 degrees C on prothrombin time, aPTT and plasma fibrinogen levels. Thromb Res. 2009; 124(1): 121-126.
33. Philip J, Sarkar RS, Pathak A. The effect of repeated freezing and thawing on levels of vitamin K-dependent coagulation factors and fibrinogen in fresh frozen plasma. Asian J Transfus Sci. 2013; 7(1): 11-15.
34. Soleimannejad M, Ebrahimi-Barough S, Soleimani M, Nadri S, Tavangar SM, Roohipoor R, et al. Fibrin gel as a scaffold for photoreceptor cells differentiation from conjunctiva mesenchymal stem cells in retina tissue engineering. Artif Cells Nanomed Biotechnol. 2018; 46(4): 805-814.
35. Nazari B, Kazemi M, Kamyab A, Nazari B, Ebrahimi-Barough S, Hadjighassem M, et al. Fibrin hydrogel as a scaffold for differentiation of induced pluripotent stem cells into oligodendrocytes. J Biomed Mater Res B Appl Biomater. 2020; 108(1): 192-200.
36. Huang YH, Molavi O, Alshareef A, Haque M, Wang Q, Chu MP, et al. Constitutive activation of STAT3 in myeloma cells cultured in a three-dimensional, reconstructed bone marrow model. Cancers (Basel). 2018; 10(6): 206.
37. Belloni D, Heltai S, Ponzoni M, Villa A, Vergani B, Pecciarini L, et al. Modeling multiple myeloma-bone marrow interactions and response to drugs in a 3D surrogate microenvironment. Haematologica. 2018; 103(4): 707-716.
38. Calimeri T, Battista E, Conforti F, Neri P, Di Martino M, Rossi M, et al. A unique three-dimensional SCID-polymeric scaffold (SCID-synth-hu) model for in vivo expansion of human primary multiple myeloma cells. Leukemia. 2011; 25(4): 707-711.

Cell J
Cell Journal(Yakhteh)
Homepage: https://www.celljournal.org/
Original Article
Vol 25, No 4, April 2023, Pages: 238-246

Comparative Epigenetic Analysis of Imprinting Genes Involved in Fertility, in Cryopreserved Human Sperms with Rapid Freezing versus Vitrification Methods

Nahid Khosronezhad, M.Sc.[1], Vahideh Hassanzadeh. Ph.D.[1]*, Maryam Hezavehei, Ph.D.[2], Abdolhossein Shahverdi, Ph.D.[2], Maryam Shahhoseini, Ph.D.[1, 3, 4]*

1. Department of Cell and Molecular Biology, Faculty of Biology, College of Science, University of Tehran, Tehran, Iran
2. Department of Embryology, Reproductive Biomedicine Research Centre, Royan Institute for Reproductive Biomedicine, ACECR, Tehran, Iran
3. Department of Genetics, Reproductive Biomedicine Research Centre, Royan Institute for Reproductive Biomedicine, ACECR, Tehran, Iran
4. Department of Biochemistry, Faculty of Basic Sciences and Advanced Technologies in Biology, University of Science and Culture, Tehran, Iran

Abstract

Objective: Choosing the optimal method for human sperm cryopreservation seems necessary to reduce cryoinjury. The aim of this study is to compare two cryopreservation methods including rapid-freezing and vitrification, in terms of cellular parameters, epigenetic patterns and expression of paternally imprinted genes (*PAX8, PEG3* and *RTL1*) in human sperm which play a role in male fertility.

Materials and Methods: In this experimental study, semen samples were collected from 20 normozoospermic men. After washing the sperms, cellular parameters were investigated. DNA methylation and expression of genes were investigated using methylation-specific polymerase chain reaction (PCR) and real-time PCR methods, respectively.

Results: The results showed a significant decrease in sperm motility and viability, while a significant increase was observed in DNA fragmentation index of cryopreserved groups in comparison with the fresh group. Moreover, a significant reduction in sperm total motility (TM, P<0.01) and viability (P<0.01) was determined, whereas a significant increase was observed in DNA fragmentation index (P<0.05) of the vitrification group compared to the rapid-freezing group. Our results also showed a significant decrease in expression of *PAX8, PEG3* and *RTL1* genes in the cryopreserved groups compared to the fresh group. However, expression of PEG3 (P<0.01) and *RTL1* (P<0.05) genes were reduced in the vitrification compared to the rapid-freezing group. Moreover, a significant increase in the percentage of *PAX8, PEG3* and *RTL1* methylation was detected in the rapid-freezing group (P<0.01, P<0.0001 and P<0.001, respectively) and vitrification group (P<0.01, P<0.0001 and P<0.0001, respectively) compared to the fresh group. Additionally, percentage of *PEG3* and *RTL1* methylation in the vitrification group was significantly increased (P<0.05 and P<0.05, respectively) compared to the rapid-freezing group.

Conclusion: Our findings showed that rapid-freezing is more suitable method for maintaining sperm cell quality. In addition, due to the role of these genes in fertility, changes in their expression and epigenetic modification may affect fertility.

Keywords: Epigenetics, Male Fertility, Rapid-Freezing, Vitrification

Citation: **Khosronezhad N, Hassanzadeh V. Hezavehei M, Shahverdi AH, Shahhoseini M. Comparative epigenetic analysis of imprinting genes involved in fertility, in cryopreserved human sperms with rapid freezing versus vitrification methods. Cell J. 2023; 25(4): 238-246. doi: 10.22074/CELLJ.2023.1974291.1171.**

Introduction

Male infertility is a complex disease, resulted from interaction between genetic and environmental factors. Several male factors, such as spermatogenesis, sperm function, sperm immotile, sperm with abnormal morphology, sexual activity and endocrine system can affect male infertility. Although 30% of the caused infertility are related to male factors, about 10% of the male infertility are diagnosed with unexplained or idiopathic infertility (1). Genetic mutations in sperm and changes in epigenetic patterns are important factors in male infertility (2). Thus, assisted reproductive techniques (ART), including sperm cryopreservation, are useful to preserve male fertility and treat infertility in men (3). However, studies have shown that cellular and molecular changes occur during cryopreservation (4). Different methods, such as rapid-freezing (liquid nitrogen vapor cooling followed by plunging into liquid nitrogen)

Received: 24/November/2022, Revised: 01/January/2023, Accepted: 16/January/2023
***Corresponding Addresses: P.O.Box: 14155-6655, Department of Cell and Molecular Biology, Faculty of Biology, College of Science, University of Tehran, Tehran, Iran**
P.O.Box: 16635-148, Department of Genetics, Reproductive Biomedicine Research Centre, Royan Institute for Reproductive Biomedicine, ACECR, Tehran, Iran
Emails: vhassanzadeh@ut.ac.ir, m.shahhoseini@royan-rc.ac.ir

Royan Institute
Cell Journal (Yakhteh)

and vitrification (directly plunging into liquid nitrogen) have been suggested to perform sperm cryopreservation (5). Isachenko et al. (6) reported that vitrification was extremely fast and there was not enough time for formation of ice crystals. Extremely high rate of temperature reduction prevented formation of intracellular ice crystals, but more studies are needed to demonstrate efficiency of this method. Despite the research efforts undertaken to develop improved human semen cryopreservation methods, it is yet unknown whether one technique is advantageous over the other (3). So far, several studies have compared these methods based on the sperm quality parameters after thawing. In addition, previous studies on the sperm of various animals showed that some epigenetic patterns, including DNA methylation and expression of some sperm genes, were changed after cryopreservation (7-9). But, studies performed to determine changes in gene expression and epigenetic patterns during different cryopreservation methods are limited (10).

Many imprinted genes, such as *PAX8*, *PEG3* and *RTL1*, are involved in sperm function and fertility11-) 13). Since defective methylation of sperm DNA and changes in the epigenetic pattern can be the main reasons underlying decline in fertility potential of sperm after thawing (14), in this study we aimed to compare effect of two cryopreservation protocols, rapid-freezing and vitrification on cell viability, mobility, morphology, DNA fragmentation, DNA methylation status and expression of *PAX8*, *PEG3* and *RTL1* genes in human sperm.

Materials and Methods

Sample collection and preparation

Semen samples were collected from 20 healthy men (normozoospermia) with 20-35 years of age, who referred to Royan Infertility Clinic in Tehran, Iran. All patients were informed about the methods of study and agreed analysis of genetic material for research purposes, while informed written consent was obtained from all patients. This study was approved by the Ethics Committee of Royan Institute (IR.ACECR.ROYAN.REC.1400.147). The exclusion criteria for this study were presence of varicocele, cigarettes smoking, alcohol consumption and exposure to chemotherapy or radiation as well as specific diseases including diabetes. Semen samples were collected in sterile semen collection tubes after 3-4 days' abstinence. After liquefaction of the samples at 37°C for 30 minutes, a basic semen analysis was undertaken within one hour according to the 2010 World Health Organization (WHO) guidelines (15). The criteria for identification as normal quality sperm were consisted of morphology (≥4% normal), concentration ($\geq 15\times10^6$ sperm/ml), motility (≥40% motile), progressive motility (PM, ≥32%) and normal viscosity (15). Recently, in most fertility centers, semen preparation is performed by swim-up or DGC method to obtain high quality sperm. For this purpose, all investigations were carried out on spermatozoa, prepared by the density gradient centrifugation technique (DGC) (16). Semen was layered on 80% Allgrade (Life Global, USA) and 20% human tubal fluid. After centrifugation at 1800 rpm for 15 minutes, the supernatant was discarded and sperms were collected from the pellet. After DGC technique, the collected pellet was resuspended in the basic medium to achieve a concentration of 60×10^6 spermatozoa/ml and finally aliquoted into three equal sub-samples for three different groups (fresh as a control group, frozen groups including rapid-freezing and vitrification). After cryopreservation, normal cells, including viable, motile sperm cells, with normal morphology, were used for analyses.

Cryopreservation

Methods for cryopreservation were according to the previous studies (17, 18). In the frozen group by rapid-freezing method, SpermFreeze™ Solution (FertiPro N.V., Belgium; contains physiologic salts, glycine, glucose, lactate, 15% glycerol, sucrose and 4.0 g/l human serum albumin) was added in droplets to the washed sperm suspension at a ratio of 0.7:1 v/v. The samples were then kept at room temperature for 10 minutes. The mixture was transferred to a volume of 1.0 ml of cryotube (Nunc, Denmark). The cryotubes were suspended in a liquid nitrogen vapor phase (15 cm above the liquid nitrogen) for 15 minutes. Then, cryotubes were immersed into a liquid nitrogen tank for storage and they were stored for 1 week (18).

In vitrification method, SpermFreeze solution was added in droplets to the washed sperm suspensions at a ratio of 0.7:1 v/v and they were kept at room temperature for 10 minutes. They were subsequently loaded into a straw (IMV, France) and immersed directly into a liquid nitrogen tank and stored for one week (17).

The samples were thawed in a water bath at 37˚C for 5 minutes, furthermore, each sample was centrifuged at 3500 rpm for 5 minutes, the upper portion containing freezing medium was removed and 1ml of human tubal fluid medium (Sigma, USA) supplemented with 5% human serum albumin (Sigma, USA) were added to the sperm pellets and incubated at 37°C for 20 minutes before sperm quality parameter analysis (18).

Sperm motility analysis

Sperm motility parameters were measured using the Semen Class Analysis Software (SCA, version 5.1; Microptic, Spain) (19). A total of 5 µl of the sperm sample was placed on a pre-warmed chamber slide (37°C) under a microscope; they were analyzed for sperm motion characteristics including total motility (TM, %), progressive motility (PM, %), curvilinear velocity (VCL, µm/s), average path velocity (VAP, µm/s), amplitude of straightness (STR, %), velocity straight linear (VSL, µm/s) and linearity (LIN, %).

Morphology assessment

Papanicolaou staining was used for assessment of sperm morphology. Briefly, 20 µl of sperm suspension smear

was made on a glass slide and dried at room temperature. The samples were then fixed in methyl alcohol (70%) and immersed in hematoxylin solution for 3 minutes. They were next rinsed in water and immersed in alcohol (95%). Subsequently, they were immersed in OG-6 stain for 1.5 minutes, ethanol (95%) 10 dips and EA-50 stain for 2.5 minutes. After washing in water, they were immersed in alcohol (96%) for three times. Upon drying at room temperature, each slide was assessed under oil immersion light microscopy at 400x magnification, by counting at least 200 sperm. Mean percentage of normal morphology of spermatozoa was determined (20).

Sperm viability

To evaluate viability, an equal amount of eosin-negrosin stain and sperm suspension were poured into a 0.5 ml microtube and pipetted several times to mixed together. After 4 minutes, a smear was made using the drops of 5 µl solution on a warm slide and they were dried at room temperature. Sperm viability was assessed by counting 200 spermatozoa on each slide under oil immersion light microscopy at 400x magnification. The sperm cells that showed regional or complete purple staining were considered as nonviable and mean percentage of spermatozoa with membrane intactness (unstained) was defined as live spermatozoa (14).

DNA fragmentation

Sperm DNA fragmentation index was measured using the sperm DNA fragmentation assay kit (SDFA; ACECR, Iran) protocol. Thirty µl of the sperm suspension was dissolved in the melted agarose and one drop (50 µl) was placed on a slide. Then, the sample was immersed in HCl solution.

After washing with water and ethanol (70, 90 and 100%), the sample was immersed in lysing solution. A total of 200 spermatozoa per sample were evaluated under a light microscope (Olympus CX21; Olympus, USA) at a magnification of 1000x (21).

RNA extraction and quantitative reverse transcription polymerase chain reaction

Total RNA was extracted from the sperm pellets using the RNA Micro Kit (Cat. No. 74004; Qiagen, Germany) as described by the manufacturer's protocol. In order to isolate total RNA from the sperms, we used TRIzol reagent and to separate the proteins, three steps of phenol-chloroform purification were done. In order to purify and evaluate RNA concentration, we used NanoDrop ND-1000® spectrophotometry (Thermo Fisher Scientific Inc., USA). Excel RT Reverse Transcription Kit-Rp1300 (Zist Fanavari Pishgam, Iran) kit was used to synthesize the first strand of cDNA by adding 100 ng/µl of the purified total RNA, while it was carried out in a total volume of 20 µl containing, 1 µl dNTP, 1 µl Random hexamer, 8 µl Purified total RNA, 4 µl RT buffer (1 X), 4 µl DEPC, 1 µl RNase inhibitor and 1 µl RT enzyme. Primer sequences were designed using PerlPrimer (Version: 1.1.21; SourceForge, USA) and GeneRunner (Version: 6.5.52; GeneRunner.net) software for:

PAX8-
F: 5′-GTCCTCTTACTCTAAGCCCA-3′
R: 3′-CCACACTACACTCTACCTCTC-5′

PEG3-
F: 5′-ACACATATTCCCAACACCCA-3′
R: 3′-CCATAATCCCACAACAACCAC-5′

RTL1-
F: 5′-CAACAGACAGGACTACATACAG-3′
R: 3′-CATCTCTTCAAGCTCCAAACC-5′.

Then, quantitative reverse transcription PCR (qRT-PCR) was carried out for two technical repeats on StepOne™ Real-Time PCR System (Applied Biosystems, USA) in a total volume of 10 µl containing, 3 µl cDNA, 1 µl of each primer and 2.5 µl SYBR Green master mix (Ampliqon real Q plus 2x; Ampliqon, Korea). Reaction was performed under the following program: initial denaturation at 95˚C for 5 minutes, followed by 45 cycles of denaturation at 95˚C for 15 secends, annealing at 60˚C for 25 seconds and extension at 72˚C for 25 seconds. Then, expression levels of the *PAX8*, *PEG3* and *RTL1* genes was evaluated using Ct values. Relative gene expression was assessed using *β-Actin* and $2^{-\Delta\Delta Ct}$ method (22).

DNA extraction and bisulfite treatment

Total sperm DNA was extracted of the sperm pellets using the DNA extraction Kit (DNrich Sperm 1012; Azma Elixir Pajooh, Iran) according to the kit instructions. Quantity of the extracted DNA was evaluated by the NanoDrop ND-1000® spectrophotometry. Then, 1-2 µg of the extracted total DNA was treated with sodium bisulfite method, as previously described by Yi et al. (23) with some modifications (24). Bisulfite treated DNA solution was purified with the FavorPrep GEL/PCR Purification Mini Kit (Cat. No: FAGCK001-2; Favorgen, Taiwan). The bisulfite-treated DNA was then analyzed using methylation-specific PCR (25, 26).

Methylation analysis using methylation-specific polymerase chain reaction assay

Difference in methylation status was measured by methylation-specific PCR (MSP) method (25, 26). Primer sequences used in the MSP method (methylated and unmethylated sequences) were designed using MethPrimer2 software (MethPrimer2.0; urogene, China) for:

PAX8-
F: 5′-TTTCGTTTAGTTTATGGAGAGGC-3′
R: 3′-GAAACGTCGTCGTACAACGT-5′
for methylated sequence,

F: 5′-TGTTTAGTTTATGGAGAGGTGG-3′
R: 3′-TAACAAAACATCATCATACAACATC-5′
for unmethylated sequence,

PEG3-

F: 5′-GGTAATCGTAGTTTGATTGGTACGT-3′
R: 3′-AAACTTCTCCGCAAAAACGA-5′
for methylated sequence,

F: 5′-GTGGTAATTGTAGTTTGATTGGTATGT-3′
R: 3′-TTATCAAAACTTCTCCACAAAAACA-5′
for unmethylated sequence,

RTL1-
F: 5′-TTTTTATTTTGGAAAGTCGGTTATC-3′
R: 3′-AACTACGACAAATACGTACGATACG-5′
for methylated sequence,

F: 5′-TTTATTTTGGAAAGTTGGTTATTGG-3′
R: 3′-CACTTTTAACTACAACAAATACATACAAT-5′
for unmethylated sequence.

Briefly, in a final volume of 25 µl reaction, 2 µl DNA was amplified with primers specific to methylated and unmethylated sequences. Then, the following cycling PCR conditions were applied: pre- denaturation at 94°C for 5 minutes, 35 cycles of denaturation at 94°C for 30 seconds, primer annealing at 60°C for 30 seconds and primer extension at 72°C for 1 minute. Final extension was performed in 4°C for 7 minutes, 30 cycles. In all experiments, fully methylated DNA and fully unmethylated DNA were employed as positive controls and DNase/RNase-free distilled water was used for the negative PCR control. Then, a volume of 10 µl of each PCR products was visualized on 2% agarose gel at Voltage 95 V for 70 minutes, with general 1X TBE buffer and DNA bands were visualized by UV-transilluminators. Band intensities of each sample was analyzed using ImageJ (NIH corporation, USA) and GraphPad Prism 8 (GraphPad PRISM V 8 analytical software; GraphPad corporation, USA) software (27).

Statistical analysis

Statistical analysis was performed using SPSS software (version 26 for Windows; IBM-SPSS Statistics, IBM Corporation, USA) and GraphPad Prism 8 software (GraphPad corporation, USA). Normality analysis of the data was evaluated with the Kolmogorov–Smirnov test. Data were analysis using one-way ANOVA. Post hoc comparisons were assessed by Kruskal-Wallis (non-parametric) and Tukey (parametric) tests. Statistically significant was considered as $P<0.05$.

Results

Effects of rapid-freezing and Vitrification methods on frozen–thawed sperm motility parameters

As shown in Table 1, percent of TM, PM, VAP, VCL and straight-line velocity (VSL) were significantly decreased in the rapid-freezing (42.97 ± 2.3, 29.03 ± 1.2, 31.34 ± 0.6, 51.69 ± 0.8 and 26.66 ± 0.5, respectively) and vitrification groups (26.35 ± 1.5, 18.43 ± 0.5, 28.74 ± 1.3, 46.15 ± 1.4 and 22.98 ± 1.2, respectively) compared to the fresh group.

Additionally, according to Table 1 and the mentioned results above, motility parameters in the vitrification group was significantly decreased compared to the rapid-freezing group (TM: $P<0.01$, PM: $P<0.01$, VCL: $P< 0.05$ and VSL: $P<0.05$).

Effects of rapid-freezing and vitrification methods on viability, morphology and DNA fragmentation

Effect of different cryopreservation methods on viability, morphology and DNA fragmentation are presented in Figure 1. Comparison of the mean values for sperm viability in the rapid-freezing group (61.95 ± 0.8) and vitrification group (42.15 ± 1.9) showed a significant reduction ($P<0.001$ and $P<0.0001$, respectively) compared to the fresh group (90.10 ± 0.6). In addition, results showed a significant reduction ($P<0.01$) in sperm viability of the vitrification group compared to the rapid-freezing group (Fig.1A). Normal morphology was not significantly affected by different frozen methods ($P>0.05$, Fig.1B).

DNA fragmentation index showed a significantly increase in the rapid-freezing (25.45 ± 1.3, $P<0.0001$) and vitrification groups (29.80 ± 1.2, $P<0.0001$) compared to the fresh group (8 ± 0.6). Moreover, the vitrification group showed a significantly increase ($P<0.05$) compared to the rapid-freezing group (Fig.1C).

Table 1: Effect of different cryopreservation (rapid and vitrification) methods on frozen-thawed human spermatozoa motility parameters

Motility parameters Groups	Total motility (%)	PM (%)	VAP (µm/s)	VCL (µm/s)	VSL (µm/s)	LIN (%)	STR (%)
Fresh semen	81.66 ± 1.584	66.54 ± 1.553	43.07 ± 0.8208	73.16 ± 1.711	36.22 ± 0.7510	51.98 ± 1.568	84.13 ± 0.8660
Rapid-freezing	42.97 ± 2.317***	29.03 ± 1.272***	31.34 ± 0.6765****	51.69 ± 0.8928****	26.66 ± 0.5509****	53.68 ± 1.000	85.32 ± 1.464
Vitrification	26.35 ± 1.540****	18.43 ± 0.5917****	28.74 ± 1.322****	46.15 ± 1.477****	22.98 ± 1.282****	51.66 ± 2.283	81.58 ± 3.435

Data are presented as mean ± SE. PM; Progressive motility, VAP; Average path velocity, VCL; Curvilinear velocity, VSL; Straight linear velocity, LIN; Linearity, STR; Amplitude of straightness, ***; P<0.001, and ****; P<0.0001.

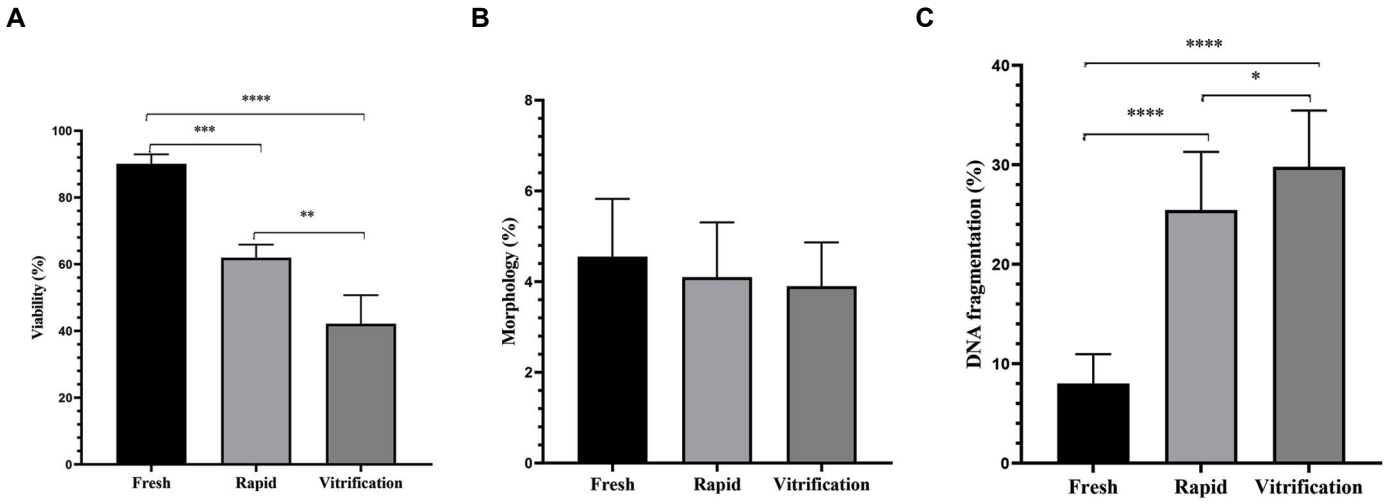

Fig.1: Effects of different cryopreservation groups on sperm cell parameters. **A.** Viability, **B.** Morphology and **C.** DNA fragmentation. *; P<0.05, **; P<0.01, ***; P<0.001, and ****; P<0.0001.

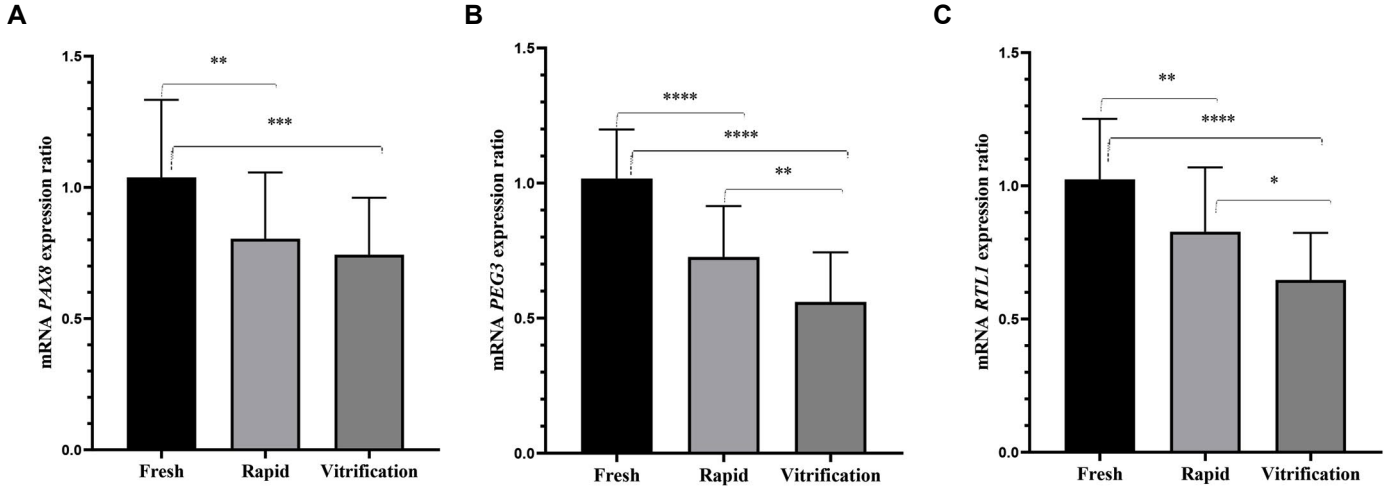

Fig.2: Assessment of gene expression in the cryopreservation groups. We used quantitative reverse transcription polymerase chain reaction (qRT-PCR) experiments to measure expression of the indicated genes. mRNA expression levels of **A.** *PAX8*, **B.** *PEG3*, **C.** *RTL1*. *; P<0.05, **; P<0.01, ***; P<0.001, and ****; P<0.0001.

Effects of the rapid-freezing and vitrification methods on expression of *PAX8*, *PEG3*, and *RTL1* genes

Our results (Fig.2A) showed that expression level of *PAX8* gene in the rapid-freezing (0.80 ± 0.05) and vitrification (0.74 ± 0.04) groups were significantly reduced (P=0.006 and P=0.0005, respectively) compared to the fresh group (1.03 ± 0.06). *PAX8* expression level was not significantly different between the two cryopreservation methods (P=0.694).

Expression level of *PEG3* gene was decreased significantly (P<0.0001) in the rapid-freezing (0.72 ± 0.03) and vitrification (0.56 ± 0.03) groups compared to the fresh group (1.01 ± 0.03). Furthermore, in the vitrification group (0.56 ± 0.03) expression level of *PEG3* gene was decreased significantly (P=0.0074) compared to the rapid-freezing group (0.72 ± 0.03). Assessment of *PEG3* gene expression is presented in Figure 2B.

According to the results in Figure 2C, it was found that expression level of *RTL1* gene in the rapid-freezing group (0.82 ± 0.04) and vitrification groups (0.64 ± 0.03) were decreased significantly (P=0.007 and P<0.0001, respectively) compared to the fresh group (1.02 ± 0.04). Additionally, expression level of *RTL1* gene was significantly reduced in the vitrification group (0.64 ± 0.03) compared to the rapid group (0.82 ± 0.04, P=0.014).

Effects of rapid-freezing and vitrification methods on *PAX8*, *PEG3* and *RTL1* gene promoter methylation status

To analyze gene promoter methylation status, PCR products were loaded on 2% agarose gels (Fig.3A, 4A, 5A) and after analyzing methylation data, ratio between methylated and unmethylated band intensities was calculated (Fig. 3B, 4B, 5B).

According to the results (Fig.3), it was found that percentage of *PAX8* methylation in the rapid-freezing (9.96 ± 0.4) and vitrification groups (9.94 ± 0.4) were significantly increased (P=0.0015 and P=0.0014, respectively) compared to the fresh group (7.34 ± 0.4).

Results of *PEG3* gene promoter methylation status in the cryopreservation and fresh groups are shown in Figure 4. As shown in Figure 4, percentage of *PEG3* gene methylation in the rapid-freezing (12.80 ± 0.7) and vitrification groups (15.17 ± 0.7) were increased significantly (P<0.0001 and P<0.0001, respectively) compared to the fresh group (5.66 ± 0.4). The results also showed that percentage of *PEG3* methylation in the vitrification group (15.17 ± 0.7) was significantly increased compared to the rapid-freezing group (12.80 ± 0.7, P=0.478).

As shown in Figure 5, percentage of *RTL1* methylation in the rapid-freezing (11.37 ± 0.7) and vitrification groups (14.10 ± 0.8) were increased significantly (P=0.0002 and P<0.0001, respectively) compared to the fresh group (7.320 ± 0.3). Besides, in the vitrification group (14.10 ± 0.8), percentage of *RTL1* methylation was significantly increased (P=0.0165) compared to the rapid-freezing group (11.37 ± 0.7).

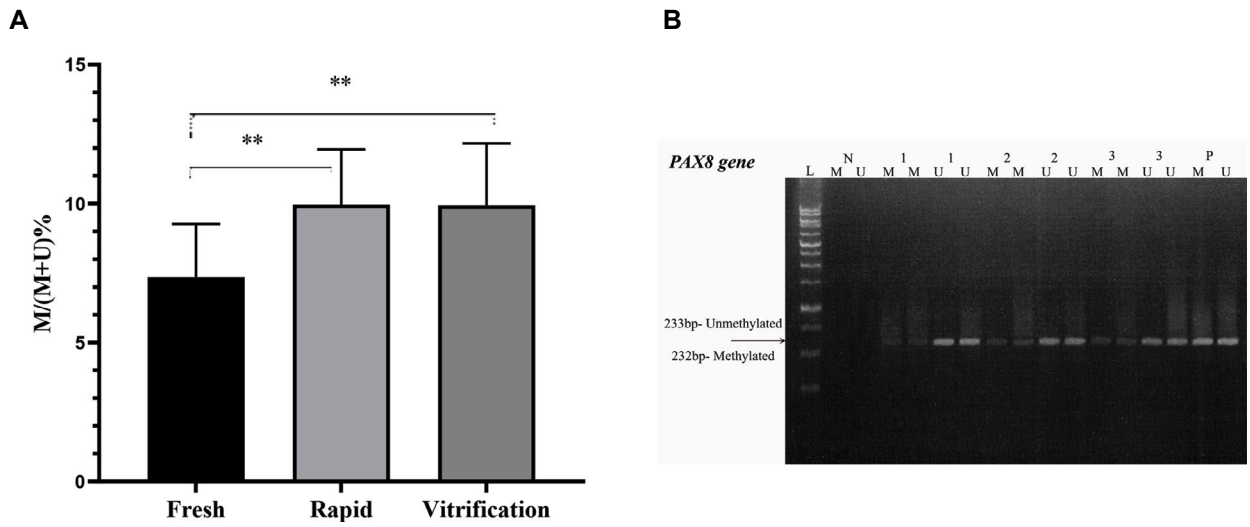

Fig.3: Methylation-specific PCR (MSP) analysis of *PAX8* gene. **A.** Percentage of *PAX8* gene promoter methylation in sperm cells after freeze-thawing process. Fresh; Control group including fresh sperm samples, Rapid; Rapid-freezing group, Vitrification; Vitrification group, and **; P<0.01. **B.** PCR products loaded on 2% agarose gel. PCR; Polymerase chain reaction, N; Negative PCR control including distilled water (for unmethylation and methylation PCR, P; Positive control including complete methylated DNA (for methylation and unmethylation PCR), M; Methylated amplicon, U; Unmethylated amplicon, Samples 1; Fresh groups, Samples 2; Rapid groups, and Samples 3; Vitrification groups.

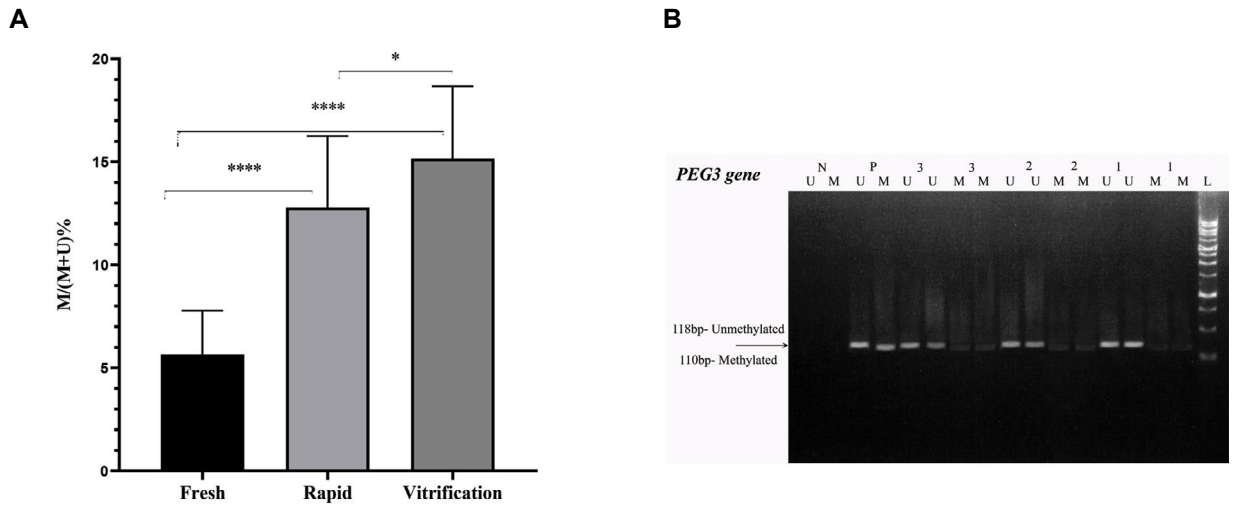

Fig.4: Methylation-specific PCR (MSP) analysis of *PEG3* gene. **A.** Percentage of *PEG3* gene promoter methylation in sperm cells after freeze-thawing process. Fresh; Control group including fresh sperm samples, Rapid; Rapid-freezing group, Vitrification; Vitrification group, *; P<0.05, ****; P<0.0001. **B.** PCR products loaded on 2% agarose gel. PCR; Polymerase chain reaction, N; Negative PCR control including distilled water (for unmethylation and methylation PCR), P; Positive control including complete methylated DNA (for methylation and unmethylation PCR), M; Methylated amplicon, U; Unmethylated amplicon, Samples 1; Fresh groups, Samples 2; Rapid groups, and Samples 3; Vitrification groups.

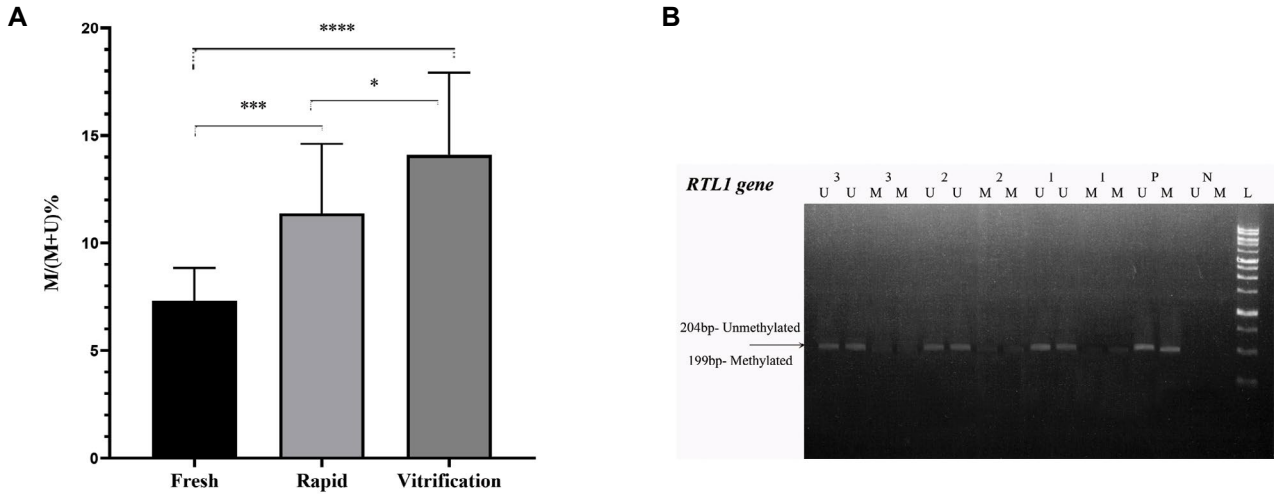

Fig.5: Methylation-specific PCR (MSP) analysis of *RTL1* gene. **A.** Percentage of *RTL1* gene promoter methylation in sperm cells after freeze-thawing process. Fresh; Control group including fresh sperm samples, Rapid; Rapid-freezing group, Vitrification; Vitrification group, *; P<0.05, ***; P<0.001, and ****, P<0.0001. **B.** PCR products loaded on 2% agarose gel. PCR; Polymerase chain reaction, N; Negative PCR control including distilled water (for unmethylation and methylation PCR), P; Positive control including complete methylated DNA (for methylation and unmethylation PCR), M; Methylated amplicon, U; Unmethylated amplicon, Samples 1; Fresh groups, Samples 2; Rapid groups, and Samples 3; Vitrification groups.

Discussion

In the recent years, sperm storage are important in the management and treatment of male infertility, but studies show that sperm quality and fertility potential are greatly reduced after freeze-thawing process. According to the previous studies, sperm quality parameters and macromolecular agents are impaired after freezing-thawing (14). Some environmental and epigenetic factors, such as temperature changes, environmental pollutants and chemicals have an effect in male infertility. So, genetic- (such as mutation-) and epigenetic-based disorders affecting spermatogenesis may be responsible for most of the idiopathic infertility cases (28). Therefore, it is necessary to determine a suitable freezing method which can reduce cryoinjury in thawed sperm. In the present study, a significant increase was observed in the DNA fragmentation index after freeze-thawing compared to the fresh group. Our findings also showed a significant increase in DNA fragmentation index of the vitrification compared to the rapid-freezing group. The main causes of sperm DNA fragmentation are increased levels of oxidative stress, protamine deficiency during chromatin packaging and apoptosis which can be related to the infertility (29). Mechanisms explaining reason of the increase in DNA fragmentation after freezing have not been identified yet, but it seems to be associated with cold shock that increases oxidative DNA damage (30). Our results showed a significant reduction in motility parameters of thawed sperm. Our findings support results of the previous studies reported that sperm motility and viability were decreased after freeze-thawing process (30-32). It has been reported that destructive effect on the mitochondria and plasma membrane can reduce sperm motility and viability after thawing (30). Furthermore, our results showed a significant decrease of sperm motility and viability in the vitrification compared to the rapid-freezing group. Our findings are in line with the results of previous studies, reported that sperm freezing by the vitrification method could reduce sperm motility and survival compared to the rapid-freezing method (33, 34). Le et al. (34) reported that PM and vitality were significantly higher in the rapid-freezing than vitrification method. Agha-Rahimi et al. (33) also compared effects of the rapid-freezing and vitrification methods on various sperm parameters. They reported that the vitrification method was not superior to the rapid-freezing of the normozoospermic spermatozoa. These results could be related to the vitrification procedure and quality of sperm that are important factors to increase the effectiveness of it (35).

In addition to damaging cellular parameters, cryopreservation can affect sperm macromolecules, such as proteins, transcripts and epigenetic patterns. Epigenetic modification, especially methylation, can cause changes in gene expression and gene silencing. In our research, a significant reduction was observed in expression of the three (*PAX8*, *PEG3* and *RTL1*) genes during the rapid-freezing and vitrification methods. Although, the highest reduction was related to the vitrification group. Our gene expression results corresponded to the previous studies, reported that expression of some sperm genes were changed after freezing compared to the fresh sperm (7, 10).

Changes in temperature, such as freezing could affect DNA methylation (36). Previous studies on the sperm of various animals, after the cryopreservation process showed epigenetic modification, including DNA methylation, after freezing (8, 9, 22) which is consistent with our results. In this study, we found that percentage of *PAX8*, *PEG3* and *RTL1* methylation was increased significantly in the rapid-freezing and vitrification groups compared to the fresh group. These results also showed that percentage of *PEG3* and *RTL1* methylation in the vitrification group was increased compared to the rapid-freezing group. Our findings supported results

of the previous studies reported that mouse embryos obtained from the cryopreserved sperm had higher DNA methylation rates than the embryos obtained from fresh sperm (22). Aurich et al. (8) also reported that sperm DNA methylation was increased in horses after freezing, which affected their successful fertility. It has been reported that cryopreservation caused epigenetic changes in the boar sperm (9). As mentioned before, *PAX8, PEG3* and *RTL1* genes have roles in male fertility and epigenetic modifications of mature sperm played an important role in the embryonic development (11-13). Previous studies reported that hypermethylation of *PEG3* gene was associated with infertility in oligospermic men (37), while changes in the level of methylation of this gene was observed in sterile male (11). Furthermore, *PEG3* gene played an important role in controlling fetal growth (38). In line with this, our results showed a decrease in the *PEG3* gene expression and hypermethylation in this gene, which may affect embryonic development. On the other hand, studies showed that hypermethylation of *PAX8* gene reduced sperm concentration and motility and it caused abnormal sperm morphology (12). Decreased expression of this gene was observed in the infertile mice (39). Due to the role of this gene in regulating synthesis of thyroid hormones (40), decreased expression and hypermethylation of this gene maybe impaired sperm production. Previous researchers reported that *RTL1* gene had a different methylation pattern in abnormal sperm compared to the fertile men (13). Our findings showed decreased expression and hypermethylation in this gene, which may lead to the impaired successful fertility. The main limitation in this project was lack of studies and resources to compare results of different freezing methods on methylation of paternal imprinting genes.

Conclusion

Our findings showed that rapid-freezing is a more suitable method for maintaining sperm cell quality after freeze-thawing process, compared to the vitrification method. Since epigenetic modifications of the imprinted genes is the main reason underlying decline in sperm motility and fertility during the freeze-thawing process, our findings indicated that rapid-freezing was a better method for sperm protection against cryo-damages compared to the vitrification method. Due to the role of *PAX8*, *PEG3* and *RTL1* genes in fertility and embryonic development, changes in the expression and epigenetic modification of these genes may affect success of fertility and embryo development, which probably can be one of the reasons for male infertility.

Acknowledgements

We thank the members of the Royan Institute and Tehran University for their beneficial suggestions. This study was financially supported by the Iran National Science Foundation (INSF, grant number: 4002824) and Royan Institute (grant number: 400000108). The authors declare no conflict of interest.

Authors' Contributions

M.Sh., V.H.; Supervision. N.Kh., V.H., M.Sh., M.H., A.Sh.; Conceptualization, Methodology, Data curation, Validation, Writing-reviewing and Editing resources. N.Kh.; Software, Formal analysis, and Writing-original draft preparation. N.Kh., M.H.; Investigation and Visualization. All authors read and approved the final manuscript.

References

1. Moein MR, Shojaeefar E, Taghizabet N, Jazayeri M, Fashami MA, Aliakbari F, et al. Prevalence of primary infertility in Iranian men; a systematic review. Men's Health Journal. 2021; 11; 5(1): e12.
2. Khosronezhad N, Colagar AH, Jorsarayi SG. T26248G-transversion mutation in exon 7 of the putative methyltransferase Nsun7 gene causes a change in protein folding associated with reduced sperm motility in asthenospermic men. Reprod Fertil Dev. 2015; 27(3): 471-480.
3. Hezavehei M, Sharafi M, Kouchesfahani HM, Henkel R, Agarwal A, Esmaeili V, et al. Sperm cryopreservation: a review on current molecular cryobiology and advanced approaches. Reprod Biomed Online. 2018; 37(3): 327-339.
4. Khosrozadeh F, Karimi A, Hezavehei M, Sharafi M, Shahverdi A. Preconditioning of bull semen with sub-lethal oxidative stress before cryopreservation: possible mechanism of mitochondrial uncoupling protein 2. Cryobiology. 2022; 104: 63-69.
5. Hu H, Ji G, Shi X, Liu R, Zhang J, Zhang H, et al. Comparison of rapid freezing versus vitrification for human sperm cryopreservation using sucrose in closed straw systems. Cell Tissue Bank. 2020; 21(4): 667-673.
6. Isachenko E, Isachenko V, Katkov II, Rahimi G, Schöndorf T, Mallmann P, et al. DNA integrity and motility of human spermatozoa after standard slow freezing versus cryoprotectant-free vitrification. Hum Reprod. 2004; 19(4): 932-939.
7. Chen X, Wang Y, Zhu H, Hao H, Zhao X, Qin T, et al. Comparative transcript profiling of gene expression of fresh and frozen-thawed bull sperm. Theriogenology. 2015; 83(4): 504-511.
8. Aurich C, Schreiner B, Ille N, Alvarenga M, Scarlet D. Cytosine methylation of sperm DNA in horse semen after cryopreservation. Theriogenology. 2016; 86(5): 1347-1352.
9. Zeng C, Peng W, Ding L, He L, Zhang Y, Fang D, et al. A preliminary study on epigenetic changes during boar spermatozoa cryopreservation. Cryobiology. 2014; 69(1): 119-127.
10. Faraji S, Rashki Ghaleno L, Sharafi M, Hezavehei M, Totonchi M, Shahverdi A, et al. Gene expression alteration of sperm-associated antigens in human cryopreserved sperm. Biopreserv Biobank. 2021; 19(6): 503-510.
11. Thiaville MM, Huang JM, Kim H, Ekram MB, Roh TY, Kim J. DNA-binding motif and target genes of the imprinted transcription factor PEG3. Gene. 2013; 512(2): 314-320.
12. Hammoud SS, Purwar J, Pflueger C, Cairns BR, Carrell DT. Alterations in sperm DNA methylation patterns at imprinted loci in two classes of infertility. Fertil Steril. 2010; 94(5): 1728-1733.
13. Kitazawa M, Tamura M, Kaneko-Ishino T, Ishino F. Severe damage to the placental fetal capillary network causes mid- to late fetal lethality and reduction in placental size in Peg11/Rtl1 KO mice. Genes Cells. 2017; 22(2): 174-188.
14. Salehi M, Mahdavi AH, Sharafi M, Shahverdi A. Cryopreservation of rooster semen: Evidence for the epigenetic modifications of thawed sperm. Theriogenology. 2020; 142: 15-25.
15. World Health Organization. WHO laboratory manual for the examination and processing of human semen. 5th ed. Geneva: World Health Organization; 2010.
16. Yamanaka M, Tomita K, Hashimoto S, Matsumoto H, Satoh M, Kato H, et al. Combination of density gradient centrifugation and swim-up methods effectively decreases morphologically abnormal sperms. J Reprod Dev. 2016; 62(6): 599-606.
17. Wang M, Todorov P, Isachenko E, Rahimi G, Wang W, von Brandenstein M, et al. Aseptic capillary vitrification of human spermatozoa: cryoprotectant-free vs. cryoprotectant-included technologies. Cryobiology. 2021; 99: 95-102.
18. Hezavehei M, Sharafi M, Fathi R, Shahverdi A, Gilani MAS. Membrane lipid replacement with nano-micelles in human sperm cryopreservation improves post-thaw function and acrosome protein

integrity. Reprod Biomed Online. 2021; 43(2): 257-268.
19. Hezavehei M, Kouchesfahani HM, Shahverdi A, Sharafi M, Salekdeh GH, Eftekhari-Yazdi P. Preconditioning of sperm with sublethal nitrosative stress: a novel approach to improve frozen-thawed sperm function. Reprod Biomed Online. 2019; 38(3): 413-425.
20. Hosseinmardi M, Siadat F, Sharafi M, Roodbari NH, Hezavehei M. Protective effect of cerium oxide nanoparticles on human sperm function during cryopreservation. Biopreserv Biobank. 2022; 20(1): 24-30.
21. Moradi M, Moochani SS, Yamini N, Javanmard D, Marjani A, Tabibzadeh AR, et al. Molecular detection of human cytomegalovirus in semen of infertile men in Tehran. IJML. 2021; 8(1): 55-61.
22. Jia G, Fu X, Cheng K, Yue M, Jia B, Hou Y, et al. Spermatozoa cryopreservation alters pronuclear formation and zygotic DNA demethylation in mice. Theriogenology. 2015; 83(6): 1000-1006.
23. Yi S, Long F, Cheng J, Huang D. An optimized rapid bisulfite conversion method with high recovery of cell-free DNA. BMC Mol Biol. 2017; 18(1): 24.
24. Ghalkhani E, Akbari MT, Izadi P, Mahmoodzadeh H, Kamali F. Assessment of DAPK1 and CAVIN3 gene promoter methylation in breast invasive ductal carcinoma and metastasis. Cell J. 2021; 23(4): 397-405.
25. Momeni A, Najafipour R, Hamta A, Jahani S, Moghbelinejad S. Expression and methylation pattern of hsa-miR-34 family in sperm samples of infertile men. Reprod Sci. 2020; 27(1): 301-308.
26. Shrestha KS, Tuominen MM, Kauppi L. Mlh1 heterozygosity and promoter methylation associates with microsatellite instability in mouse sperm. Mutagenesis. 2021; 36(3): 237-244.
27. Moon KY, Lee PH, Kim BG, Park MK, Jang AN. Claudin 5 transcripts following acrolein exposure affected by epigenetic enzyme. J Clin Toxicol. 2015; 5 (268): 1000268.
28. Khosronezhad N, Hosseinzadeh Colagar A, Mortazavi SM. The Nsun7 (A11337)-deletion mutation, causes reduction of its protein rate and associated with sperm motility defect in infertile men. J Assist Reprod Genet. 2015; 32(5): 807-815.
29. Tavalaee M, Razavi S, Nasr-Esfahani MH. Influence of sperm chromatin anomalies on assisted reproductive technology outcome. Fertil Steril. 2009; 91(4): 1119-1126.
30. Gholami D, Ghaffari SM, Shahverdi A, Sharafi M, Riazi G, Fathi R, et al. Proteomic analysis and microtubule dynamicity of human sperm in electromagnetic cryopreservation. J Cell Biochem. 2018; 119(11): 9483-9497.
31. Isachenko V, Maettner R, Petrunkina AM, Sterzik K, Mallmann P, Rahimi G, et al. Vitrification of human ICSI/IVF spermatozoa without cryoprotectants: new capillary technology. J Androl. 2012; 33(3): 462-468.
32. O'Connell M, McClure N, Lewis SE. The effects of cryopreservation on sperm morphology, motility and mitochondrial function. Hum Reprod. 2002; 17(3): 704-709.
33. Agha-Rahimi A, Khalili MA, Nabi A, Ashourzadeh S. Vitrification is not superior to rapid freezing of normozoospermic spermatozoa: effects on sperm parameters, DNA fragmentation and hyaluronan binding. Reprod Biomed Online. 2014; 28(3): 352-358.
34. Le MT, Nguyen TTT, Nguyen TT, Nguyen VT, Nguyen TTA, Nguyen VQH, et al. Cryopreservation of human spermatozoa by vitrification versus conventional rapid freezing: effect on motility, viability, morphology and cellular defects. Eur J Obstet Gynecol Reprod Biol. 2019; 234: 14-20.
35. Li YX, Zhou L, Lv MQ, Ge P, Liu YC, Zhou DX. Vitrification and conventional freezing methods in sperm cryopreservation: a systematic review and meta-analysis. Eur J Obstet Gynecol Reprod Biol. 2019; 233: 84-92.
36. Xu R, Li S, Guo S, Zhao Q, Abramson MJ, Li S, et al. Environmental temperature and human epigenetic modifications: a systematic review. Environ Pollut. 2020; 259: 113840.
37. Kim J, Frey WD, He H, Kim H, Ekram MB, Bakshi A, et al. Peg3 mutational effects on reproduction and placenta-specific gene families. PLoS One. 2013; 8(12): e83359.
38. Reik W, Walter J. Genomic imprinting: parental influence on the genome. Nat Rev Genet. 2001; 2(1): 21-32.
39. Houshdaran S, Cortessis VK, Siegmund K, Yang A, Laird PW, Sokol RZ. Widespread epigenetic abnormalities suggest a broad DNA methylation erasure defect in abnormal human sperm. PLoS One. 2007; 2(12): e1289.
40. Wistuba J, Mittag J, Luetjens CM, Cooper TG, Yeung CH, Nieschlag E, et al. Male congenital hypothyroid Pax8-/- mice are infertile despite adequate treatment with thyroid hormone. J Endocrinol. 2007; 192(1): 99-109.

Cell J
Cell Journal(Yakhteh)
Homepage: https://www.celljournal.org/
Original Article
Vol 25, No 4, April 2023, Pages: 247-254

3,5,3'-Triiodo-L-Thyronine Regulates Actin Cytoskeleton Dynamic in The Differentiated PC-12 Cells during Hypoxia through An αvβ3 Integrin

Tamar Barbakadze, Ph.D.[1, 2], Elisabed Kvergelidze, M.Sc.[1, 2], Judit Bátor, Ph.D.[3, 4], József Szeberényi, D.Sc.[3], David Mikeladze, D.Sc.[1, 2*]

1. Faculty of Natural Sciences and Medicine, Ilia State University, Tbilisi, Georgia
2. Laboratory of Biochemistry, Ivane Beritashvili Center of Experimental Biomedicine, Tbilisi, Georgia
3. Department of Medical Biology and Central Electron Microscopic Laboratory, Medical School, University of Pécs, Pécs, Hungary
4. Janos Szentagothai Research Centre, University of Pécs, Pécs, Hungary

Abstract

Objective: Thyroid hormones are involved in the pathogenesis of various neurological disorders. Ischemia/hypoxia that induces rigidity of the actin filaments, which initiates neurodegeneration and reduces synaptic plasticity. We hypothesized that thyroid hormones via alpha-v-beta-3 (αvβ3) integrin could regulate the actin filament rearrangement during hypoxia and increase neuronal cell viability.

Materials and Methods: In this experimental study, we analysed the dynamics of actin cytoskeleton according to the G/F actin ratio, cofilin-1/p-cofilin-1 ratio, and p-Fyn/Fyn ratio in differentiated PC-12 cells with/without T3 hormone (3,5,3'-triiodo-L-thyronine) treatment and blocking αvβ3-integrin-antibody under hypoxic conditions using electrophoresis and western blotting methods. We assessed NADPH oxidase activity under the hypoxic condition by the luminometric method and Rac1 activity using the ELISA-based (G-LISA) activation assay kit.

Results: The T3 hormone induces the αvβ3 integrin-dependent dephosphorylation of the Fyn kinase (P=0.0010), modulates the G/F actin ratio (P=0.0010) and activates the Rac1/NADPH oxidase/cofilin-1 (P=0.0069, P=0.0010, P=0.0045) pathway. T3 increases PC-12 cell viability (P=0.0050) during hypoxia via αvβ3 integrin-dependent downstream regulation systems.

Conclusion: The T3 thyroid hormone may modulate the G/F actin ratio via the Rac1 GTPase/NADPH oxidase/cofilin1signaling pathway and αvβ3-integrin-dependent suppression of Fyn kinase phosphorylation.

Keywords: Actin Filament, Hypoxia, Integrin, PC-12, Thyroid Hormone

Citation: **Barbakadze T, Kvergelidze E, Bátor J, Szeberényi J, Mikeladze D. 3,5,3'-Triiodo-L-thyronine regulates actin cytoskeleton dynamic in the differentiated PC-12 cells during hypoxia through an αvβ3 integrin. Cell J. 2023; 25(4): 247-254. doi: 10.22074/CELLJ.2022.557501.1059.**

Introduction

The thyroid hormones, including 3,5,3´-triiodo-L-thyronine (T3) and L-thyroxine (T4), play a significant role as a regulator of cell growth, development, and metabolism Thyroid hormones involve in the pathogenesis of various neurological diseases. There is evidence linking alterations in thyroid hormone levels to the pathogenesis of Alzheimer disease (1). Also, Thyroid dysfunction was observed in children with autism spectrum disorder (2). Low T3 plasma level after an acute ischemic stroke is associated with a greater stroke severity and worse functional outcomes (3, 4). However, the relationship between thyroid hormones, functional post-stroke outcomes, and recovery time is complex and requires further investigation.

Thyroid hormones primarily target the nuclear receptor; however, recent investigations have suggested a non-nuclear, non-genomic action (5, 6). The non-genomic effects of thyroid hormones occur partly due to the activation of the cell surface-exposed integrin alpha-v-beta-3 (αvβ3) receptor (5). Thyroid hormones binding to the αvβ3 receptor can enhance the adhesion to extracellular matrix substrates (7) and activate the protein kinase B (Akt) and extracellular signal-regulated kinase (ERK) signalling pathways (8, 9). The αvβ3 receptor seems to contain a T3-specific binding site and a region at which both T4 and T3 bind in the hormone-binding domain (6). Binding to the T3-specific site activates the phosphoinositide 3-kinase (PI3K) pathway. In contrast, the T4 does not activate the PI3K pathway, but acts on the ERK-dependent signalling (9). In the differentiation state, PC-12 cells are predominantly regulated by the T3 via the P13K/Akt pathway (8, 9), suggesting that T3 and T4 act differently on the intracellular regulatory systems via the αvβ3 integrin.

Received: 10/July/2022, Revised: 16/September/2022, 22/November/2022
***Corresponding Address: Faculty of Natural Sciences and Medicine, Ilia State University, Tbilisi, Georgian**
Email: davit_mikeladze@iliauni.edu.ge

Royan Institute
Cell Journal (Yakhteh)

Generally, a cytoskeleton is responsible for various functions in all cell types, such as the organization of subcellular organelles and regulating cell motility and dynamics (10). Dysregulation of the cytoskeletal organization contributes to many pathological disorders, including hypoxia-related diseases (11, 12). Therefore, the cytoskeleton dynamic nature helps its components rapid rearrangement in response to extracellular signals (10). The Actin is the central component of the cytoskeleton that contributes to most cell functions and a tissue organization (13). Thyroid hormones are involved in an actin polymerization in the central nervous system (14). Several actin-binding proteins control an actin polymerization and its dynamic. They maintain a monomeric G-actin pool, promote a F-actin polymerization, restrict an actin filament length, and regulate a filament assembly and disassembly (13). There is an evidence that an actin polymerization is mainly modulated by the rT3 and T4, but not by the T3 in astrocytes, which directly regulates the F-actin elongation in the neurites of neurons (15). However, there are not enough data about the integrin-mediated action of thyroid hormones on the actin polymerization during hypoxia.

The thyroid hormone-αvβ3 integrin interaction results in a small guanosine triphosphatase (GTPase) signalling (16), which controls the cytoskeleton. A Rho family GTPases (Rho, Rac) acts on the actin cytoskeleton by modulating the actin-binding protein activity (17). The reciprocal effects of Rho and Rac (Rac activation and Rho inhibition) on a dendritic motility can be involved in a dendritic dynamic (18). The Rho family members play a critical role in the mediating ischemia/reperfusion injury-induced nicotinamide adenine dinucleotide phosphate (NADPH) oxidase activation, reactive oxygen species (ROS) generation, and oxidative stress in the brain, which greatly contributes to neuronal degeneration and cognitive dysfunction after cerebral ischemia (19).

Actin-depolymerizing factor/cofilin can severe filaments increasing their depolymerization and thus regulating the dynamics of actin filaments (20). Cofilins play an important role in normal development, and dysregulation of their functions causes severe complications of tissue homeostasis and health (21, 22). They can be potentially involved in the progression of neurodegenerative disorders forming cofilin-actin rods that affect normal neuronal function (23). Cofilin phospho-regulation is crucial for a wide variety of cellular processes, such as neuronal development, and synaptic plasticity. Through it a variety of extracellular stimuli regulate actin cytoskeletal reorganization (20).

Recent data highlighted the importance of cytoskeletal dynamic in hypoxia (17); however, further research is needed to determine the role of thyroid hormones in the recovery of cellular pathological changes caused by hypoxia-ischemic processes. Despite of the growing interest in the actin cytoskeleton and hypoxia interactions, the molecular mechanisms of these interactions are not completely understood. We hypothesized that thyroid hormones via the αvβ3 integrin signalling and actin dynamic could affect the hypoxia-induced cell damage and increase the cell survival during hypoxia.

Materials and Methods

In this experimental study, differentiated PC-12 cells were used for investigation the role of T3 thyroid hormone in cell survival during hypoxia. This study was approved by the LEPL Ilia State University Committee of Establishing Ethical Norms Adherence in Research Projects (R/135-22).

Cell line culturing

In this experimental study, PC-12 pheochromocytoma cells (CRL-1721™, ATCC, USA) were used. PC-12 cells display a chromaffin cell-like morphology, but undergo rapid changes following treatment with the nerve growth factor (NGF), including neurite outgrowth. These cells are widely employed as model systems to examine the signal transduction process in neurons, predominantly of the dopaminergic origin. PC-12 cells were cultured in the T25 flasks (690 170, Greiner Bio-One GmbH, Austria) in a humidified atmosphere containing 5% CO_2 at 37°C in a high-glucose Dulbecco's modified Eagle's medium (DMEM, 30-2002™, ATCC, USA) supplemented with 10% heat-inactivated horse serum (HS, H1138, Sigma-Aldrich, USA), 5% fetal bovine serum (FBS, F2442, Sigma-Aldrich, USA), and 100 U/mL penicillin/streptomycin (15140148, Gibco™, USA) as well as 50 µg/mL gentamicin sulphate (15750060, Gibco™, USA). To induce differentiation, PC-12 cells were incubated in a low serum-containing DMEM 1% HS and 1% FBS (H1138 and F2442, Sigma-Aldrich, USA) supplemented with 100 ng/mL NGF (N-245 Alomone Labs, Israel) in T25 flasks for five days. The NGF-containing medium was replaced every two days with a fresh complete DMEM medium. Cells were considered differentiated if the length of one or more neurites exceeded the diameter of the cell body. Cell viability was counted using Trypan blue dye assay (145-0013, Bio-Rad, USA) and an Automated Cell Counter (TC20TM, Bio-Rad, USA) (24). Differentiated PC-12 cells (5×10^6 cells per sample) were treated with T3 and αvβ3 integrin blocking antibody 1 µg/mL (23C6; sc-7312, Santa Cruz, USA), and incubated for 1 hour under hypoxic condition. The 10 nM T3 (T6397, Sigma-Aldrich, USA) concentration was used in this experiment. The αvβ3 blocking antibody 1 µg/mL (23C6; sc-7312, Santa Cruz, USA) was used as an αvβ3 integrin inhibitor (25) to evaluate the involvement of the αvβ3 integrin in thyroid hormone-induced effects. Hypoxia conditions (0-1% oxygen) were maintained using nitrogen gas in a BioSpherix C-Chamber placed in a CO_2 incubator and controlled by a controller (ProOx Model P110, BioSpherix, USA). Hypoxia was maintained for an hour. A differentiated PC-12 cells (5×10^6 cells per sample) without any treatment during one-hour hypoxia was used as a control (control, H).

Preparation of cell fractions from the PC-12 cell line for electrophoresis and western blotting

After one hour of exposition to the hypoxic condition (0-1% oxygen), PC-12 cells (5×10^6 cells per sample) were detached from the cell culture flasks using 0.025% trypsin/EDTA (59418C, Sigma-Aldrich, USA) containing phosphate-buffered saline (PBS, 137 mM NaCl (S9888, Sigma-Aldrich, USA), 2.7 mM KCl (P3911, Sigma-Aldrich, USA), 10 mM Na_2HPO_4 (S9763, Sigma-Aldrich, USA), and 1.8 mM KH_2PO_4 (P8709, Sigma-Aldrich, USA pH=7.4) (incubation with trypsin containing buffer for 1 minute at 37°C) and scraped using scrapers (CSL2518, Bioland Scientific LLC, USA). After the detachment and scraping of the PC-12 cells from the flasks, trypsin inactivation was performed using resuspension of detached PC-12 cells in one volume of aprotinin-containing PBS (1 mkg/mL) (78432, Thermo Scientific™, USA) and pelleted by centrifugation at 300 × g. After centrifugation, the pelleted PC-12 cells were washed twice with 5 ml PBS buffer. Washed PC-12 cells (as pellet) were lysed using a lysis buffer (20 mM 4-(2-hydroxyethyl)-1-piperazine ethane sulfonic acid (HEPES, H3375, Sigma-Aldrich, USA), pH=7.4, 10 mM KCl (P3911, Sigma-Aldrich, USA), 10 mM $MgCl_2$ (M8266, Sigma-Aldrich, USA), 1 mM ethylenediaminetetraacetic acid (EDTA, E9884, Sigma-Aldrich, USA), 1 mM ethylene glycol-bis (β-aminoethylether)-N, N, N′, N′-tetraacetic acid (EGTA, 324628, Millipore, USA), 250 mM sucrose (35580, Serva, Germany), 1 mM dithiothreitol (DTT, 43819, Sigma-Aldrich, USA), and protease inhibitor cocktail (P8340, Sigma-Aldrich, USA)), and passed through a 25 Ga needle ten times using a 1 mL syringe. Lysed cells were centrifuged at 720 × g for 5 minutes, nuclei and intact cells were removed, and the supernatant was used for electrophoresis and western blotting analysis.

F-actin and G-actin fractionation

Fractionation was performed according to the method described by Bhambhvani et al. (26), with some modifications. Incubated PC-12 cells were homogenized in the F-actin stabilization buffer 0.1 M 1,4-piperazinediethanesulfonic acid, pH=6.9 (PIPES, sc-216099, ChemCruz, USA), 30% glycerol (G7893, Sigma-Aldrich, USA), 5% dimethyl sulfoxide (DMSO, D8418, Sigma-Aldrich, USA), 1 mM $MgSO_4$ (39773.01, Serva, Germany), 1 mM EGTA (324628, Millipore, USA), 1% Triton X-100 (X100, Sigma-Aldrich, USA), 1 mM adenosine triphosphate (ATP, A1852, Sigma-Aldrich, USA), and protease inhibitor (P8340, Sigma-Aldrich, USA). The protein concentration of the homogenates was measured using the Pierce Micro BCA™ Protein Assay Kit (23235, Thermo Fisher Scientific, USA), incubated at 37°C for 10 minutes and then, centrifuged at 720 × g for 5 minutes at room temperature. The supernatant was centrifuged at 134,000 × g at 37°C for one hour in an ultracentrifuge (CS150NX, Himac, Japan) to separate G-actin (in the supernatant) from F-actin (in pellet) fractions. Actin proteins were detected in the both fractions by sulfate-polyacrylamide gel electrophoresis (SDS-PAGE) and western blotting using an anti-β actin antibody (sc-47778, Santa Cruz, USA).

Western blotting

For the analysis of cofilin1, p-cofilin1 (phosphorylated cofilin), Fyn, and p-Fyn (phosphorylated Fyn) proteins in the supernatant of cell lysates (see "Preparation of cell fractions") and β-actin in the F (pellet) and G (supernatant) fractions (see in the F-actin and G-actin fractionation section), appropriate samples (the same amount of protein) were boiled at 90°C with Laemmli 2× Concentrate Sample Buffer containing 4% SDS, 20% glycerol, 10% 2-mercaptoethanol, 0.004% bromphenol blue and 0.125 M Tris HCl, pH approx. 6.8. (S3401, Sigma-Aldrich, USA) for 5 minutes, cooled at room temperature, and centrifuged at 16,000 × g 3 minutes using centrifuge (Sigma 3-16 PK, Germany), followed by separation via sodium dodecyl SDS-PAGE on 7.5-15% gels and transfer to nitrocellulose membranes (88018, Thermo Scientific, USA) (26). After blocking with 5% bovine serum albumin (8076.1, Roth, Germany) dissolved in TBST [Tris-HCl-buffer: 250 mM Tris-HCl (648317, Millipore, USA), 27 mM KCl (P3911, Sigma-Aldrich, USA), 1.37M NaCl (S9888, Sigma-Aldrich, USA), pH=7.4] with 0.05% Tween 20 (P1379, Sigma-Aldrich, USA), then nitrocellulose membranes were incubated with the appropriate primary antibodies dissolved in the blocking solution: anti-cofilin1 at ratio 1:500 (sc-53934, Santa Cruz Biotechnology, USA), anti-p-cofilin1at ratio 1:500 (sc-271921, Santa Cruz Biotechnology, USA), anti-Fyn at ratio 1:500 (sc-434, Santa Cruz Biotechnology,USA), anti-p-Fyn at ratio 1:500 (sc-377555, Santa Cruz Biotechnology, USA). This step was done according to the manufacturing protocol. Subsequently, the membranes were incubated with secondary antibodies at ratio 1:2000 (ab112458, Abcam, USA). Immunolabeled bands were visualized using enhanced chemiluminescence (sc-2048, Santa Cruz Biotechnology, USA) and analysed by the Image J (1.53k, National Institute of Health, USA). After the chemiluminescence visualisation the p-cofilin1, nitrocellulose membrane was stripped using stripping buffer [1 L Stripping Buffer: 15 g glycine (3187.2, Roth, Germany), 1 g sodium dodecyl sulphate (SDS, 11667289001, Sigma-Aldrich, USA), 10 mL Tween 20 (P1379, Sigma-Aldrich, USA), pH=2.2] and re-probed for cofilin1 analyzing. After the chemiluminescence visualisation the p-Fyn, nitrocellulose membrane was stripped using stripping buffer (1 L Stripping Buffer: 15 g glycine, 1 g SDS, 10 mL Tween 20, pH=2.2) and re-probed for Fyn protein detection using the stripping method. Briefly, after the first chemiluminescence visualisation, the membranes were incubated with fresh stripping buffer using a volume that will cover the membrane, incubated at room temperature for 10 minutes, buffer was discarded and incubation with fresh

stripping buffer was repeated. After this step, buffer was discarded and membrane was washed for 10 minutes in PBS. Washing procedure in PBS was repeated. Finally, membrane was washed twice in TBST for 5-5 minutes. All procedures were performed at room temperature. The stripped and washed membrane was blocked in 5% bovine serum albumin TBST solution for the next western blotting.

NADPH oxidase assay

NADPH oxidase was analysed using lucigenin, according to the method described by Zhang et al. (27), with modifications by Wang and Lou (22). Differentiated PC-12 cells (1×10^6) were washed with PBS and disrupted by sonication in ice-cold Krebs buffer [130 mM NaCl (S9888, Sigma-Aldrich, USA), 5 mM KCl (P3911, Sigma-Aldrich, USA), 2 mM $MgCl_2$ (M8266, Sigma-Aldrich, USA), 1.5 mM $CaCl_2$ (C1016, Sigma-Aldrich, USA), 5 mM glucose (G8270, Sigma-Aldrich, USA), 35 mM phosphoric acid (04102, Sigma-Aldrich, USA), and 20 mM HEPES (H3375, Sigma-Aldrich, USA), pH=7.4]. After centrifugation at 1000 x g, the pellet was resuspended with Krebs buffer, contained 0.5 mM lucigenin (sc-202698, ChemCruz, USA). NADPH oxidase produces free radicals in the result of addition of NADPH (0.1 mM), as the substrate, and in the presence of lucigenin induces luminescence, which intensity was measured using microplate fluorescence reader (Twinkle LB979, Berthold, USA) with bottom optics in the clear-bottomed plates. Luminescence readings increased linearly within 5 minutes and were expressed as Relative Light Units (RLU/minute).

Rac1, activation assay

Rac1 activation assay was performed using the Rac1,2,3 G-LISA Activation Assay Kit (BK125, Cytoskeleton, USA), according to the manufacturer's protocol. The cytosolic fraction of PC-12 cells was used. The results were expressed as optical density (OD) per mg of total protein.

Cytotoxicity assay

Cytotoxicity was analysed by monitoring the release of lactate dehydrogenase (LDH) into the culture medium from hypoxia-exposed damaged PC-12 cells. LDH was assayed using the LDH assay kit (88954, Pierce™, USA). Released LDH from damaged PC-12 cells was analysed using a microplate spectrophotometer reader (ELx808, BioTek, USA) with an optical density at a wavelength of 490 nm and 680 nm.

Statistical analysis

Statistical analysis was performed by SPSS software (SPSS v. 25, IBM, USA). One-Way analysis of variance and Tukey's Supplementary Test statistical method were used to evaluate the significance of the experimental data. A value of $P<0.05$ was considered as statistically.

Results

To study the non-genomic αvβ3 integrin-mediated effects of T3 thyroid hormone during hypoxia, we treated differentiated PC-12 cells with T3 and αvβ3-integrin inhibitor (αvβ3 blocking antibody), and exposed to hypoxic condition for one hour. We found, that T3 thyroid hormone increased the viability of PC-12 cells (P=0.0050) during hypoxia. This pro-survival effect of T3 hormone was abolished by the αvβ3 antibody (P=0.0153), which underlined the integrin-mediated regulation of cell viability during hypoxia (Fig.1).

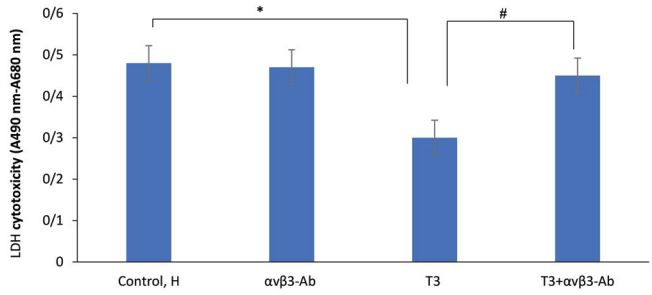

Fig.1: Analysis of the cytotoxicity in differentiated PC-12 cells under hypoxia with/without 10 nM T3 hormone and αvβ3 antibody (αvβ3-Ab, 1 µg/ml) during 1 hour hypoxia by the LDH test as described in "Materials and Methods. Results of triplicate experiments are shown as mean ± SEM. Error-bars denote one standard error of the mean and asterisk and hash indicate a statistically significant difference. LDH; Lactate dehydrogenase, *; P=0.0050 vs. control and #; P=0.0153 vs. T3 hormone treatment.

Next, we analysed the actin cytoskeletal contents, monomer-G actin and filament polymer-F actin, and determined the G/F actin ratio. Our results showed that treatment of cells with T3 thyroid hormone increased the G/F actin ratio (P=0.0010) during hypoxia. The impact of T3 hormone was abolished by the addition of an anti-αvβ3 integrin antibody (P=0.0020, Fig.2A, 2B).

Furthermore, we have found that T3 hormone treatment increased the cofilin1/p-cofilin1 ratio (P=0.0045) during hypoxia by decreasing phosphorylation of cofilin1 (reduced p-cofilin content), which was abolished by the αvβ3-integrin blocking antibody (P=0.0058, Fig.3A, B). To evaluate the integrin downstream regulator of the cofilin1/p-cofilin1 ratio, we further analysed the effect of T3 hormone on the phosphorylation of the Fyn kinase (a member of the Src-family of kinases) in the differentiated PC-12 cells during hypoxia. In the hypoxic cells, we found that T3 hormone reduced the content of the phosphorylated Fyn kinase and accordingly decreased the p-Fyn/Fyn ratio (P=0.0010, Fig.4A, B). This ratio is restored to the control level by an αvβ3-integrin blocking antibody (P=0.0138).

In addition, we analysed the Rac activity and found that in the hypoxic cells, addition the T3 hormone increased the Rac activity (P=0.0069), and this effect was eliminated after the treatment the cells with αvβ3-integrin blocking antibody (P=0.0078, Fig.5A). As one of the most important targets of Rac, we assessed the NADPH oxidase activity and found that the T3 hormone adding to the hypoxic cells induces an elevation of NADPH oxidase activity (P=0.0010). This effect was abolished after treating the cells with anti-αvβ3 integrin (P=0.0014, Fig.5B).

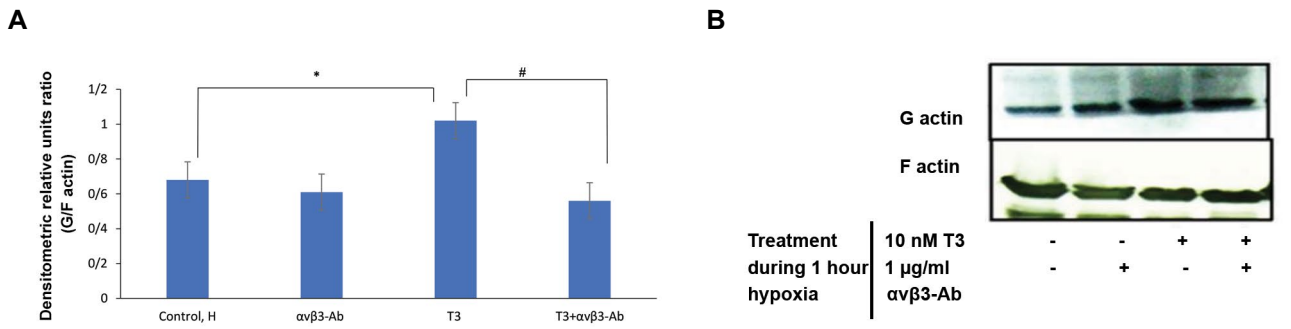

Fig.2: Immunoblotting analysis. **A.** Diagram Analysis of the G- and F-actin content in differentiated PC-12 cells under hypoxia with/without 10 nM T3 hormone and αvβ3 antibody (αvβ3-Ab, 1 μg/ml) during 1 hour hypoxia. Results of triplicate experiments are shown as mean ± SEM. Error-bars denote one standard error of the mean and asterisk and hash indicate a statistically significant difference. *; P=0.0010 vs. control and #; P=0.0020 vs. T3 hormone treatment. **B**. Western blots of the G and F actins in the differentiated PC-12 cells with/without 10 nM T3 hormone treatment and αvβ3 antibody (αvβ3-Ab, 1 μg/ml) during 1 hour hypoxia. Bands were quantified by Image J.

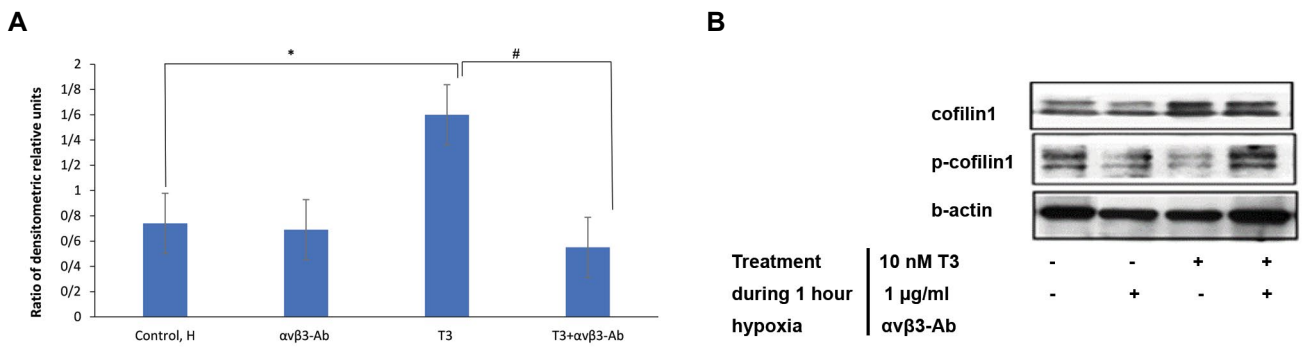

Fig.3: Immunoblotting analysis. **A.** Ratio of cofilin1/p-cofilin1 in the differentiated PC-12 cells with/without 10 nM T3 and αvβ3 antibody (αvβ3-Ab, 1 μg/ml) during 1 hour hypoxia. Results of triplicate experiments are shown as mean ± SEM. Error-bars denote one standard error of the mean and asterisk and hash indicate a statistically significant difference. *; P=0.0045 vs. control and #; P=0.0058 vs. T3 treatment. **B.** Western blots of cofilin1 p-cofilin1, and beta-actin (loading control) in differentiated PC-12 cells with/without 10 nM T3 hormone and αvβ3 antibody (αvβ3-Ab, 1 μg/ml) during one-hour hypoxia. Bands were quantified by Image J.

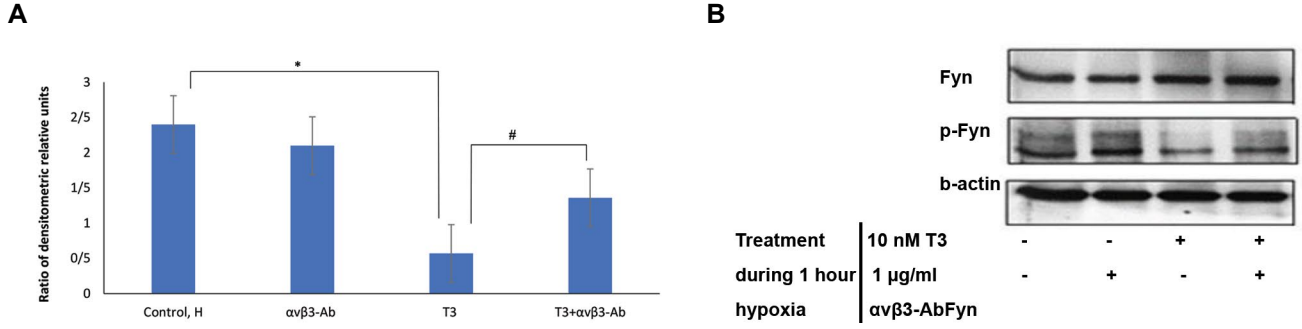

Fig.4: Immunoblotting analysis. **A.** Diagram of the p-Fyn/Fyn ratio in differentiated PC-12 cells with/without 10 nM T3 and αvβ3 antibody (αvβ3-Ab, one μg/ml) during 1 hour hypoxia. Results of triplicate experiments are shown as mean ± SEM. Error-bars denote one standard error of the mean and asterisk and hash indicate a statistically significant difference. *; P=0.0010 vs. control and #; P=0.0138 vs. T3 treatment. **B.** Western blots of p-Fyn, Fyn and beta-actin (loading control) in the differentiated PC-12 cells with/without 10 nM T3 hormone and αvβ3 antibody (αvβ3-Ab, 1 μg/ml) during one-hour hypoxia. Bands were quantified by Image J.

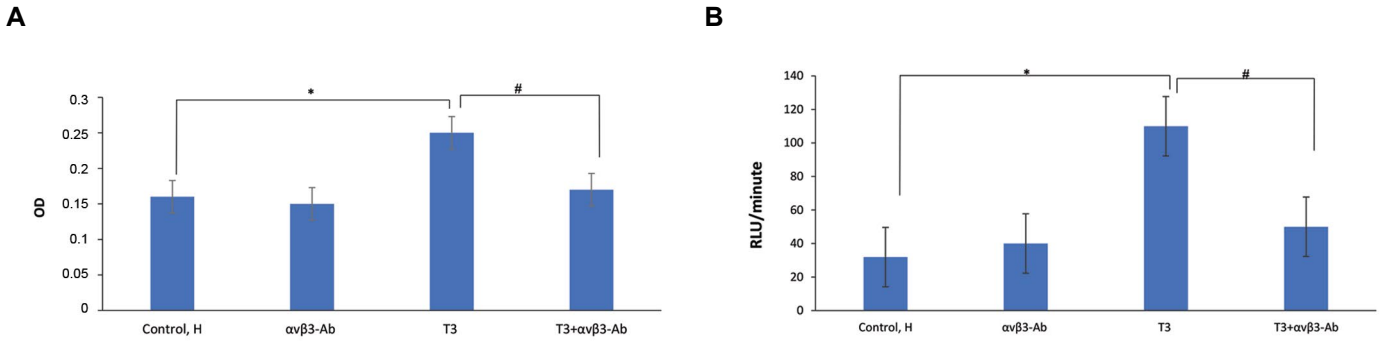

Fig.5: Analysis of the Rac 1 and NADPH oxidase activity in the differentiated PC-12 cells with/without 10 nM T3 hormone and αvβ3 antibody (αvβ3-Ab, 1 µg/ml) during 1 hour hypoxia. **A.** Level of Rac1 in the differentiated PC-12 cells with/without 10 nM T3 hormone and αvβ3 antibody (αvβ3-Ab,1 µg/ml) during one h hypoxia. Results of triplicate experiments are shown as mean ± SEM. Error-bars denote one standard error of the mean and the asterisk and hash indicate a statistically significant difference *; P=0.0069 vs. control and #; P=0.0078 vs. T3 hormone treatment. **B.** NADPH oxidase activity in the differentiated PC-12 cells with/without 10 nM T3 hormone and αvβ3 antibody (αvβ3-Ab, 1 µg/ml) during 1 hour hypoxia. NADPH oxidase activity was measured as Relative Light Unit per minute (RLU/minute). Results of triplicate experiments are shown as mean ± SEM. Error-bars denote one standard error of the mean and asterisk or hash indicates a statistically significant difference. *; P=0.0010 vs. control and #; P=0.0014 vs. T3 hormone treatment.

The schematic representation of the results is described in Figure 6.

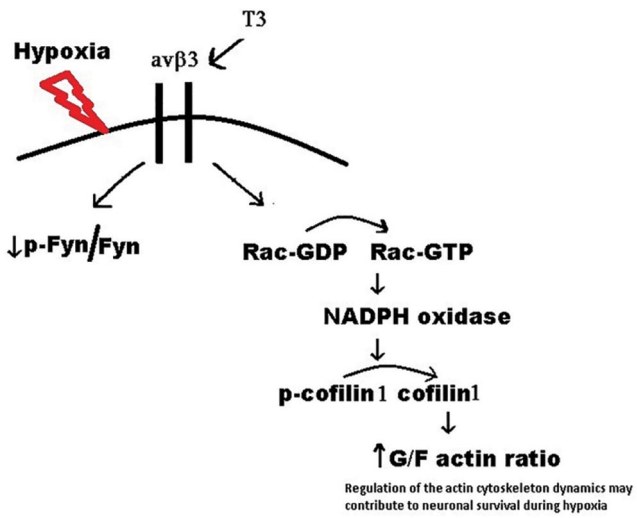

Fig.6: Schematic representation of the role of T3 hormone in actin cytoskeletal dynamic in the differentiated PC-12 cells during hypoxia. T3 hormone via αvβ3 integrin suppresses Fyn activation and, on the other hand, through the Rac1/NADPH oxidase/cofilin1 pathway increases the G/F actin ratio. In this way, extracellular T3 hormone regulates the neuronal actin filament dynamic via the αvβ3 integrin receptor during hypoxia.

Discussion

Thyroid hormones (T3 and T4) are crucial agents for normal brain development that contribute to recovery and neuronal regeneration after brain injury. These hormones act mainly through the nuclear receptors, but nongenomic actions of the T3 hormone were also found in the brain (28). We found that the T3 hormone treatment for one hour during hypoxia increased the viability of PC-12 cells. This pro-survival effect of the T3 hormone treatment was abolished by the αvβ3 antibody, which underlined the integrin-mediated T3-dependent modulation of the cell viability during hypoxia. This finding suggests that cell viability mainly depends on the presence of a T3 hormone in the extracellular medium, which contributes to the αvβ3-mediated pro-survival signalling during hypoxia.

Hypoxia induces F-actin filament accumulation due to the inactivation of actin-binding and severing protein, cofilin, by LIM kinase-mediated phosphorylation (17). Therefore, maintaining the typical G/F actin ratio is crucial for the actin filament dynamic regulation in the neuronal cell viability. In neurons, cofilin-1 may contribute to degenerative processes by forming cofilin-actin rods (23, 29). Based on these observations, we analysed the cytoskeletal content of actin, actin monomer-G actin, and filament polymer-F actin and determined the G/F actin ratio, a marker of cytoskeletal dynamics (30). According our results, the increased G/F actin ratio is mainly regulated through the αvβ3 integrin receptor and this effect is correlated with the reduction of p-cofilin1 levels. Thus, changes in actin dynamics appear to be the result of the cofilin1 dephosphorylation.

Hypoxia induces an actin rearrangement in several cell types and tissues, presumably via the Rho GTPase signalling (17). The Rho family GTPases play an important role in the control of cellular morphology. There are several studies on the role of the Fyn, a member of the Src family of kinases, in the inactivation of the Rho and activation of the Rac, which triggers morphological alterations. Also, Rho and Rac exhibit contrasting effects on the cell morphological complexity (31, 32). On the other hand, the Fyn activation has an undesirable effect on neurons, that makes them more vulnerable to a synaptotoxicity. The opposite effect is achieved by reducing the Fyn activation, and while it may be neuroprotective, an excessive inhibition could lead to poor long-term potential and hypothetically may influence the cognitive function in humans. Thus, a

therapeutic aim to maintain a delicate balance between activation and inhibition of the Fyn is likely to optimize the neural networks function (33, 34). Overactivation of the Src family protein tyrosine kinases, including the Fyn, has been implicated in the pathogenesis of cerebral ischemia and can initiate apoptosis (35). Based on these observations, we analysed the effect of thyroid hormones on the phosphorylation of the Fyn in differentiated PC-12 cells during hypoxia. We found that the T3 hormone treatment decreased and maintained a moderate p-Fyn/Fyn ratio, suggesting that the T3 hormone regulates the actin cytoskeleton dynamic via αvβ3 integrin through the dephosphorylation of the Fyn. Thus, our results agree with the observation that suppression of the Fyn kinase phosphorylation switches on the anti-apoptotic signalling cascade, especially in dopaminergic cells, and confirms the suggestion that pharmacological inhibitors directed at the Fyn activation could prove to be a therapeutic target in the treatment of dopaminergic degeneration during various neurological disorders including Parkinson's disease (36).

Several studies have shown that the Rac activation promotes the formation of lamellipodia and filopodia. Simultaneously, the Rho activity prevents neurite initiation, while inducing neurite retraction (37). It is demonstrated that Rac-mediated ROS production downregulates Rho activity (38). There is evidence that the Rac1 GTPase also can promote multiple pathological events and signalling pathways that collectively contribute to the neuronal damage and cognitive dysfunction following the cerebral ischemia (19). The Rac1 participates in a ROS formation via an NADPH oxidase activation in different cell lines. According to our findings, T3 hormone induced a moderate NADPH oxidase activation through binding the Rac1 to NADPH oxidase 2 (NOX2) in the differentiated PC-12 cells during the hypoxia condition. This effect is regulated through αvβ3 integrin (39).

In our opinion, non-genomic mechanisms, initiated by T3 thyroid hormone via αvβ3 integrin could contribute to the recovery of lost neurological functions after an ischemic stroke. Nevertheless, quantitative live cell imaging is needed for a more precise analysis of the non-genomic-dependent cytoskeleton rearrangement during ischemia.

The thyroid hormones level is significantly associated with post-stroke outcomes (40). According to our observations, one of the most critical targets of thyroid hormones is the αvβ3 integrin, which can participate in the hypoxic brain repair processes and have a pro-survival role in the neuronal cells during hypoxia. This receptor plays a central and complex role in the cell-cell and cell-matrix interactions that mediate cell adhesion, migration, and invasion. Additionally, αvβ3 integrin exerts intracellular effects on the actin cytoskeleton organization by regulating various signalling processes. As a cell surface receptor, this integrin has a central role in the pathophysiology of many brain diseases and is a potential target of new neurological drug development. Modulation of the thyroid hormone signalling in the post-ischemic brain may be a promising therapeutic strategy that may regulate endogenous repair mechanisms.

Conclusion

In conclusion, our results show that T3 can regulate the actin filament dynamics by the increasing the alteration of the G/F actin ratio via the Rac1 GTPase/NADPH oxidase/cofilin1 pathway and αvβ3-integrin-dependent suppression of Fyn kinase phosphorylation. These findings suggest, that the T3 regulates the neuronal actin cytoskeleton dynamics via αvβ3 integrin, which increases neuronal cell viability during hypoxia. In the future, we suppose to study the precise pathways of Fyn kinase regulation by T3 through αvβ3 integrin during hypoxia.

Acknowledgments

This research was supported by the Shota Rustaveli National Science Foundation of Georgia (SRNSF), Tbilisi, Georgia. (Grant No. PHDF-19-751). The authors would like to thank the World Federation of Scientists (WFS, Erice, Italy) for financial support of this research (WFS National Scholarship related to the WFS Planetary Emergency "Medicine and Biotechnology"). The authors declare that there are no conflicts of interest.

Authors' Contributions

E.K., J.B., T.B.; Contributed to all experimental work, and reviewed the literature for the manuscript. T.B., J.S., D.M.; Participated in study design, data collection and evaluation, drafting, and statistical analysis. D.M Performed editing and approved the final version of this manuscript for submission. All authors approved the manuscript for submission.

References

1. Tan ZS, Vasan RS. Thyroid function and Alzheimer's disease. J Alzheimers Dis. 2009; 16(3): 503-507.
2. Frye RE, Wynne R, Rose S, Slattery J, Delhey L, Tippett M, et al. Thyroid dysfunction in children with autism spectrum disorder is associated with folate receptor α autoimmune disorder. J Neuroendocrinol. 2017; 29(3).
3. Alevizaki M, Synetou M, Xynos K, Pappa T, Vemmos KN. Low triiodothyronine: a strong predictor of outcome in acute stroke patients. Eur J Clin Invest. 2007; 37(8): 651-657.
4. Bunevicius A, Iervasi G, Bunevicius R. Neuroprotective actions of thyroid hormones and low-T3 syndrome as a biomarker in acute cerebrovascular disorders. Expert Rev Neurother. 2015; 15(3): 315-326.
5. Bergh JJ, Lin HY, Lansing L, Mohamed SN, Davis FB, Mousa S, et al. Integrin alphaVbeta3 contains a cell surface receptor site for thyroid hormone that is linked to activation of mitogen-activated protein kinase and induction of angiogenesis. Endocrinology. 2005; 146(7): 2864-2871.
6. Davis PJ, Leonard JL, Lin HY, Leinung M, Mousa SA. Molecular basis of nongenomic actions of thyroid hormone. Vitam Horm. 2018; 106: 67-96.
7. Cohen K, Flint N, Shalev S, Erez D, Baharal T, Davis PJ, et al. Thyroid hormone regulates adhesion, migration and matrix metalloproteinase 9 activity via αvβ3 integrin in myeloma cells. Oncotarget. 2014; 5(15): 6312-6322.
8. Barbakadze T, Natsvlishvili N, Mikeladze D. Thyroid hormones differentially regulate phosphorylation of ERK and Akt via integrin αvβ3 receptor in undifferentiated and differentiated PC-12 cells.

Cell Biochem Funct. 2014; 32(3): 282-286.
9. Cheng SY, Leonard JL, Davis PJ. Molecular aspects of thyroid hormone actions. Endocr Rev. 2010; 31(2): 139-170.
10. McKayed, KK, Simpson JC. Actin in action: imaging approaches to study cytoskeleton structure and function. Cells. 2013; 2(4): 715-731.
11. Tojkander S, Gateva G, Lappalainen P. Actin stress fibers – assembly, dynamics and biological roles. J Cell Sci. 2012; 125(Pt 8): 1855-1864.
12. Eira J, Silva CS, Sousa MM, Liz MA. The cytoskeleton as a novel therapeutic target for old neurodegenerative disorders. Prog Neurobiol. 2016; 141: 61-82.
13. Pollard TD, Cooper JA. Actin, a central player in cell shape and movement. Science. 2009; 326(5957): 1208-1212.
14. Davis PJ, Goglia F, Leonard JL. Nongenomic actions of thyroid hormone. Nat Rev Endocrinol. 2016; 12(2): 111-121.
15. Farwell AP, Dubord-Tomasetti SA, Pietrzykowski AZ, Stachelek SJ, Leonard JL. Regulation of cerebellar neuronal migration and neurite outgrowth by thyroxine and 3,3',5'-triiodothyronine. Brain Res Dev Brain Res. 2005; 154(1): 121-135.
16. Berrier AL, Martinez R, Bokoch GM, LaFlamme SE. The integrin beta tail is required and sufficient to regulate adhesion signaling to Rac1. J Cell Sci. 2002; 115(Pt 22): 4285-4291.
17. Zieseniss A. Hypoxia and the modulation of the actin cytoskeleton - emerging interrelations. Hypoxia (Auckl). 2014; 2: 11-21
18. Wong WT, Faulkner-Jones BE, Sanes JR, Wong RO. Rapid dendritic remodeling in the developing retina: dependence on neurotransmission and reciprocal regulation by Rac and Rho. J Neurosci. 2000; 20(13): 5024-5036.
19. Raz L, Zhang QG, Zhou CF, Han D, Gulati P, Yang LC, et al. Role of Rac1 GTPase in NADPH oxidase activation and cognitive impairment following cerebral ischemia in the rat. PLoS One. 2010; 5(9): e12606.
20. Mizuno K. Signaling mechanisms and functional roles of cofilin phosphorylation and dephosphorylation. Cell Signal. 2013; 25(2): 457-469.
21. Wang W, Mouneimne G, Sidani M, Wyckoff J, Chen X, Makris A, et al. The activity status of cofilin is directly related to invasion, intravasation, and metastasis of mammary tumors. J Cell Biol. 2006; 173(3): 395-404.
22. Wang Y, Lou MF. The regulation of NADPH oxidase and its association with cell proliferation in human lens epithelial cells. Invest Ophthalmol Vis Sci. 2009; 50(5): 2291-2300.
23. Bamburg JR, Bernstein BW. Actin dynamics and cofilin-actin rods in alzheimer disease. Cytoskeleton (Hoboken). 2016; 73(9): 477-497.
24. Goloshvili G, Barbakadze T, Mikeladze D. Sodium nitroprusside induces H-Ras depalmitoylation and alters the cellular response to hypoxia in differentiated and undifferentiated PC12 cells. Cell Biochem Funct. 2019; 37(7): 545-552.
25. Scarlett A, Parsons MP, Hanson PL, Sidhu KK, Milligan TP, Burrin JM. Thyroid hormone stimulation of extracellular signal-regulated kinase and cell proliferation in human osteoblast-like cells is initiated at integrin alphaVbeta3. J Endocrinol. 2008; 196(3): 509-517.
26. Bhambhvani HP, Mueller TM, Simmons MS, Meador-Woodruff JH. Actin polymerization is reduced in the anterior cingulate cortex of elderly patients with schizophrenia. Transl Psychiatry. 2017; 7(12): 1278.
27. Zhang W, Wang Y, Chen CW, Xing K, Vivekanandan S, Lou MF (2006) The positive feedback role of arachidonic acid in the platelet-derived growth factor-induced signaling in lens epithelial cells. Mol Vis. 2006; 12: 821-831.
28. Liu YY, Brent GA. Thyroid hormone and the brain: Mechanisms of action in development and role in protection and promotion of recovery after brain injury. Pharmacol Ther. 2018; 186: 176-185.
29. Hoffmann L, Rust MB, Culmsee C. Actin(g) on mitochondria – a role for cofilin1 in neuronal cell death pathways. Biol Chem. 2019; 400(9): 1089-1097.
30. Menon S, Gupton SL. Building blocks of functioning brain: cytoskeletal dynamics in neuronal development. Int Rev Cell Mol Biol. 2016; 322: 183-245.
31. Arthur WT, Noren NK, Burridge K. Regulation of Rho family GTPases by cell-cell and cell-matrix adhesion. Biol Res. 2002; 35(2): 239-246.
32. Liang X, Draghi NA, Resh MD. Signaling from integrins to Fyn to Rho family GTPases regulates morphologic differentiation of oligodendrocytes. J Neurosci. 2004; 24(32): 7140-7149.
33. Nygaard HB, van Dyck CH, Strittmatter SM. Fyn kinase inhibition as a novel therapy for Alzheimer's disease. Alzheimers Res Ther. 2014; 6(1): 8.
34. Matrone C, Petrillo F, Nasso R, Ferretti G. Fyn tyrosine kinase as harmonizing factor in neuronal functions and dysfunctions. Int J Mol Sci. 2020; 21(12): 4444.
35. Du CP, Tan R, Hou XY. Fyn kinases play a critical role in neuronal apoptosis induced by oxygen and glucose deprivation or amyloid-β peptide treatment. CNS Neurosci Ther. 2012; 18(9): 754-761.
36. Saminathan H, Ghosh A, Zhang D, Song C, Jin H, Anantharam V, et al. Fyn kinase-mediated PKCδ Y311 phosphorylation induces dopaminergic degeneration in cell culture and animal models: implications for the identification of a new pharmacological target for parkinson's disease. Front Pharmacol. 2021; 12: 631375.
37. Govek EE, Newey SE, Van Aelst L. The role of the Rho GTPases in neuronal development. Genes Dev. 2005; 19(1): 1-49.
38. Nimnual AS, Taylor LJ, Bar-Sagi D. Redox-dependent downregulation of Rho by Rac. Nat Cell Biol. 2003; 5(3): 236-241.
39. Kvergelidze E, Barbakadze T, Mikeladze D. Thyroid Hormone T3 Regulates NOX2 activity and BDNF secretion in differentiated PC-12 cells during hypoxia via αvβ3 integrin. Bull Georg Natl Acad Sci. 2022; 16(2): 115-121.
40. Talhada D, Santos CRA, Gonçalves I, Ruscher K. Thyroid hormones in the brain and their impact in recovery mechanisms after stroke. Front Neurol. 2019; 10: 1103.

Cell J
Cell Journal(Yakhteh)
Homepage: https://www.celljournal.org/
Original Article
Vol 25, No 4, April 2023, Pages: 255-263

Fabrication of Cell-Laden AME-Loaded Collagen-Based Hydrogel Promotes Fibroblast Proliferation and Wound Healing *In Vitro*

Mohammad Azimi Alamouty, M.Sc.[1], Niloufar Shayan Asl, M.Sc.[2], Abdollah Safari, Ph.D.[3], Marzieh Ebrahimi, Ph.D.[4, 5*], Hamed Daemi, Ph.D.[1, 6*]

1. Department of Tissue Engineering, Faculty of Basic Sciences and Advanced Technologies in Medicine, Royan Institute, ACECR, Tehran, Iran
2. Department of Tissue Engineering, School of Advanced Technologies in Medicine, Tehran University of Medical Sciences, Tehran, Iran
3. Department of Mathematics, Statistics, and Computer Science, Faculty of Science, University of Tehran, Tehran, Iran
4. Department of Stem Cells and Developmental Biology, Cell Science Research Center, Royan Institute for Stem Cell Biology and Technology, ACECR, Tehran, Iran
5. Department of Regenerative Medicine, Cell Science Research Center, Royan Institute for Stem Cell Biology and Technology, ACECR, Tehran, Iran
6. Department of Cell Engineering, Stem Cells and Developmental Biology, Cell Science Research Center, ACECR, Royan Institute, Tehran, Iran

Abstract

Objective: The biological factors secreted from cells and cell-based products stimulate growth, proliferation, and migration of the cells in their microenvironment, and play vital roles in promoting wound healing. The amniotic membrane extract (AME), which is rich in growth factors (GFs), can be loaded into a cell-laden hydrogel and released to a wound site to promote the healing of the wound. The present study was conducted to optimize the concentration of the loaded AME that induces secretion of GFs and structural collagen protein from cell-laden AME-loaded collagen-based hydrogels, to promote wound healing *in vitro*.

Materials and Methods: In this experimental study, fibroblast-laden collagen-based hydrogel loaded with different concentrations of AME (0.1, 0.5, 1, and 1.5 mg/mL, as test groups) and without AME (as control group), were incubated for 7 days. The total proteins secreted by the cells from the cell-laden hydrogel loaded with different concentrations of AME were collected and the levels of GFs and type I collagen were assessed using ELISA method. Cell proliferation and scratch assay were done to evaluate the function of the construct.

Results: The results of ELISA showed that the concentrations of GFs in the conditioned medium (CM) secreted from the cell-laden AME-loaded hydrogel were significantly higher than those secreted by only the fibroblast group. Interestingly, the metabolic activity of fibroblasts and the ability of the cells to migrate in scratch assay significantly increased in the CM3-treated fibroblast culture compared to other groups. The concentrations of the cells and the AME for preparation of CM3 group were 10^6 cell/mL and 1 mg/mL, respectively.

Conclusion: We showed that 1 mg/ml of AME loaded in fibroblast-laden collagen hydrogel significantly enhanced the secretion of EGF, KGF, VEGF, HGF, and type I collagen. The CM3 secreted from the cell-laden AME-loaded hydrogel promoted proliferation and scratch area reduction *in vitro*.

Keywords: Amniotic Membrane Extract, Fibroblast, Growth Factor, Hydrogel, Wound Healing

Citation: Azimi Alamouty M, Shayan Asl N, Safari A, Ebrahimi M, Daemi H. Fabrication of cell-laden AME-loaded collagen-based hydrogel promotes fibroblast proliferation and wound healing in vitro. Cell J. 2023; 25(4): 255-263. doi: 10.22074/CELLJ.2023.561869.1129.

Introduction

Wound healing is a complex biological process that requires the successful completion of different healing stages, namely homeostasis, inflammation, proliferation, and regeneration (1). During the wound healing process, cytokines and growth factors (GFs) are the vital biological factors that stimulate the synthesis of DNA and cell mitosis (2). In addition, they can regulate various cellular functions, such as proliferation, migration, differentiation, morphogenesis, and apoptosis, which accelerate wound healing (3). Recently, the action mechanisms of several GFs have been revealed in this process, and some of them, including epidermal GF (EGF), hepatocyte GF (HGF), keratinocyte GF (KGF), platelet-derived GF (PDGF), transforming GF beta (TGF-b), vessel endothelial GF (VEGF), fibroblast GFs (FGF), and insulin GF (IGF), are commercially available for both clinical use and research (4). Among them EGF, HGF, FGF, and KGF stimulate the proliferation of fibroblast, keratinocyte, and vascular endothelial cells by different mechanisms (5). VEGF

Received: 11/September/2022, Revised: 17/December/2022, Accepted: 24/January, 2023
*Corresponding Addresses: P.O.Box: 16635-148, Department of Stem Cells and Developmental Biology, Cell Science Research Center, Royan Institute for Stem Cell Biology and Technology, ACECR, Tehran, Iran
P.O.Box: 16635-148, Department of Tissue Engineering, Faculty of Basic Sciences and Advanced Technologies in Medicine, Royan Institute, ACECR, Tehran, Iran
Emails: m.ebrahimi@royan-rc.ac.ir, h.daemi@royaninstitute.org

Royan Institute
Cell Journal (Yakhteh)

affects angiogenesis and granulation tissue formation in the early stages of healing (6), while PDGF is vital for inflammation, granulation, and epithelial regeneration through wound healing stages (2, 7). Although the roles of different GFs during healing process have been studied by different researchers, all monotherapies based on the GFs have failed (8).

Today, using cell-based products, such as cell-laden skin substitutes on the wound bed, remain a promising strategy in skin regeneration (9). Skin substitutes have been introduced to the wound care market since 1975 (10). They can modulate the physicochemical and biological features of the wound environment through different molecular mechanisms including interactions among GFs, cells, and extracellular matrix (ECM) (11). Fibroblasts are known as important cells for skin wound reconstruction and repair through skin substitute implantation (12). They can produce a suitable concentration and combination of cytokines, and provide ECM components that promote wound healing (13, 14).

The amniotic membrane (AM) as a naturally-occurring biologically-active construct has been used both as wound dressing and tissue replacement for different types of wounds during recent years (15, 16). It contains various GFs such as PDGF, KGF, HGF, bFGF, EGF, and VEGF, and also glycosaminoglycans (GAGs) for example, hyaluronic acid in its construct. Therefore, it can increase the proliferation of human skin fibroblasts and also mesenchymal stem cells (17-20). A variety of research have revealed the importance of GAGs and their analogues in acceleration of skin cell migration (21, 22). In addition to being a source of GFs, the AM has the potentials to act as a highly bioactive and natural scaffold for the growth, migration, and adhesion of keratinocytes and fibroblasts, resulting in wide-ranging applications in skin tissue engineering (19). Furthermore, AM reduces the risk of infection, owing to its antimicrobial properties, which not only acts as a biological barrier, but also expresses several antimicrobial molecules such as beta3-defensin and elafin (23). Additionally, human amniotic epithelial cells (HAECs) produce high levels of cytokines, which are largely effective in wound healing for acute and chronic wound models (24).

Recently, we developed an extract from AM called AM extract (AME), and evaluated its role on skin wound epithelialization (25, 26) and corneal damage (27). Based on our previous studies, we assumed that the biological behaviors of fibroblasts may be affected by some specific concentrations of AME. Therefore, the main aim of this study is to evaluate the effects of different concentrations of AME loaded in hydrogels on GFs and structural proteins that release from cell-laden collagen-based hydrogels and induce fibroblast proliferation and accelerate wound healing *in vitro*.

Materials and Methods

In this experimental study, human amniotic membranes (HAMs) were obtained from Royan Stem Cell Technology (Iran). All HAMs were negative for microbial, fungal, and viral contamination. Dulbecco's Modified Eagle Medium/F12 (DMEM/F12), fetal bovine serum (FBS), and fungizone were obtained from Gibco. Trypsin, ethylenediaminetetraacetic acid (EDTA), penicillin/streptomycin, acetic acid, 3-(4,5-dimethylthiazol-2-yl)-2,5-diphenyl tetrazolium bromide (MTT) and L-glutamine were supplied by Sigma-Aldrich. Sodium hydroxide (NaOH) and trypan blue were purchased from Merck. Mitomycin C (MMC) (ab120797) was purchased from Abcam. Rat tail collagen and human dermal fibroblasts (HDFs) were obtained from Royan Institute and Stem Cell Bank of the Pasteur Institute, respectively.

Preparation of amniotic membrane extract

The AME was prepared according to our previous study. Briefly, The HAMs were cut into small pieces, were immersed in liquid nitrogen and then pulverized with a grinder machine (SC-7880 Silver Crest). The prepared powder was dispersed in DMEM/F12 medium and sonicated (UP200S-Heilescher) three times at low temperature (0°C) for a maximum power of 20% of the working cycle for 10 minutes. The homogenate was centrifuged at 4000 g for 10 minutes, then 15,000 g for 5 minutes. Finally, the supernatant was filtered through a 0.2 μm filter, aliquoted and kept frozen at -70°C until use (27).

Fibroblast cell culture

HDF cells in passages 5-6 were cultured in DMEM/F12 medium with FBS (10%), penicillin-streptomycin (100 units/mL), and fungizone (0.25 μg/mL) (28). Culture flasks were incubated at 37°C, with 5% CO_2 concentration and 95% relative humidity. Once the cells reached 80% confluence, fibroblasts were removed from the culture flasks with trypsin/EDTA (0.1% w/v, 0.02% w/v) and transferred into T-25 flasks. This study was approved by the Royan Institute Ethics Committee (IR.ACECR.ROYAN.REC.1398.157).

Preparation of cell-laden amniotic membrane extract-loaded collagen hydrogel

Fibroblasts were counted by trypan blue and then encapsulated in a physically-crosslinked collagen hydrogel (0.6 mg/mL). To this end, a stock solution of type I collagen (obtained from rat tail) at a concentration of 1.2 mg/mL was dissolved in acetic acid (0.1 % v/v). Cell-laden collagen hydrogels were prepared through mixing of the collagen solution (1 mL), DMEM/

F12 supplemented with 10% FBS (1.1 mL), NaOH aqueous solution (0.1 mL, 0.1 M), the cell suspension (0.20 mL, 1×10^6 cells/mL) and varying concentrations of AME (0.1, 0.5, 1, and 1.5 mg/mL) at 0°C. The resulting mixture was poured into a mold and stored at 37°C to form a hydrogel structure. The prepared hydrogels, which were in a disc shape (diameter of 10 mm and thickness of 1 mm, Fig.1), were transferred to a Petri dish containing cultured medium, and were incubated in DMEM/F12 (500 µL) at 37°C, 5% CO_2 and 95% relative humidity for We selected day 7 based on our previous research (22) and other similar reports (8, 29, 30). Moreover, performing a pilot study at different timepoints (1, 3, 7 and 14 days) post-incubation confirmed that day 7 is the optimal time for performing a total protein assay (data not shown). The medium containing total proteins released from the constructs in each group (Table 1) was referred to as conditioned medium (CM) and was stored at -80°C.

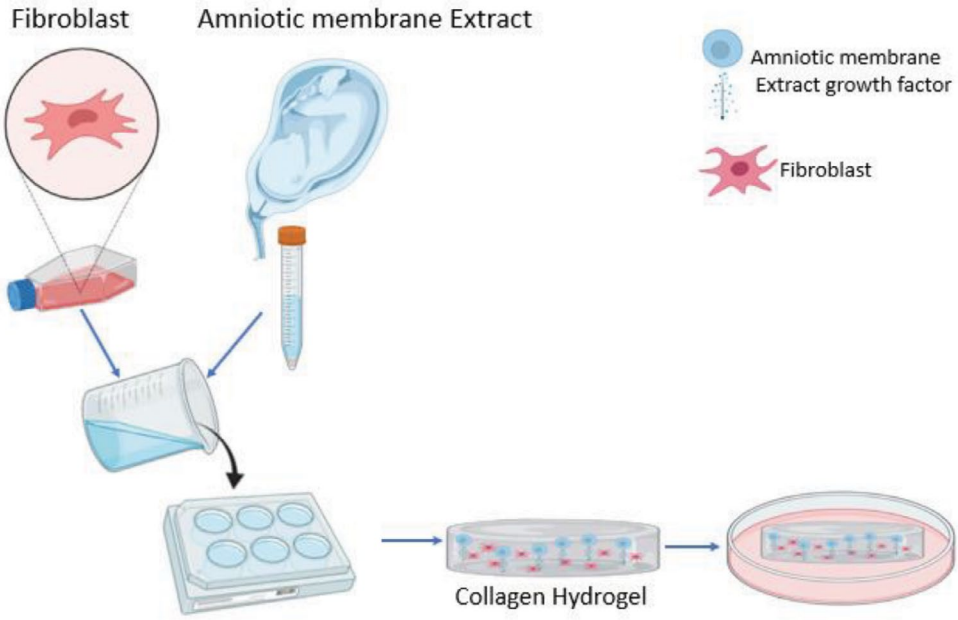

Fig.1: Schematic representation for preparation of cell-laden, amniotic membrane extract (AME)-loaded collagen hydrogel. The AME and fibroblasts were combined with collagen solution and poured into a mold. The resulting hydrogel was placed in culture medium, and the subsequent conditioned medium was removed for analysis after days 7.

Table 1: Different experimental groups to assess their efficacy on GFs secreted from hydrogels

Group	Ingredients	AME concentration in hydrogel (mg/mL)	Fibroblast (cells/mL)
AME	Only AME	1	-
CM1	AME+FIB	0.1	1×10^6
CM2	AME+FIB	0.5	1×10^6
CM3	AME+FIB	1	1×10^6
CM4	AME+FIB	1.5	1×10^6
FIB	FIB	-	1×10^6

CM (1-4); The conditioned medium, which is total proteins secreted by the cell-laden hydrogel that was loaded with different concentrations of AME, AME; Amniotic membrane extract,FIB; Fibroblast, and GFs; Growth factors.

Quantitative analysis of growth factors secreted by the cells from conditioned medium

The total protein levels for AME and CM were evaluated using the bicinchoninic acid (BCA) method. CM samples as the analytes were collected from each group and stored at -80°C. In general, 25 µL of the analyte and serially diluted standards (0.063,,0.125 1.5 ,1 ,0.75 ,0.5 ,0.25, and 2 µg/µL) were added to each 96-wells plate. The plate was covered, incubated at 37°C for 30 minutes, cooled down to room temperature and then, the optical density (OD) of the samples was read in triplicates by a spectrophotometer (Multiskan Spectrum, Thermo Scientific) at 520-570 nm. In this context, cumulative concentrations of the growth factors EGF, KGF, HGF, and VEGF, as well as some important proteins present in AME, such as the structural protein (type I collagen), were evaluated using enzyme-linked immunosorbent assay (ELISA) kits (R&D systems) according to the manufacturers' protocols.

Effect of conditioned medium on fibroblast proliferation

Human fibroblasts were cultured (2.5×10^5/well) in a 6-well plate at 37°C, 5% CO_2 concentration and 95% relative humidity. The cells were seeded and cultured in a culture medium (1 mL) with penicillin G/streptomycin (1%), and L-glutamine (200 mM). The collected CM samples (1 mL) were added to each well. The cells cultured in the presence of FBS (10%) and the basal culture medium (DMEM) were considered as the positive and negative controls, respectively. After 24, 48, and 72 hours of cell seeding, the wells (three wells for each group) were washed with phosphate buffer saline (PBS) and their viability was assessed using the MTT assay. In addition, the cell counting was performed using trypan blue at predetermined timepoints. Each test was repeated three times.

The effect of conditioned medium on fibroblast migration

The effect of each CM sample on *in vitro* cell migration in the fibroblast cultures was evaluated using scratch assay. Briefly, the cells (2.5×10^5/well) were cultured in 6-well plates and during the time that they were incubated at 37°C for 2 hours, proliferation of the cells was inhibited using mitomycin-C (5 µg/mL) (31). After reaching 80% of confluency, the population of the HDFs were scratched with a pipette tip along a straight line. After washing the cell debrides with PBS, the cultured cells were treated with serum-free culture medium containing CM samples. The serum-free, CM-free medium and complete culture medium (DMEM/F12 containing FBS 10%) were selected as negative and positive control samples, respectively. At 0, 12, 24, and 48 hours after scratching, digital images of the cells were taken by an Olympus device and analyzed by Image-J software. Each experiment was repeated three times for every timepoint. The amount of scratch closure (%) was calculated as follows:

$$\text{Amount of scratch closure (\%)}=[(S_0 - S)/S_0]\times100$$

where S_0 is the scratch area at time 0, and S is the scratch area at times 3, 12, 24, and 48 hours.

Statistical analysis

All experiments were performed at least three times, and the results were expressed as mean ± standard deviation (SD). Due to our sample sizes, Kruskal-Wallis Rank Sum Test (non-parametric version of ANOVA test) was used to compare the median of the outcomes across groups. In addition, following a significant Kruskal-Wallis test, Dunn's test was employed for multiple pairwise comparisons along with adjusted P values to account for multiple testing (using Bonferroni approach). A $P<0.05$ was considered significant for all statistical tests. All analyses were performed using R Statistical Software (v4.2.2; R Core Team 2022).

Results

The content of growth factors and structural proteins in prepared amniotic membrane extract

The concentration of GFs and structural proteins in AME is an important parameter that can affect its biological properties. Our results indicated that the concentration of type I collagen and different GFs including EGF, HGF, KGF and VEGF were 341 ± 38.1 µg/mL, 2.3 ± 0.05 µg/mL, 58.1 ± 1.6 µg/mL, 0.28 ± 0.01 µg/mL and 0.23 ± 0.02 µg/mL in AME at a concentration of 1 mg/mL, respectively. The contents of GFs and type I collagen in AME with concentrations of 0.1, 1, 0.5, and 1.5 mg/mL is shown in Figure 2.

Quantitative analysis of conditioned medium

As mentioned earlier, AME can affect the secretion patterns of fibroblasts in cell-laden hydrogels. Therefore, we constructed different experimental groups, which mixed both the fibroblast cells (1×10^6 cell/mL) and AME (0.1, 0.5, 1 and 1.5 mg/mL) with the collagen solution, and prepared a cell-laden, AME-loaded collagen hydrogel through a simple physical crosslinking (Fig.1). The concentrations of GFs secreted from the HDFs were measured on day 7 of the cultures. As shown in Figure 2, we observed a significant difference in concentrations of all GFs and type I collagen when we compared AME 1 mg/mL and the CM3 group (contained secretion factors of fibroblasts loaded in collagen hydrogel and AME). Moreover, the CM4 group showed a significant difference compared to the cell group (FIB) in all cases and with AME (1.5 mg/mL) in type I collagen (657 ± 34.03 µg/mL). Figure 2A shows a higher concentration of HGF in the CM2 (52.5 ± 0.76 µg/mL) and CM3 (81.2

± 0.1.02 µg/mL) groups compared to the AME 0.5 mg/mL (29.4 ± 0.60 µg/mL) and AME 1 mg/mL (58.7 ± 1.12 µg/mL) groups, respectively. The concentration of VEGF secreted from the hydrogel loaded with AME (1 mg/mL), (CM3), indicated a higher concentration (0.35 ± 0.02 µg/mL) compared to only fibroblasts (0.02 ± 0.004 µg/mL) and AME 1 mg/mL (0.23 ± 0.02 µg/mL) groups (Fig.2D). In addition, CM1 (0.14 ± 0.02 µg/mL) and CM2 (0.19 ± 0.01 µg/mL) groups showed a higher volume of VEGF compared to only 0.1 and 0.5 mg/mL of the AME (0.02 ± 0.003 µg/mL, 0.12 ± 0.04 µg/mL), respectively.

Finally, concentration of type I collagen (381 ± 18.5 µg/mL) significantly increased in CM3 group compared to AME (1 g/mL) and fibroblast-only group (342 ± 25.04 µg/mL and 0.22 ± 0.12 µg/mL).

Effects of conditioned medium on cell proliferation

To evaluate the influence of different concentrations of AME on cell proliferation, HDF cells were treated with CM containing various concentrations of AME, and the secreted substances from the 3D cultured fibroblasts were analyzed at different timepoints (24, 48, and 72 hours). Expectedly, the HDFs showed a normal spindle-shaped morphology in all groups (Fig.3A). There was a visual, upward trend in proliferation of the HDFs from the cells treated with CM1 to CM3 groups, where the concentration of AME varied from 0.1 mg/mL up to 1 mg/mL. In this context, the CM3 group revealed the highest cell count compared to the other CM groups, as well as the cell group treated with FBS as the positive control group. To evaluate the metabolic activity of the cells quantitatively, the MTT assay was also assessed at 24, 48, and 72 hours timepoints. As shown in Figure 3B, the same trend of increasing OD values was observed for CM1-CM3 samples from 24 to 72 hours. This result well confirmed the proliferative role of AME on AME-treated HDFs, where the highest effective concentration of AME was 1 mg/mL. However, we observed a lower OD value for the CM4 (0.43 ± 0.02) group compared to both the CM3 (0.79 ± 0.01) and the positive control groups (0.72 ± 0.01) (26, 32). The number of viable cells of HDFs treated with the CM3 group was counted with trypan blue under inverted light microscope and reported as 2.7×10^6, 3.51×10^6, 4.5×10^6 at 24, 48 and 72 hours, respectively (Fig.3C). These data demonstrated a significant increase in the cell number for the CM-treated HDFs compared to the CM4 and negative control groups during 48 and 72 hours timepoints, respectively. Figure 3C also showed that the number of live cells increased significantly in CM1-CM3 groups compared to the negative control at different timepoints.

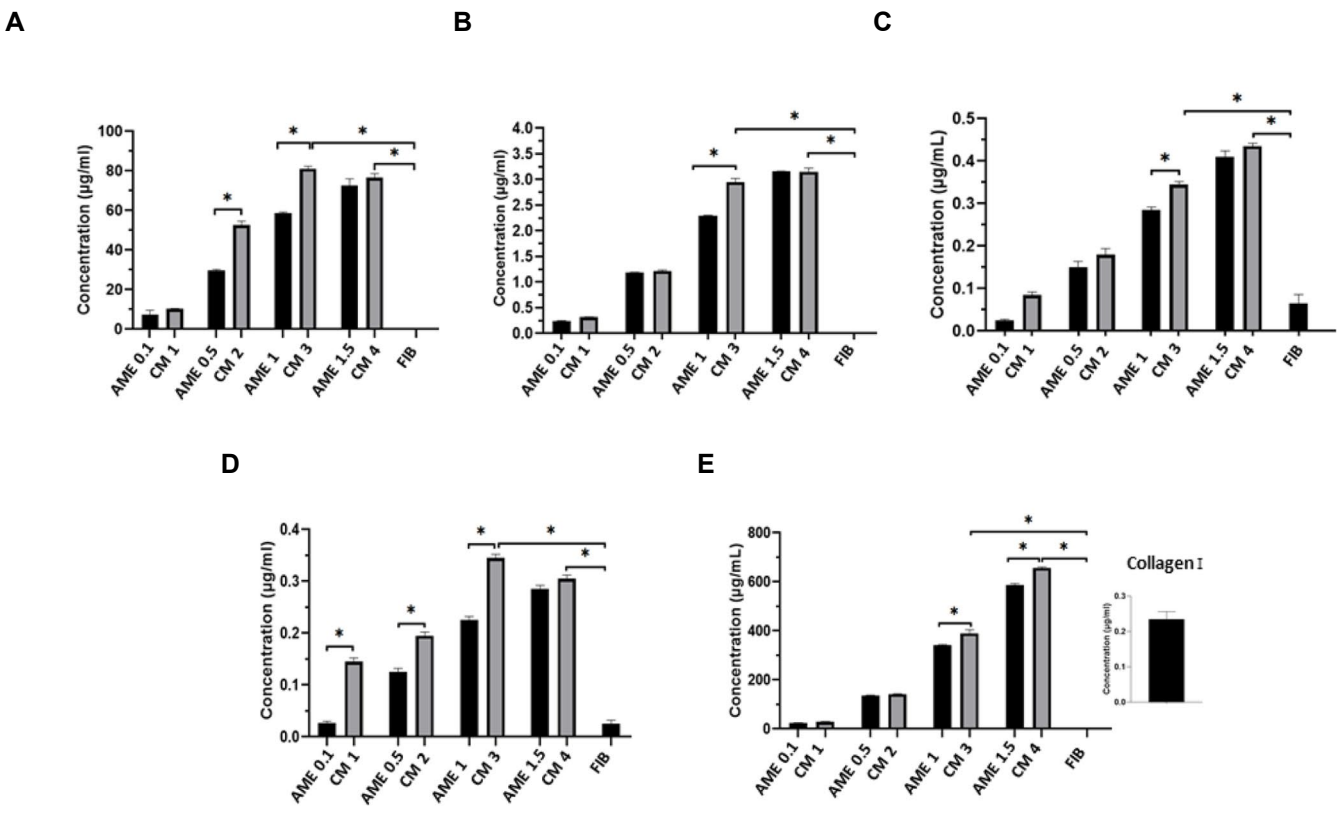

Fig.2: Quantification of concentrations of GFs and collagen type I with ELISA. The concentration of each biological factor was measured at a volume of 1 mL of AME and the related CM. **A.** HGF, **B.** EGF, **C.** KGF, **D.** VEGF, **E.** Type I collagen. Data is represented as mean ± SEM, (n=3). *; P≤ 0.05. GFs; Growth factors, AME; Amniotic membrane extract, CM; Conditioned medium, HGF; Hepatocyte growth factor, EGF; Epidermal growth factor, KGF; Keratinocyte growth factor, VEGF; Vessels endothelial growth factor, and FIB; Fibroblast.

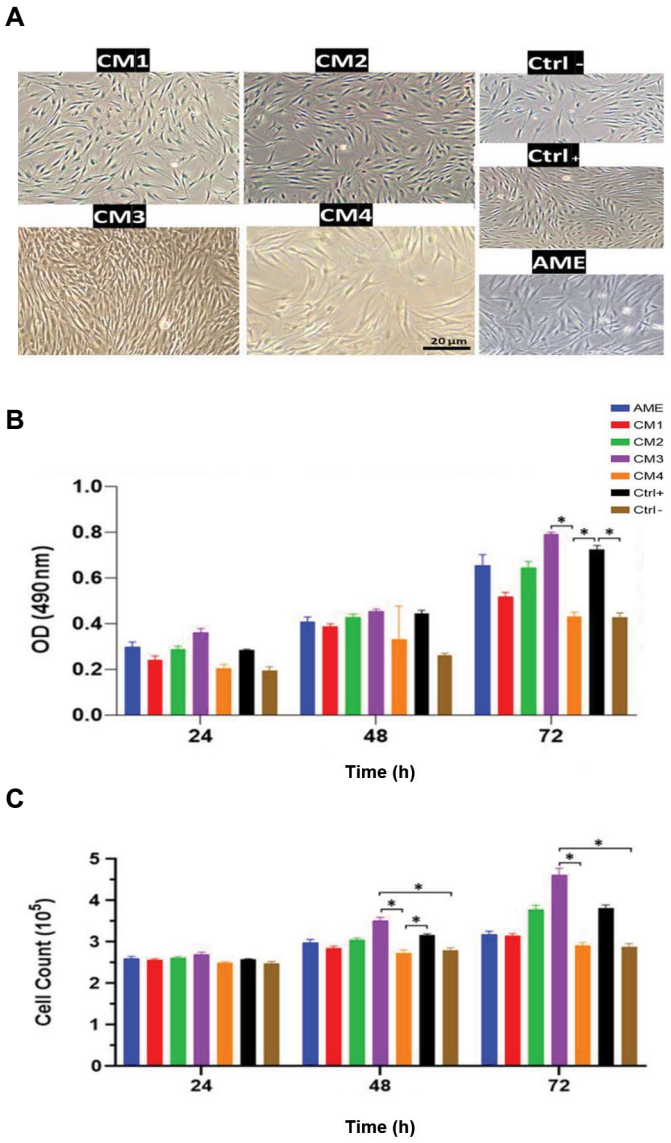

Fig.3: *In vitro* cytocompatibility of the cell-laden AME-loaded hydrogels. **A.** Microscopic images from HDFs morphology treated with different CM and control groups. **B.** Investigation of cell viability using MTT assay at 12, 48, and 72 hours timepoints. **C.** The cell number was evaluated by trypan blue at 12, 48 and 72 hours (*; P≤0.05). Data represent mean ± SEM, n=3. Ctrl-; Negative control, Ctrl+; Positive control, AME; Amniotic membrane extract, HDF; Human dermal fibroblasts, CM; Condition medium, and OD; Optical density.

Scratch assay

Cell migration is a key stage in facilitating the healing process during all phases of wound healing. Therefore, the effects of CM on *in vitro* cell migration of HDFs was studied using scratch assay, as a mimic of *in vivo* wound closure, at 0, 3, 12, and 24 hours post-injury (Fig.4A). The microscopic images from the scratched areas of the wells showed that cell migration could be observed in all groups after the 3 hours timepoint (Fig.4B). Quantitative analysis of *in vitro* wound closure illustrated that the CM3 group had the highest potential to promote cell migration compared to the other groups. According to Figure 4B, the scratched area was significantly reduced in the wells treated with CM3 group (67.1 ± 2.6%) as compared to AME (31 ± 0.8%) and CM4 groups (27.4 ± 1.3%) at 12 hours post-injury. In addition, the scratched area was significantly reduced in CM2 group (56.6 ± 0.8%) as compared to CM4 group after 12 hours. In addition, the reduction of the scratched area in CM3 group was significantly higher (96.4 ± 1.45%) than the wells treated with the negative control (62.3 ± 0.85%) and CM4 groups (71.4 ± 0.7%) after 48 hours.

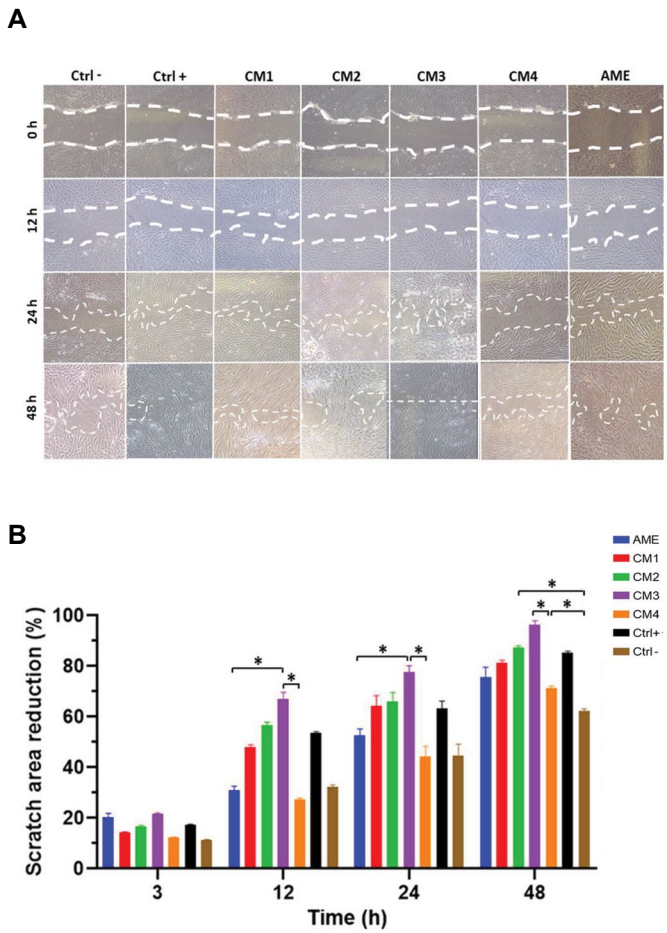

Fig.4: *In vitro* scratch assay analysis. **A.** The microscopic images illustrated different contents of migration for HDFs due to the different concentrations of AME, **B.** The amount of reduced scratched area (%) was quantified at different timepoints (*; P≤0.05). Data represent mean ± SEM, n=3. Ctrl-; Negative control, Ctrl+; Positive control, HDF; Human dermal fibroblasts, CM; Condition medium, and AME; Amniotic membrane extract,

Discussion

Combination of the cells and their signaling elements, such as GFs, on an engineered platform creates biological constructs that actively regenerate tissue (15). Previous research has shown that allogenic fibroblasts loaded into hydrogel scaffolds may provide an out-of-shelf skin substitute. Meanwhile, to have an effective cell-therapy product with this

strategy is less promising, because cryopreservation of the cells reduces viability of the cells by almost 50% and inhibits protein production by 70-98% (11, 28). Furthermore, both the time-consuming process for production of the cell-based skin substitutes and their long-term storage are both challenging (33). In state of the art, using secretory factors of cells for in situ growth and proliferation of the cells in the wound bed, to promote healing of the injured tissue may be an effective alternative method. Therefore, researchers have shifted to load the CM obtained from the fibroblasts, human umbilical cord perivascular cells (34) and adipose tissue-derived mesenchymal stem cell (35) into 3D scaffolds and probe their healing efficacy to develop new skin substitutes. In this line, it has been shown that fibroblast cells are capable of producing more GFs under the effect of exogenous GFs, which control proliferation and migration of the cells in a wound microenvironment (36).

AME contains biological components and cytokine cocktail that are effective in the wound healing process (37). We recently indicated that the presence of AME in the culture medium promotes proliferation of fibroblasts and corneal epithelium (28, 29). In this study, we aimed to investigate the effects of AME on proliferation and migration of encapsulated fibroblasts into a collagen hydrogel to optimize the effective concentration of AME for use in next-generation AME-loaded cell-based products. For this aim, cell-laden, AME-loaded collagen hydrogels were prepared through simultaneous loading of AME and fibroblasts into a collagen hydrogel, and the paracrine effect of AME on protein synthesis of the HDFs was examined. Additionally, we analyzed the secretory factors released from resulting hydrogel. The results revealed that the amount of nearly all GFs secreted in CM, which promote the growth and proliferation of the fibroblasts (38), increased by increasing the AME concentration from 0.1 mg/mL to 1.5 mg/mL. Iijima et al. (36) reported that fibroblasts produce higher amounts of VEGF and HGF when they are laminated with a membrane containing EGF at a concentration of 0.1 to 0.2 $\mu g/cm^2$ compared to a membrane treated with 0.5 $\mu g/cm^2$ of EGF. In addition, other researchers have shown that the CM, as a pool of secretory factors released from AME-loaded hydrogel, can promote regeneration of a damaged tissue by inducing proliferation, migration, angiogenesis, biosynthesis and ECM remodeling (34, 35). Likewise, our results showed that the concentration of type I collagen, which is a component of the skin ECM, increased in fibroblasts treated with different concentrations of AME (0.1-1.5 mg/mL). The ECM formation promotes proper communication between fibroblasts and it facilitates formation and maintenance of hair follicles, sweat glands, and nerves and vessels (39, 40).

Similar to recent research findings, we found that the CM extracted from cell-laden AME-loaded collagen hydrogel can stimulate proliferation and migration of the HDFs. Based on the results of MTT assay, proliferation of HDFs treated with the CM3 group were obvious compared to the cells that were treated with either CM4 or the control groups. The results of both viability and scratch assays on the CM-treated HDFs well demonstrated that proliferation and migration of the HDFs were both concentration- and time-dependent (28, 34). The best results for fibroblast migration were observed for the cells treated with 1 mg/mL of AME (CM3) group. It was also observed that HDFs treated with CM1-CM3 groups had a significant increase in proliferation compared to the CM4 group after 24 and 48 hours. Also, the number of live HDFs treated with CM1-CM3 groups during 48-72 hours showed a significant increase compared to the negative control group. However, we found that the higher concentrations of AME (< 1 mg/mL) is inappropriate for the cells, consistent with our previous results (26), which may be due to the accumulation of proliferative cytokines in CM4 group and further apoptosis of the cells. Based on our results, the concentration of 1 mg/mL of AME as an exogenous promoting substance for proliferation and migration of the HDFs was selected as the optimum concentration to be used for healing of the injured skin tissue for future studies.

Conclusion

This study was performed to pursue the *in vitro* effects of different concentrations of AME on biological factors that can be released from the cell-laden hydrogels, as well as the effects of secreted materials in CM on cell proliferation and migration. The results of this study indicated that the contents of GFs (EGF, KGF, VEGF and HGF) and the structural protein (type I collagen) secreted from the cell-laden AME-loaded collagen hydrogel may be increased in the presence of AME (0.1-1 mg/mL). The *in vitro* analyses revealed that the prepared CM from the cell-laden AME-loaded hydrogels increases proliferation and migration of fibroblasts. In this regard, the CM3 group (containing the AME and HDFs in concentrations of 1 mg/mL and 10^6 cell/mL, respectively) showed the greatest effect on secretion of GFs and collagen, as well as on proliferation and migration of the fibroblasts compared to the other groups. Our results showed that the cell-laden hydrogels reinforced by AME are potentially better solutions as pharmaceutical formulation for clinical use. However, advanced research, including *in vivo* evaluations must be performed before this new strategy could be introduced to the clinic.

Acknowledgments

This study was sponsored by the Faculty of Basic

Sciences and Modern Medical Technologies, Royan Research Institute, Tehran, Iran. The authors are grateful to the Royan Cord blood bank for their assistance in this research. Department of Tissue Engineering, School of Advanced Technologies in Medicine, Royan Institute, Tehran, Iran for Grant-in-Aid for Scientific Research. The authors report no conflicts of interest.

Authors' Contributions

M.A.A.; Protocol designed, conducted the experiments, and wrote the first draft of the manuscript. N.Sh.A.; Sample preparation and analyzed data. A.S.; Re-analyzed the statistical data and results. M.E., H.D.; Supervised the project and edited the manuscript. All authors read and approved the final manuscript.

References

1. Erickson JR, Echeverri K. Learning from regeneration research organisms: the circuitous road to scar free wound healing. Dev Biol. 2018; 433(2): 144-154.
2. Yamakawa S, Hayashida K. Advances in surgical applications of growth factors for wound healing. Burns Trauma. 2019; 7: 10.
3. Barrientos S, Stojadinovic O, Golinko MS, Brem H, Tomic-Canic M. Growth factors and cytokines in wound healing. Wound Repair Regen. 2008; 16(5): 585-601.
4. Gainza G, Villullas S, Pedraz JL, Hernandez RM, Igartua M. Advances in drug delivery systems (DDSs) to release growth factors for wound healing and skin regeneration. Nanomedicine. 2015; 11(6): 1551-1573.
5. Blitstein-Willinger E. The role of growth factors in wound healing. Skin Pharmacol Physiol. 1991; 4(3): 175-182.
6. Park JW, Hwang SR, Yoon IS. Advanced growth factor delivery systems in wound management and skin regeneration. Molecules. 2017; 22(8): 1259.
7. Behm B, Babilas P, Landthaler M, Schreml S. Cytokines, chemokines and growth factors in wound healing. J Eur Acad Dermatol Venereol. 2012; 26(7): 812-820.
8. Helary C, Zarka M, Giraud-Guille MM. Fibroblasts within concentrated collagen hydrogels favour chronic skin wound healing. J Tissue Eng Regen Med. 2012; 6(3): 225-237.
9. Motamed S, Taghiabadi E, Molaei H, Sodeifi N, Hassanpour SE, Shafieyan S, et al. Cell-based skin substitutes accelerate regeneration of extensive burn wounds in rats. Am J Surg. 2017; 214(4): 762-769.
10. Snyder DL, Sullivan N, Schoelles KM. Skin substitutes for treating chronic wounds. Rockville (MD): Agency for Healthcare Research and Quality (US); 2012.
11. Sharma P, Kumar A, Dey AD, Behl T, Chadha S. Stem cells and growth factors-based delivery approaches for chronic wound repair and regeneration: a promise to heal from within. Life Sci. 2021; 268: 118932.
12. Hur W, Lee HY, Min HS, Wufuer M, Lee CW, Hur JA, et al. Regeneration of full-thickness skin defects by differentiated adipose-derived stem cells into fibroblast-like cells by fibroblast-conditioned medium. Stem Cell Res Ther. 2017; 8(1): 92.
13. Wong T, McGrath JA, Navsaria H. The role of fibroblasts in tissue engineering and regeneration. BJD. 2007; 156: 1149-1155.
14. Kubo K, Kuroyanagi Y. A study of cytokines released from fibroblasts in cultured dermal substitute. Artif Organs. 2005; 29(10): 845-849.
15. Yildirimer L, Thanh NT, Seifalian AM. Skin regeneration scaffolds: a multimodal bottom-up approach. Trends Biotechnol. 2012; 30(12): 638-648.
16. Boateng J, Catanzano O. Advanced therapeutic dressings for effective wound healing--a review. J Pharm Sci. 2015; 104(11): 3653-3680.
17. Eming SA, Martin P, Tomic-Canic M. Wound repair and regeneration: mechanisms, signaling, and translation. Sci Transl Med. 2014; 6(265): 265sr6.
18. Koizumi N, Inatomi T, Sotozono C, Fullwood NJ, Quantock AJ, Kinoshita S. Growth factor mRNA and protein in preserved human amniotic membrane. Curr Eye Res. 2000; 20(3): 173-177.
19. Elkhenany H, El-Derby A, Abd Elkodous M, Salah RA, Lotfy A, El-Badri N. Applications of the amniotic membrane in tissue engineering and regeneration: the hundred-year challenge. Stem Cell Res Ther. 2022; 13(1): 8.
20. Mahmoudi-Rad M, Abolhasani E, Moravvej H, Mahmoudi-Rad N, Mirdamadi Y. Acellular amniotic membrane: an appropriate scaffold for fibroblast proliferation. Clin Exp Dermatol. 2013; 38(6): 646-651.
21. Sadeghi A, Zare-Gachi M, Najjar-Asl M, Rajabi S, Fatemi MJ, Forghani SF, et al. Hybrid gelatin-sulfated alginate scaffolds as dermal substitutes can dramatically accelerate healing of full-thickness diabetic wounds. Carbohydr Polym. 2022: 120404.
22. Sahraneshin-Samani F, Kazemi-Ashtiani M, Karimi H, Shiravandi A, Baharvand H, Daemi H. Regioselective sulfated chitosan produces a biocompatible and antibacterial wound dressing with low inflammatory response. Biomater Adv. 2022; 139: 213020.
23. Sangwan VS, Basu S. Antimicrobial properties of amniotic membrane. Br J Ophthalmol. 2011; 95(1): 1-2.
24. Zheng Y, Zheng S, Fan X, Li L, Xiao Y, Luo P, et al. Amniotic epithelial cells accelerate diabetic wound healing by modulating inflammation and promoting neovascularization. Stem Cells Int. 2018; 1082076.
25. Azimi Alamouti M, Shayan N, Momeni M, Nouri M, Koohkan A, Hajizadeh-Saffar E, et al. Investigation on the safety of amniotic membrane extracts in improving diabetic foot ulcers (phase 1 clinical trial study). Iran J Endocrinol Metab. 2019; 18(3): 126-134.
26. Momeni M, Zarehaghighi M, Hajimiri M, Khorasani G, Dinarvand R, Nekookar A, et al. In vitro and in vivo investigation of a novel amniotic-based chitosan dressing for wound healing. Wound Repair Regen. 2018; 26(1): 87-101.
27. Asl NS, Nejat F, Mohammadi P, Nekoukar A, Hesam S, Ebrahimi M, et al. Amniotic membrane extract eye drop promotes limbal stem cell proliferation and corneal epithelium healing. Cell J. 2019; 20(4): 459-468.
28. Zaulyanov L, Kirsner RS. A review of a bi-layered living cell treatment (Apligraf) in the treatment of venous leg ulcers and diabetic foot ulcers. Clin Interv Aging. 2007; 2(1): 93-98.
29. Hadjizadeh A, Doillon CJ. Directional migration of endothelial cells towards angiogenesis using polymer fibres in a 3D co-culture system. J Tissue Eng Regen Med. 2010; 4(7): 524-531.
30. Sarrigiannidis SO, Rey JM, Dobre O, González-García C, Dalby MJ, Salmeron-Sanchez M. A tough act to follow: collagen hydrogel modifications to improve mechanical and growth factor loading capabilities. Mater Today Bio. 2021; 10: 100098.
31. Cen R, Wang L, He Y, Yue C, Tan Y, Li L, et al. Dermal fibroblast migration and proliferation upon wounding or lipopolysaccharide exposure is mediated by stathmin. Front Pharma. 2021; 12: 781282.
32. Yeh MK, Liang YM, Cheng KM, Dai NT, Liu CC, Young JJ. A novel cell support membrane for skin tissue engineering: Gelatin film cross-linked with 2-chloro-1-methylpyridinium iodide. Polymer (Guildf). 2011; 52(4): 996-1003.
33. Maarof M, Mh Busra MF, Lokanathan Y, Bt Hj Idrus R, Rajab NF, Chowdhury SR. Safety and efficacy of dermal fibroblast conditioned medium (DFCM) fortified collagen hydrogel as acellular 3D skin patch. Drug Deliv Transl Res. 2019; 9(1): 144-161.
34. Kim MH, Wu WH, Choi JH, Kim JH, Hong SH, Jun JH, et al. Conditioned medium from the three-dimensional culture of human umbilical cord perivascular cells accelerate the migration and proliferation of human keratinocyte and fibroblast. J Biomater Sci Polym Ed. 2018; 29(7-9): 1066-1080.
35. Kraskiewicz H, Hinc P, Krawczenko A, Bielawska-Pohl A, Paprocka M, Witkowska D, et al. HATMSC secreted factors in the hydrogel as a potential treatment for chronic wounds-in vitro study. Int J Mol Sci. 2021; 22(22): 12241.
36. Iijima E, Daichi Toyoda D, Yamamoto A, Kuroyanagi M, Yoshimitsu Kuroyanagi Y. In vitro analysis of VEGF and HGF production by fibroblast in cultured dermal substitute combined with

eEFG-incorporating top dressing. Open J Regen Med. 2014; 3(1): 13-21.
37. Chopra A, Thomas BS. Amniotic membrane: a novel material for regeneration and repair. J Biomim Biomater Tissue Eng. 2013: 18(1): 1000106.
38. Anitua E, Pino A, Orive G. Plasma rich in growth factors promotes dermal fibroblast proliferation, migration and biosynthetic activity. J Wound Care. 2016; 25(11): 680-687.
39. Murphy SV, Skardal A, Song L, Sutton K, Haug R, Mack DL, et al. Solubilized amnion membrane hyaluronic acid hydrogel accelerates full-thickness wound healing. Stem Cells Transl Med. 2017; 6(11): 2020-2032. 8(8(12): 2083. 8(12): 2083.
40. Urciuolo F, Casale C, Imparato G, Netti PA. Bioengineered Skin substitutes: the role of extracellular matrix and vascularization in the healing of deep wounds. J Clin Med. 2019; 8(12): 2083.

Cell J
Cell Journal(Yakhteh)
Homepage: https://www.celljournal.org/
Original Article
Vol 25, No 4, April 2023, Pages: 264-272

Down-Regulation of CEND1 Expression Contributes to The Progression and Temozolomide Resistance of Glioma

Zhou Houjun, M.D., Bai Peng, M.D.*

Neurosurgery Department 2, The Affiliated Hospital of Kunming Medical University, Kunming, Yunnan, China

Abstract

Objective: This study was conducted to clarify the expression characteristics of cell cycle exit and neuronal differentiation 1 (CEND1) in glioma and its effects on the proliferation, migration, invasion, and resistance to temozolomide (TMZ) of glioma cells.

Materials and Methods: In this experimental study, CEND1 expression in glioma tissues and its relationship with patients' survival were analyzed through bioinformatics. Quantitative real-time polymerase chain reaction (qRT-PCR) and immunohistochemistry were performed to detect CEND1 expression in glioma tissues. The cell counting kit-8 (CCK-8) method was adopted to detect cell viability and the effects of different concentrations of TMZ on the inhibition rate of glioma cell proliferation, and the median inhibitory concentration of TMZ (IC_{50} value) was calculated. 5-Bromo-2'-deoxyuridine (BrdU), wound healing and Transwell assays were performed to evaluate the impacts of CEND1 on glioma cell proliferation, migration, and invasion. Besides, the Kyoto Encyclopedia of Genes and Genomes (KEGG) analysis, Gene Ontology (GO) analysis, and Gene Set Enrichment Analysis (GSEA) were applied to predict the pathways regulated by CEND1. Nuclear factor-kappa B p65 (NF-κB p65) and phospho-p65 (p-p65) expression were detected by Western blot.

Results: CEND1 expression was reduced in glioma tissues and cells, and its low expression was significantly associated with the shorter survival of glioma patients. CEND1 knockdown promoted glioma cell growth, migration, and invasion, and increased the IC50 value of TMZ, whereas up-regulating CEND1 expression worked oppositely. Genes co-expressed with CEND1 were enriched in the NF-κB pathway, and knocking down CEND1 facilitated p-p65 expression, while CEND1 overexpression suppressed p-p65 expression.

Conclusion: CEND1 inhibits glioma cell proliferation, migration, invasion, and resistance to TMZ by inhibiting the NF-κB pathway.

Keywords: CEND1, Glioma, Proliferation, Temozolomide

Citation: **Houjun Z, Peng B. Down-regulation of CEND1 expression contributes to the progression and temozolomide resistance of glioma. Cell J. 2023; 25(4): 264-272. doi: 10.22074/CELLJ.2022.557567.1074.**

Introduction

Glioma is a common neurological malignancy, and glioma cases account for 60% of all intracranial tumors (1, 2). Up till now, the treatment options for glioma include surgery, radiotherapy, and chemotherapy, which improve the prognosis of some glioma patients (3). However, due to the biological characteristic of invasive growth of glioma, glioma has a high recurrence rate; the patients' prognosis is still unfavorable (4, 5). With the application of the first-line chemotherapeutic drug temozolomide (TMZ), a growing number of glioma patients have become resistant to TMZ (6). In this context, an in-depth exploration into the drug resistance mechanism of TMZ is highly significant for improving the prognosis of glioma patients.

Cell cycle exit and neuronal differentiation (CEND1) is a specific transmembrane protein highly expressed in the brain and mainly located on the organelle membranes such as the endoplasmic reticulum membrane and mitochondrial outer membrane; reportedly, it regulates the differentiation of neuronal precursors (7, 8). The defect of CEND1 causes impaired cerebellar development and motor coordination disorder in mice (9). Besides, CEND1 can terminate the cell cycle progression and trigger the differentiation of neurons (10). The role of CEND1 in tumors has also been reported. In invasive breast cancer, it is revealed that CEND1 expression is epigenetically inhibited by methylation, which indicates that CEND1 may play a tumor-suppressive role ininvasive breast cancer (11). However, the expression characteristics and biological functions of CEND1 in glioma remain unclear.

In this study, bioinformatics analysis indicated that CEND1 expression in glioma tissues was significantly reduced and was linked to the patient's poor prognosis. We investigated the expression pattern of CEND1 in

Received: 11/July/2022, Revised: 22/August/2022, Accepted: 15/December/2022
***Corresponding Address: Neurosurgery Department 2, The Affiliated Hospital of Kunming Medical University, Kunming, Yunnan, China**
Email: sggg78351@163.com

Royan Institute
Cell Journal (Yakhteh)

gliomas, its biological functions, and its underlying mechanism.

Materials and Methods

Clinical samples

From January 2015 to January 2018, 40 cases of tumor samples (glioma) and 20 cases of normal brain tissue (NBT) samples were collected from glioma patients. All tissues, after being surgically removed, were frozen in liquid nitrogen. Every patient signed the informed consent form prior to the surgery. The diagnoses of glioma were histologically confirmed by three independent pathologists. The study got the approval of the Ethics Committee of the Affiliated Hospital of Kunming Medical University (SCXK(Dian)K2019-0004).

Cell culture and transfection

From the Type Culture Collection of the Chinese Academy of Sciences (Shanghai, China), glioma cell lines (U251, U251/TMZ, U87, and U87/TMZ) and normal human brain astrocyte cell line (HEB) were obtained. U251/TMZ and U87/TMZ were glioma cells that were resistant to TMZ treatment. All the cells were cultured in Dulbecco's modified Eagle's medium (DMEM, Invitrogen, Carlsbad, CA, USA) containing 10% fetal bovine serum (FBS), 100 U/ml penicillin and 100 µg/ml streptomycin (Invitrogen, Carlsbad, CA, USA) at 37˚C in 5% CO_2 and 100% humidity. CEND1 overexpression plasmid was constructed via cloning the cDNA of the CEND1 sequence into the pcDNA3.1 vector (GenePharma Co., Ltd., Shanghai, China). And the empty pcDNA3.1 vector was used as a negative control (NC). Small interfering RNA (siRNA) normal control (si-NC: 5′-AGGCCAGCGTCTTCCACTCACCCAA-3′) and siRNAs targeting CEND1 (si-CEND1#1: 5′-AGGCCGACCCTGCCCTTCTCAACAA-3′ and si-CEND1 #2: 5′-GACCCTGCCCTTCTCAACAACCACA-3′) were constructed with the Silencer™ siRNA Construction Kit (Ambion, Austin, TX, USA) according to the manufacturer's instructions. Glioma cells were transferred into 6-well plates (3×10^5 cells/well) and cultured for 24 hours with a serum-free medium. After that, cell transfection was performed employing Lipofectamine® 2000 (Invitrogen, Thermo Fisher Scientific, Inc.) following the supplier's instructions. After 24 hours, the serum-free medium was replaced by a complete medium, followed by the culture for 24 hours. Quantitative real-time polymerase chain reaction (qRT-PCR) was performed to detect the transfection efficiency.

Quantitative real-time polymerase chain reaction

Glioma tissues and cells were harvested, and total RNA was extracted using TRIzol reagent (Invitrogen, Shanghai, China). A NanoDrop1000 spectrophotometer (NanoDrop Technologies LLC, DE, USA) was employed to detect the concentration and purity of RNA. A TaKaRa Reverse Transcription Kit (TaKaRa Inc., Japan) was utilized to reversely transcribe RNA into cDNA. The cDNA, as the template, was mixed with SYBR Premix Eaq™ II (Takara, Dalian, China), primers, and DEPC water, and then the amplification was performed. The following are the primer sequences:

CEND1-
F: 5′-ATGGAATCCCGAGGAAAGTCA-3′
R: 5′-GCCTGAGGCACCTTGGTATC-3′

GAPDH-
F: 5′-CATGGGTGTGAACCATGAGA-3′
R: 5′-CAGTGATGGCATGGACTGTG-3′.

The $2^{-\Delta\Delta Ct}$ method was used for the calculation of the relative expression of *CEND1*, with *GAPDH* as the endogenous control.

Immunohistochemistry

The histological sections of the glioma were baked at 56˚C for 2 hours before being deparaffinized and rehydrated. Subsequently, antigen retrieval was performed, and the sections were blocked in 3% bull serum albumin for 30 minutes. After that, the sections were incubated with the primary Recombinant Anti-CEND1 antibody (ab113076, 1:500, Abcam, Shanghai, China) at 4˚C overnight in a wet box. On the second day, the sections were incubated with the secondary Goat anti-rabbit IgG H&L antibody (ab150077, 1:1000, Abcam, Shanghai, China) at room temperature for 30 minutes in a wet box. Then, the sections were stained with diaminobenzidine and observed under a microscope. The color development was terminated after the color or the tissues turned brown. Eventually, the sections were sealed with neutral gum. The images were analyzed with the Image-Pro Plus 6.0 software, and the intensity of staining and the percentage of stained cells were evaluated and quantified by three independent pathologists. IHC score was calculated based on the staining intensity score (0, no staining; 1, weak staining; 2, moderate staining; and 3, intense staining) and the proportion score (0, no staining; 1, 1-25% of the tumor cells were stained; 2, 26-50%; 3, 51-75%; and 4, more than 75% of the tumor cells were stained). IHC score=staining intensity score × proportion score. IHC score was used to evaluate the expression of CEND1: 0-3 points, negative; 4-7 points, weakly positive; 8-12 points, strongly positive.

Cell counting kit-8 assay

U251/TMZ and U87/TMZ cells during the logarithmic growth phase were transferred to 96-well plates (5×10^3 cells/well), with 3 replicate wells in each group. After culturing cells in the incubator for 3 hours, different concentrations of TMZ (0, 1, 5, 10, 20, 40, and 60 µmol/L) were added, with 3 parallel wells in each group. After another 24 hours, the cells were incubated with 10 µL of CCK-8 reagent (Beyotime Biotechnology, Shanghai, China) for 2 hours. An automatic microplate reader was

used to measure the absorbance (OD) of the cells in each well at 450 nm wavelength. The following equation is for calculating cell survival rate and the inhibition rate of the drug on cells: cell survival rate (%)=(control group OD value-drug group OD value)/control group OD value. Ultimately, SPSS 22.0 software (SPSS Inc.,Chicago, IL, USA) was adopted to calculate the median inhibitory concentration of the drug (IC_{50} value).

5-bromo-2'-deoxyuridine assay

U87/TMZ and U251/TMZ cells were transferred to 24-well plates. After the cells were cultured in serum-free medium for 24 hours, the cells were incubated with 10 μmol/L of BrdU solution (Beyotime, Shanghai, China) in a complete medium for 4 hours at 37°C. After the medium was removed, the cells were rinsed 3 times with phosphate buffer saline (PBS), fixed with 70% ethanol for 10 minutes at 4°C, and then washed 3 times with PBS. Then, 2 mol/L of HCl was added to denature the cellular DNA at 37°C for 60 minutes before the cells were washed 3 times with PBS. After that, the cells were blocked with 3% bovine serum albumin (KPL, Gaithersburg, MD, USA) at room temperature for 1 hour, followed by the rinse with PBS 3 times, 5 minutes for each time. Subsequently, the cells were incubated overnight at 4°C with anti-BrdU monoclonal antibody (ab8152, 1:300, Abcam, Shanghai, China) and then with goat anti-mouse fluorescent secondary Goat Anti-Mouse IgG H&L antibody (ab150113, 1:1000, Abcam, Shanghai, China) at room temperature for 2 hours. After counterstaining the cell nucleus with DAPI, the cells were observed under a fluorescence microscope. In 10 randomly selected non-overlapping fields, the number of BrdU-positive cells was counted, and the average was calculated.

Scratch wound healing assay

After the confluency of U251/TMZ and U87/TMZ cells cultured in a 6-well plate reached about 90%, the cells were scratched with a sterile pipette tip and then cultured with serum-free medium. The width of the scratch was observed at 0 and 24 hours, respectively. Scratch wound healing rate=(scratch width 0 hour after scratching-scratch width 24 hours after scratching)/scratch width 0 hour after scratching×100%.

Transwell assays

The density of cell suspension was diluted to 1×10^5 cells/ml with a serum-free medium. The upper compartment of the Transwell chamber (Corning, NY, USA) was added with 200 μL of cell suspension, and 500 μL of complete medium was added to the lower compartment. After 24 hours, the cells in the upper compartment were wiped off with cotton swabs, and the cells attaching to the below surface of the membrane were washed twice with PBS and then fixed with paraformaldehyde for 30 minutes. Subsequently, the cells were stained for 30 minutes with 0.1% crystal violet, followed by being washed with PBS. Under an inverted microscope (DMI4000, Leica, Germany), the number of cells passing through the membrane was counted, and the cells were photographed. Three random fields were observed, and the average of the cell number was calculated. Matrigel-coated Transwell chamber was used in the invasion assay, and the remaining steps were the same as those in the migration assay.

Western blot

For each sample, 100 mg of glioma tissues or 2×10^7 cells were added to 1 ml of RIPA lysis buffer (Pierce, Rockford, IL, USA). The tissue or cells were lysed on the ice for 30 minutes. Next, the total cell protein was extracted, and a BCA kit (Rockford, IL, USA) was applied for determining the protein concentration. The protein, after electrophoresis, was transferred to the polyvinylidene fluoride (PVDF) membranes (Millipore, Billerica, MA, USA), and the membranes were then blocked with 5% skimmed milk for 1 hour at room temperature. Subsequently, the membranes were incubated with primary antibodies at 4°C overnight and then with secondary Goat Anti-Rabbit IgG H&L antibody (HRP) (ab6721, 1:5000) for 2 hours at room temperature. Besides, the protein bands were detected by a Bio-Rad chemiluminescence apparatus (Bio-Rad, Berkeley, CA, USA), with GAPDH as the internal control, and the Image J software was used for the quantitative analysis of the protein bands. The primary antibodies included: the anti-nuclear factor-kappa B p65 (NF-κB p65) antibody (ab32536, 1:2000) and the anti-phospho-p65 (p-p65) antibody (ab97726, 1:2000). All antibodies were bought from Abcam (Shanghai, China).

Statistical analysis

The statistical analysis was conducted employing SPSS 21.0 software (SPSS Inc., Chicago, IL, USA). All the experiments were repeated 3 times. All measurement data were expressed by "mean ± standard deviation". The comparison between the two groups was performed with the t test. $P<0.05$ represented that a difference was of statistical significance.

Results

CEND1 expression is downregulated in glioma tissues and cell lines

First of all, GEPIA (http://gepia.cancer-pku.cn/) and UALCAN (http://ualcan.path.uab.edu/cgi-bin/ualcan-res.pl) databases were utilized to analyze CEND1 expression in glioma, and it was revealed that CEND1 expression was downregulated in both low-grade glioma and glioblastoma (Fig.1A, B). Moreover, the GEPIA database indicated that low CEND1 expression was also linked to the shorter overall survival of the patients (Fig.1C). Additionally, qRT-PCR was performed to detect the CEND1 mRNA expression in 20 cases of NBT samples and 40 cases of glioma tissue samples, and it was shown that CEND1 mRNA expression was significantly upregulated in glioma tissues (Fig.1D). Furthermore,

CEND1 protein expression in glioma tissues was detected by IHC, the results of which showed that there was a lower positive rate of CEND1 protein expression in the glioma tissues compared with NBT (P=0.044, Chi-square=4.07, Fig.1E).

The effects of CEND1 on glioma cell viability, sensitivity to TMZ, migration, and invasion

Additionally, we performed the western blot to detect the expression of CEND1 in different cell lines. It showed that the expression of CEND1 in immortalized glial cell line HMC3 was lowly expressed, while its expression in primary human neuron cells was highly expressed, and its expression was reduced in glioma cell lines (U251 and U87); the results also indicated that CEND1 expression was downregulated in U251/TMZ and U87/TMZ cells as opposed to U251 and U87 cells (Fig.2A). The expression of CEND1 was lower in U87 cells, so U87 cells were selected for subsequent CEND1 overexpression experiments; the expression of CEND1 was higher in U251 cells, so U251 cells were selected for subsequent CEND1 knockdown experiments. Western blot (Fig.2B) and immunofluorescence (Fig.2C) were performed to confirm the successful construction of the CEND1 overexpression model and CEND1 knockdown model. Since transfection with si-CEND1#2 exhibited a greater silencing effect, si-CEND1#2 was used for subsequent experiments. CCK-8 assay revealed that CEND1 knockdown markedly promoted U251/TMZ cell viability and increased the IC_{50} value of TMZ (Fig.2D), and CEND1 overexpression remarkably suppressed U251/TMZ cell viability and decreased the IC_{50} value of TMZ (Fig.2E). BrdU assay suggested that CEND1 knockdown facilitated U251/TMZ cell proliferation, and CEND1 overexpression observably inhibited U87/TMZ cell proliferation (Fig.3A, B). Scratch wound healing and Transwell assays showed that knocking down CEND1 promoted U251/TMZ cell migration and invasion, and CEND1 overexpression suppressed U87/TMZ cell migration and invasion (Fig.3C-F).

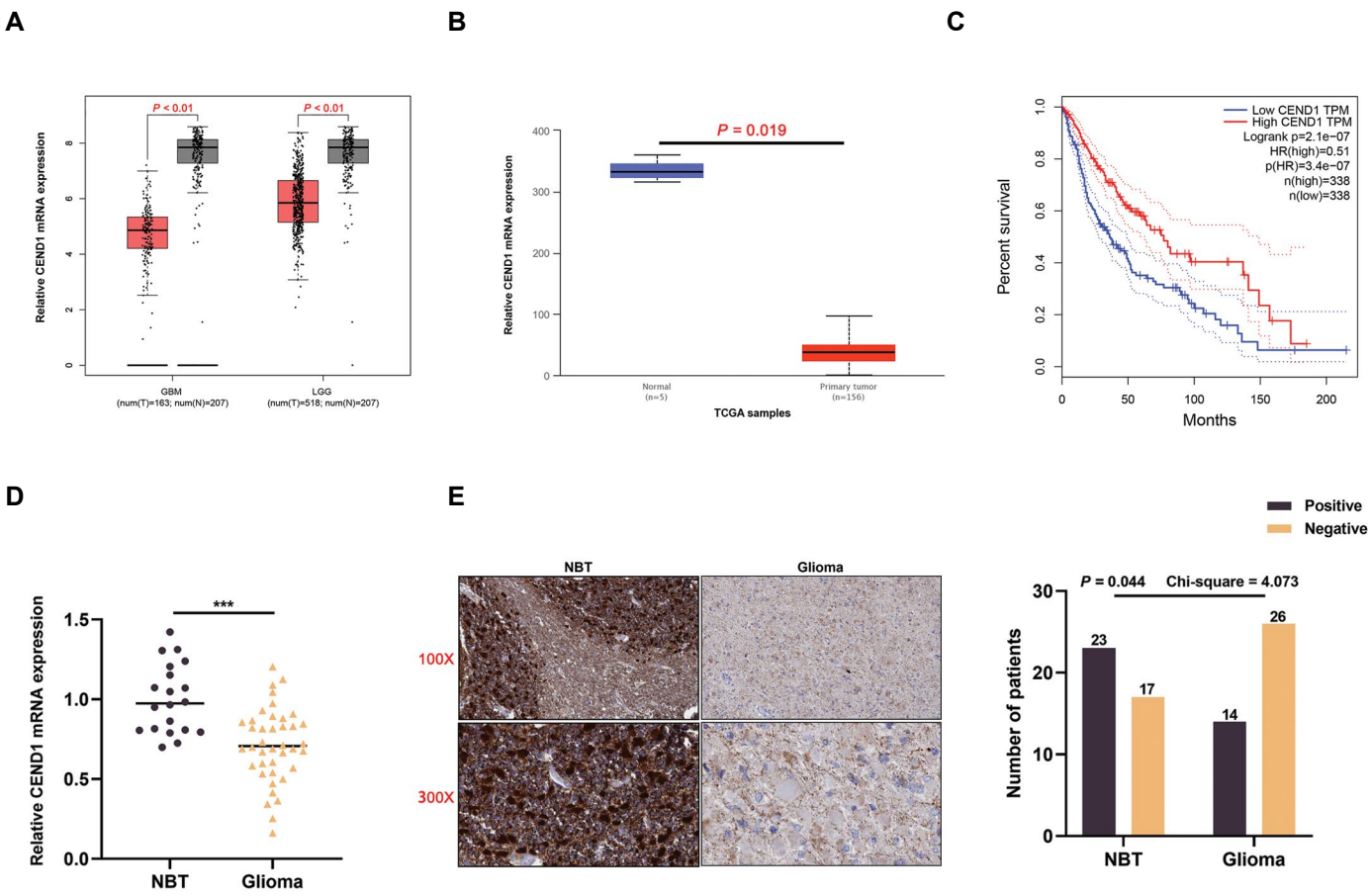

Fig.1: Expression of CEND1 in glioma tissues and cell lines. **A.** CEND1 mRNA expression in glioma tissues (red column) and normal brain tissues (grey column) was analyzed by the GEPIA database (log2|FC|>1.0 and P<0.05 as the selection criteria). **B.** CEND1 mRNA expression in glioma tissues (red column) and normal brain tissues (blue column) was analyzed by the UALCAN database (log2|FC|>1.0 and P<0.05 as the selection criteria). **C.** The relationship between CEND1 expression and the glioma patients' overall survival was analyzed by the GEPIA database. **D.** CEND1 mRNA expression in 20 NBT and 40 glioma tissues was detected by qRT-PCR. **E.** CEND1 protein expression in 20 NBT and 40 glioma tissues was detected by IHC assay. Then, the samples were diagnosed by pathologists. CEND1; Cell cycle exit and neuronal differentiation 1, ***; P<0.001, GBM; Glioblastoma multiforme, LGG; Lower grade glioma, NBT; Normal brain tissue, and qRT-PCR; Quantitative real-time polymerase chain reaction.

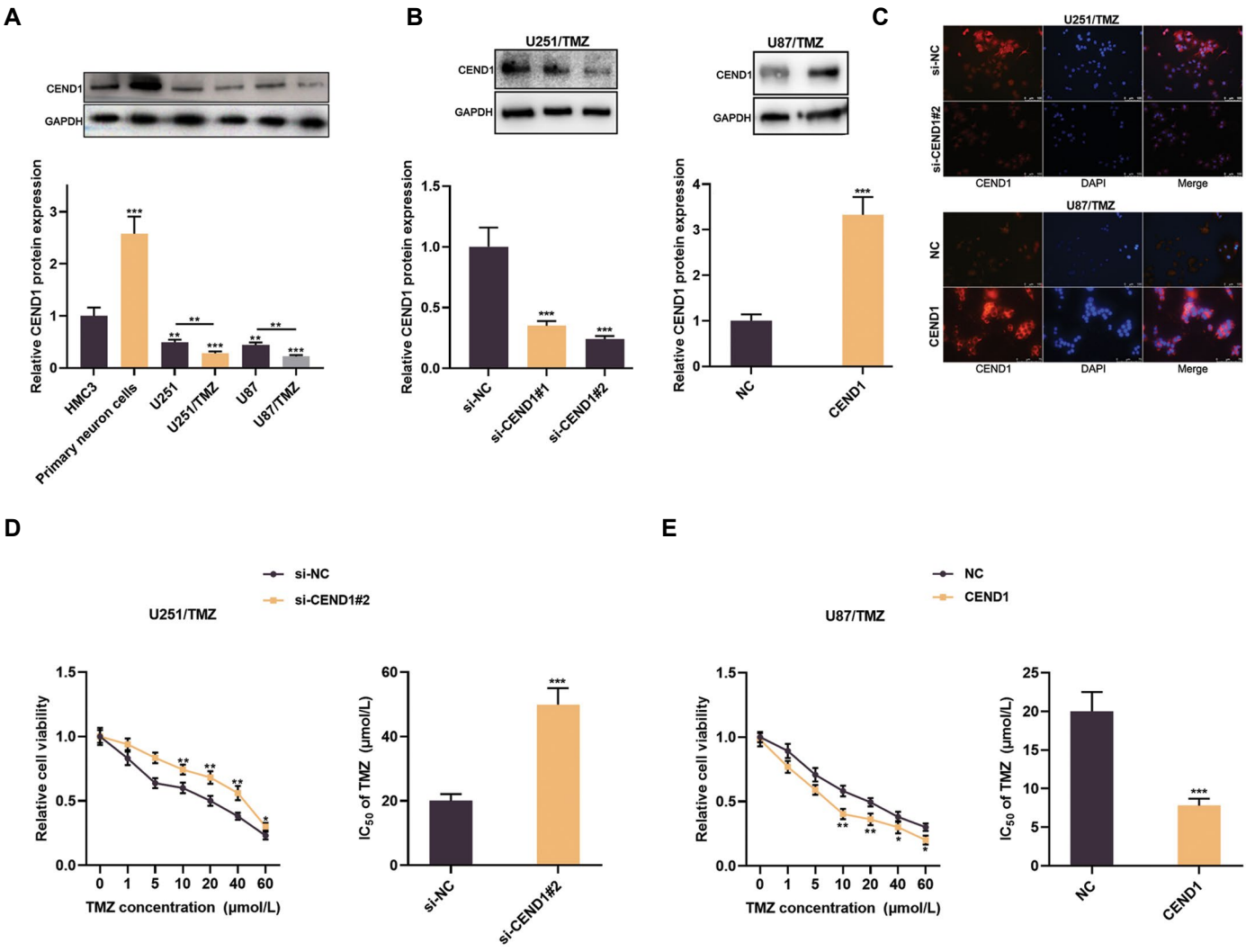

Fig.2: Effects of CEND1 on the resistance of glioma cells to TMZ. **A.** CEND1 protein expression in glioma cell lines, glial cell line HMC3, and primary neuron cells was detected by Western blot. **B, C.** After transfecting si-NC, si-CEND#1, and si-CEND#2 into U251/TMZ cells and transfecting NC and CEND1 into U87/TMZ cells, Western blot and immunofluorescence were utilized to confirm the successful construction of the CEND1 knockdown model and the CEND1 overexpression model. **D.** After transfecting si-NC or si-CEND#2 into U251/TMZ cells, the CCK-8 assay was conducted to detect the effects of knocking down CEND1 on the IC_{50} value of TMZ. **E.** After transfecting NC or CEND1 overexpression plasmid into U87/TMZ cells, the CCK-8 assay was performed to detect the effects of CEND1 overexpression on the IC_{50} value of TMZ. ***; P<0.001, CEND1; Cell cycle exit and neuronal differentiation 1, TMZ; Temozolomide, si-NC; Negative control siRNA, si-CEND1; CEND1 siRNA, and IC_{50}; Half maximal inhibitory concentration.

CEND1 knockdown activates the NF-κB pathway

To expound the downstream mechanism by which CEND1 functions in glioma, the cBioPortal database was adopted to screen the genes co-expressed with CEND1 (Spearman's $r < -0.56$, $P<0.05$) The enrichment analysis was conducted using the Kyoto Encyclopedia of Genes, Genomes (KEGG), and Gene Ontology (GO) databases. GO analysis revealed that the genes co-expressed with CEND1 were associated with multiple biological processes (BP), cellular components (CC), and molecular functions (MF), including the toll-like receptor 7 signaling pathway, SCAR complex, lamellipodium, and toll-like receptor 2 binding and so on (Fig.4A). KEGG analysis implied that the genes co-expressed with CEND1 were associated with the NF-κB pathway (Fig.4B). Then, Gene Set Enrichment Analysis (GSEA) analysis was performed using the LinkedOmics database (http://www.linkedomics.org/). The results revealed that NF-κB pathways positively correlated with low expression of CEND1 (Fig.4C). After transfected with si-NC, si-CEND1#2, control plasmids, and CEND1 overexpression plasmids for 24 hours, the U251/TMZ and U87/TMZ cells were collected and followed with the Western blot analysis. It was revealed that knocking down CEND1 enhanced p-p65 expression while up-regulating CEND1 reduced p-p65 expression in

glioma cells. Additionally, after CEND1 was depleted, the expression levels of CD133 and CD15 were up-regulated, while after CEND1 was overexpressed, those were downregulated (Fig.4D), which suggested that reduced CEND1 expression in glioma cells contributed to increased stemness of glioma cells. The aforementioned findings suggested that CEND1 could probably regulate glioma cell proliferation, migration, invasion, and sensitivity to TMZ by modulating the NF-κB pathway.

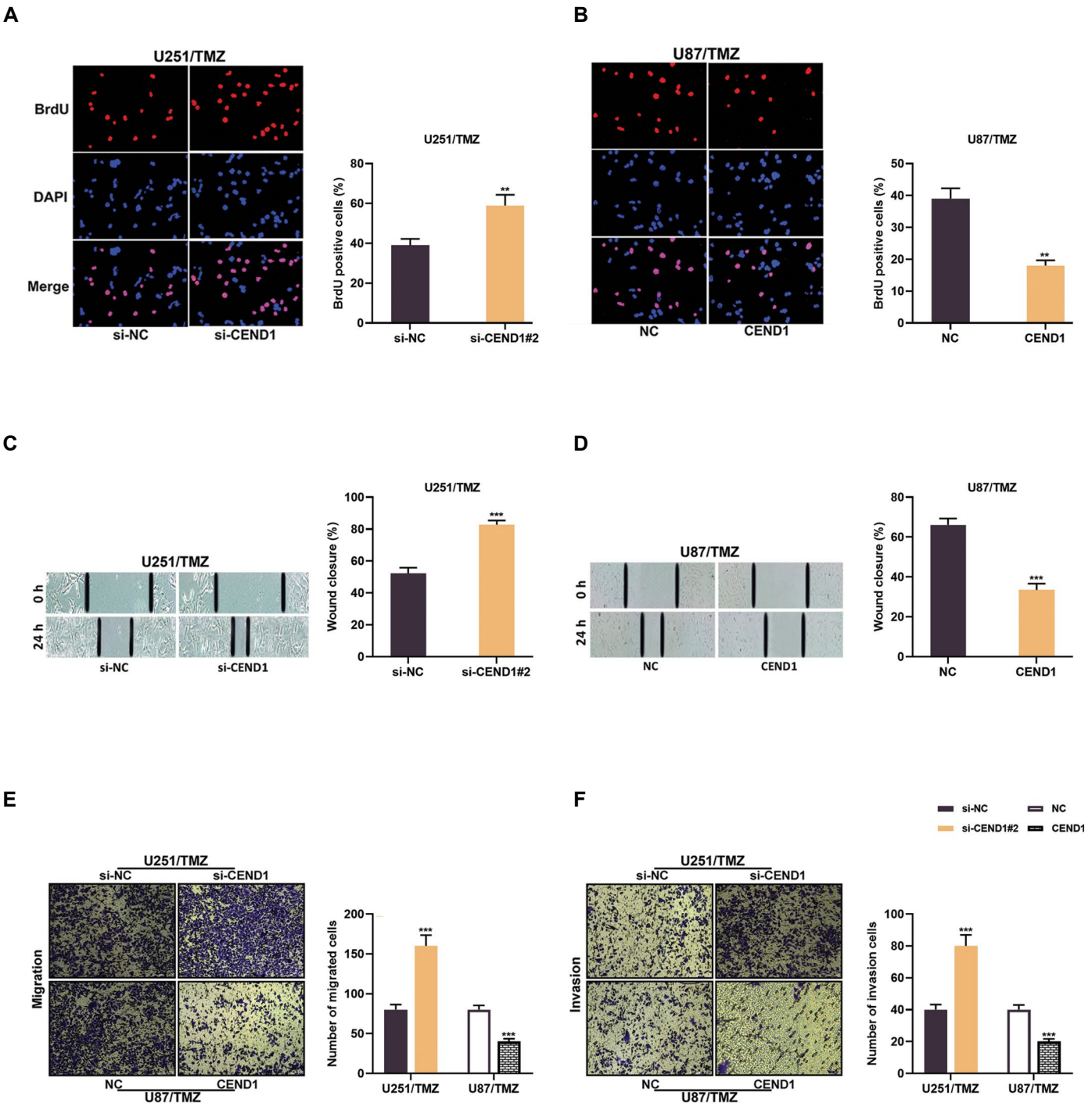

Fig.3: Effects of CEND1 on glioma cell proliferation, migration, and invasion. **A, B.** After transfecting si-NC or si-CEND#2 into U251/TMZ cells and transfecting NC or CEND1 overexpression plasmid into U87/TMZ cells, BrdU assay was performed to detect the effects of CEND1 overexpression or knockdown on U251/TMZ and U87/TMZ cell proliferation. **C, D.** A scratch wound-healing assay was conducted to detect the effects of CEND1 overexpression or knockdown on U251/TMZ and U87/TMZ cell wound healing. **E.** The effects of CEND1 overexpression or knockdown on U251/TMZ and U87/TMZ cell migration were detected by the Transwell migration assay. **F.** Transwell invasion assay was conducted to determine the effects of CEND1 overexpression or knockdown on U251/TMZ and U87/TMZ cell invasion. **; P<0.01, ***; P<0.001, CEND1; Cell cycle exit and neuronal differentiation 1, TMZ; Temozolomide, si-NC; Negative control siRNA, and si-CEND1; CEND1 siRNA.

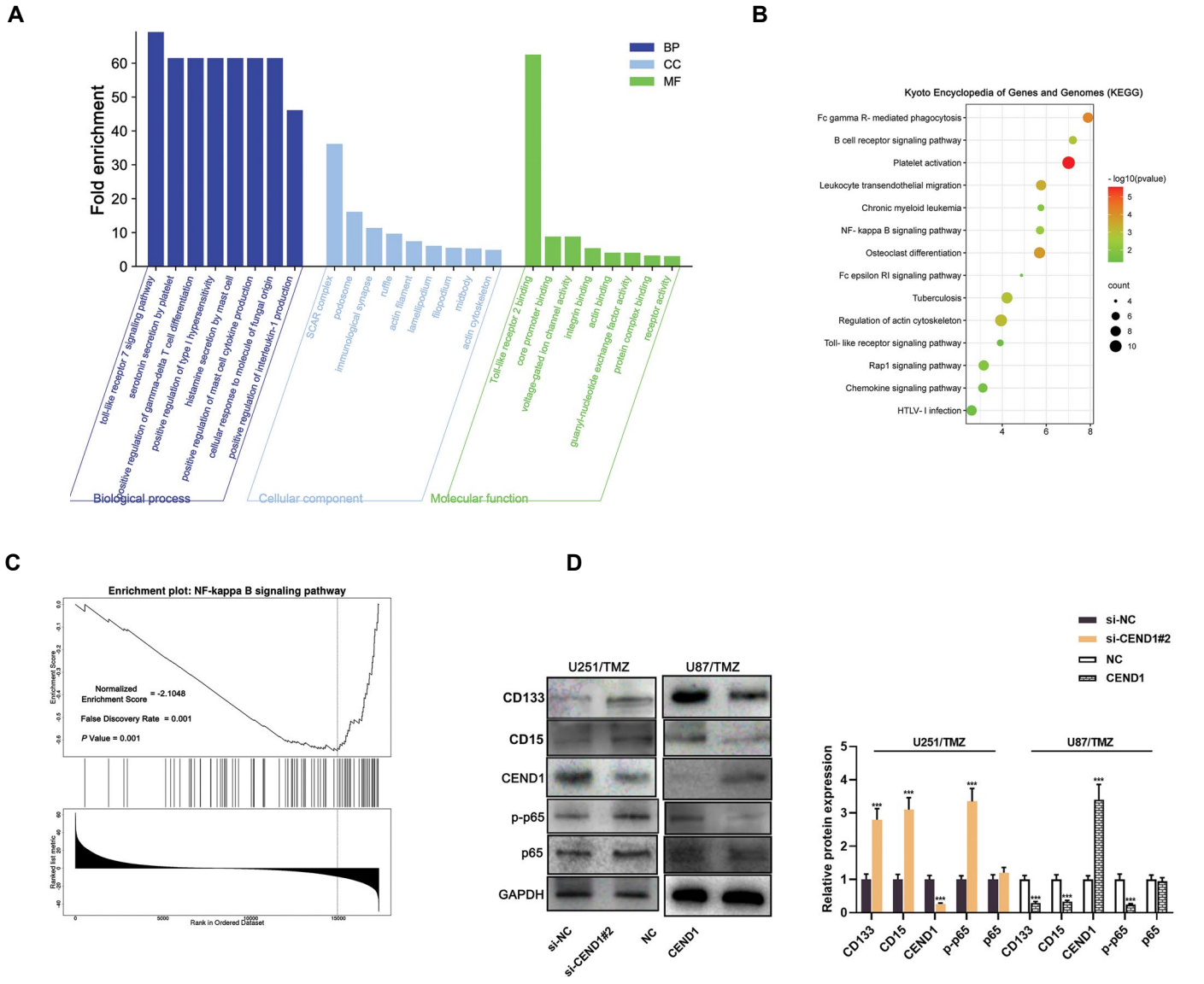

Fig.4: CEND1 knockdown can activate the NF-κB pathway. **A.** cBioPortal database was adopted to screen 200 genes that were co-expressed with CEND1 (Spearman's r<-0.56, P<0.05). The GO database was adopted to analyze the pathways in BP, CC, and MF where these genes were enriched. **B.** KEGG database was used to perform pathway enrichment analysis of these genes. **C.** Through the LinkedOmics database, CEND1 was analyzed for Gene Set Enrichment Analysis (GSEA). **D.** The effects of CEND1 knockdown or overexpression on p65, p-p65, CD133, and CD15 were detected by Western blot. ***; P<0.001, CEND1; Cell cycle exit and neuronal differentiation 1, NF-κB; Nuclear factor-kappa B, GO; Gene Ontology, BP; Biological processes, CC; Cellular components, MF; Molecular functions, TMZ; Temozolomide, si-NC; negative control siRNA, and si-CEND1; CEND1 siRNA.

Discussion

CEND1 expression is significantly elevated during the differentiation of neural precursor cells into neurons, and this process is accompanied by an increase in p53 protein expression, which suggests that CEND1 can activate the p53-p21 signaling pathway to prolong the G1 phase of the cells, thus arresting the cell cycle (10, 12, 13). It is reported that in a mouse model, after CEND1 knockdown, the proliferation of granule cell precursors is promoted, radial granule cell migration is delayed, and the differentiation of Purkinje cells is blocked (14). Some studies indicated that there are many genes involved in the development of glioma. The downregulation of ABCE1 expression significantly reduces the protein expressions of p-PI3K, p-Akt, and NF-κB in glioma cells, thus inhibiting glioma cell growth (15). CRNDE knockdown represses the expressions of LC3 II/I, Beclin1, and Atg5 and increases the p62 expression to inhibit autophagy due to the activation of PI3K/Akt/mTOR pathway, thus promoting TMZ chemosensitivity in glioma (16). In neuroblastoma, CEND1 is an important molecular target for histone deacetylase (HDAC) inhibition, and CEND1 knockdown reduces the impacts of trichostatin-A (TSA) on inhibiting tumor cell proliferation and inducing cell differentiation (17). Another study reports that the functional interaction among CEND1, RanBPM, and Dyrk1B affects the balance between the proliferation and the differentiation of neuroblastoma cells in mice; CEND1 restrains neuroblastoma cell proliferation through modulating cyclin D1 pathway (12). Consistently, our study revealed

that CEND1 probably functioned as a tumor suppressor in glioma. We demonstrated that CEND1 expression was downregulated in glioma tissues and was associated with the increased tumor grade and shorter survival time of the patients. In addition, knocking down CEND1 significantly facilitated cell multiplication, migration, and invasion, and enhanced the TMZ resistance, whereas CEND1 overexpression induced the opposite effects. The above-mentioned evidence supported that CEND1 was a potential prognostic marker for glioma patients, and the restoration of CEND1 might be a novel strategy to reduce the aggressiveness of glioma and prolong the survival of glioma patients.

Known as a kind of imidazole tetrazine derivative, TMZ is an oral alkylating agent and is distributed throughout the body without liver metabolism, and it can easily penetrate the blood-brain barrier and enter the cerebrospinal fluid to exert its pharmacologic efficacy; these properties allow TMZ to be a chemotherapy drug extensively used for glioma treatment (18-21). TMZ effectively inhibits postsurgical glioma recurrence, and it has become the first-line chemotherapy agent to treat high-grade glioma (21). TMZ transforms into the active compound 5-(3-methyltriazene-1-yl) imidazole-4-carboxamide (MTIC), thus suppressing the growth of various tumor cells and inducing apoptosis (22, 23). O6 methylguanine induced by TMZ is pivotal in the anti-tumor activity of TMZ, and the methylated guanine cannot bind to the thymine and can induce mismatch repair during DNA replication, leading to breaks of DNA, blocking DNA replication, and ultimately arresting the cells in the G2/M phase (24). The mechanism of glioma resistance to TMZ is complex, and reportedly, O-6-methylguanine-DNA methyltransferase (MGMT) mediates TMZ resistance (25). Additionally, there are some studies reporting that DNA damage repair is also implicated in TMZ resistance (26, 27). The present study revealed that CEND1 knockdown facilitated the resistance of glioma cells to TMZ while CEND1 overexpression worked oppositely. Interestingly, MGMT protein is not expressed in U87 and U251 cells (28-30), which are used in the present study, so the effects of CEND1 on TMZ chemosensitivity may not depend on the MGMT pathway.

NF-κB is first discovered in B cell extracts in 1986, and it is a nucleoprotein factor that can specifically bind to the enhancer sequence of the gene of immunoglobulin K light chain (31). The activation of NF-κB can up-regulate the expressions of multiple immune and inflammatory factors and induce an inflammatory response and other BP (32, 33). NF-κB family has 5 members: Rela (p65), RelB, C-Rel, NF-kappa B1 (p50/p105), and NF-kappa B 2 (p52/p100); they form a complex in the form of homodimers or heterodimers, among which p50/p65 heterodimer is the most important form (34). In tumorigenesis and development, p65 partakes in the regulation of gene transcription and modulates downstream target genes such as vascular endothelial growth factor (VEGF), chemokine receptors (such as CXCR4), matrix metalloproteinase 2/9, (MMP2/9), etc. (35). NF-κB is also involved in glioma progression. Specifically, lncRNA-ATB overexpression can activate the NF-κB pathway to promote the aggression of glioma cells (36). Moreover, knocking down WWP1 can activate the NF-κB pathway to increase the p65 phosphorylation expression level, thereby facilitating the malignant behaviors of glioma cells (37). The present study authenticated that CEND1 knockdown could activate NF-κB signaling, which indicated that CEND1 suppressed glioma cell proliferation and migration via regulating the NF-κB pathway.

Conclusion

To sum up, CEND1 expression is reduced in glioma and is associated with unfavorable prognosis; CEND1 overexpression inhibits the aggressiveness of glioma cells and reduces their resistance to TMZ via regulating NF-κB signaling. In the following studies, more patients are required to be enrolled to further validate the value of CEND1 as a prognostic biomarker.

Acknowledgements

We thank Hubei Yican Health Industry Co., Ltd (Wuhan, China) for its linguistic assistance during the preparation of this manuscript. This study is supported by Yunnan Provincial Scientific Research Fund Project (Approval No. 2020J0159). There is no conflict of interest in this study.

Authors' Contributions

Z.H., B.P.; Conceived, designed the experiments, performed the experiments, and wrote the manuscript. Z.H.; Analyzed the data. All authors read and approved the final manuscript.

References

1. Weller M, Wick W, Aldape K, Brada M, Berger M, Pfister SM, et al. Glioma. Nat Rev Dis Primers. 2015; 1: 15017.
2. Delgado-López PD, Corrales-García EM. Survival in glioblastoma: a review on the impact of treatment modalities. Clin Transl Oncol. 2016; 18(11): 1062-1071.
3. Tang A, Liang J, Mai Y, Sun H. Advances in research on glioma microenvironment and immunotherapeutic targets. Journal of Cancer Discovery. 2022; 1(1): 14-29.
4. Zhu P, Du XL, Lu G, Zhu JJ. Survival benefit of glioblastoma patients after FDA approval of temozolomide concomitant with radiation and bevacizumab: a population-based study. Oncotarget. 2017; 8(27): 44015-44031.
5. Zhu Y, Zhang X, Wang L, Ji Z, Xie M, Zhou X, et al. Loss of SH3GL2 promotes the migration and invasion behaviours of glioblastoma cells through activating the STAT3/MMP2 signalling. J Cell Mol Med. 2017; 21(11): 2685-2694.
6. Yang JK, Yang JP, Tong J, Jing SY, Fan B, Wang F, et al. Exosomal miR-221 targets DNM3 to induce tumor progression and temozolomide resistance in glioma. J Neurooncol. 2017; 131(2): 255-265.
7. Gaitanou M, Segklia K, Matsas R. Cend1, a story with many tales: from regulation of cell cycle progression/exit of neural stem cells to brain structure and function. Stem Cells Int. 2019; 2019: 2054783.
8. Patsavoudi E, Merkouri E, Thomaidou D, Sandillon F, Alonso G, Matsas R. Characterization and localization of the BM88 antigen in the developing and adult rat brain. J Neurosci Res. 1995; 40(4): 506-518.
9. Sergaki MC, Guillemot F, Matsas R. Impaired cerebellar development and deficits in motor coordination in mice lacking the neuronal protein BM88/Cend1. Mol Cell Neurosci. 2010; 44(1): 15-29.
10. Politis PK, Makri G, Thomaidou D, Geissen M, Rohrer H, Matsas R. BM88/CEND1 coordinates cell cycle exit and differentiation

of neuronal precursors. Proc Natl Acad Sci USA. 2007; 104(45): 17861-17866.
11. Fleischer T, Frigessi A, Johnson KC, Edvardsen H, Touleimat N, Klajic J, et al. Genome-wide DNA methylation profiles in progression to in situ and invasive carcinoma of the breast with impact on gene transcription and prognosis. Genome Biol. 2014; 15(8): 435.
12. Tsioras K, Papastefanaki F, Politis PK, Matsas R, Gaitanou M. Functional interactions between BM88/Cend1, Ran-binding protein M and Dyrk1B kinase affect cyclin D1 levels and cell cycle progression/exit in mouse neuroblastoma cells. PLoS One. 2013; 8(11): e82172.
13. Politis PK, Thomaidou D, Matsas R. Coordination of cell cycle exit and differentiation of neuronal progenitors. Cell Cycle. 2008; 7(6): 691-697.
14. Sergaki MC, Guillemot F, Matsas R. Impaired cerebellar development and deficits in motor coordination in mice lacking the neuronal protein BM88/Cend1. Mol Cell Neurosci. 2010; 44(1): 15-29.
15. Zhang P, Chen XB, Ding BQ, Liu HL, He T. Down-regulation of ABCE1 inhibits temozolomide resistance in glioma through the PI3K/Akt/NF-κB signaling pathway. Biosci Rep. 2018; 38(6): BSR20181711.
16. Zhao Z, Liu M, Long W, Yuan J, Li H, Zhang C, et al. Knockdown lncRNA CRNDE enhances temozolomide chemosensitivity by regulating autophagy in glioblastoma. Cancer Cell Int. 2021; 21(1): 456.
17. Politis PK, Akrivou S, Hurel C, Papadodima O, Matsas R. BM88/Cend1 is involved in histone deacetylase inhibition-mediated growth arrest and differentiation of neuroblastoma cells. FEBS Lett. 2008; 582(5): 741-748.
18. Athanassiou H, Synodinou M, Maragoudakis E, Paraskevaidis M, Verigos C, Misailidou D, et al. Randomized phase II study of temozolomide and radiotherapy compared with radiotherapy alone in newly diagnosed glioblastoma multiforme. J Clin Oncol. 2005; 23(10): 2372-2377.
19. Zou Y, Chen M, Zhang S, Miao Z, Wang J, Lu X, et al. TRPC5-induced autophagy promotes the TMZ-resistance of glioma cells via the CAMMKβ/AMPKα/mTOR pathway. Oncol Rep. 2019; 41(6): 3413-3423.
20. Xu X, Wang Z, Liu N, Cheng Y, Jin W, Zhang P, et al. Association between SOX9 and CA9 in glioma, and its effects on chemosensitivity to TMZ. Int J Oncol. 2018; 53(1): 189-202.
21. Zhu Y, Jia J, Zhao G, Huang X, Wang L, Zhang Y, et al. Multi-responsive nanofibers composite gel for local drug delivery to inhibit recurrence of glioma after operation. J Nanobiotechnology. 2021; 19(1): 198.
22. Thomas A, Tanaka M, Trepel J, Reinhold WC, Rajapakse VN, Pommier Y. Temozolomide in the Era of Precision Medicine. Cancer Res. 2017; 77(4): 823-826.
23. Stéphanou A, Ballesta A. pH as a potential therapeutic target to improve temozolomide antitumor efficacy: a mechanistic modeling study. Pharmacol Res Perspect. 2019; 7(1): e00454.
24. Yan Y, Xu Z, Dai S, Qian L, Sun L, Gong Z. Targeting autophagy to sensitive glioma to temozolomide treatment. J Exp Clin Cancer Res. 2016; 35: 23.
25. Brigliadori G, Foca F, Dall'Agata M, Rengucci C, Melegari E, Cerasoli S, et al. Defining the cutoff value of MGMT gene promoter methylation and its predictive capacity in glioblastoma. J Neurooncol. 2016; 128(2): 333-339.
26. Luo H, Chen Z, Wang S, Zhang R, Qiu W, Zhao L, et al. c-Myc-miR-29c-REV3L signalling pathway drives the acquisition of temozolomide resistance in glioblastoma. Brain. 2015; 138(Pt 12): 3654-3672.
27. Christmann M, Diesler K, Majhen D, Steigerwald C, Berte N, Freund H, et al. Integrin αVβ3 silencing sensitizes malignant glioma cells to temozolomide by suppression of homologous recombination repair. Oncotarget. 2017; 8(17): 27754-27771.
28. van Nifterik KA, van den Berg J, van der Meide WF, Ameziane N, Wedekind LE, Steenbergen RD, et al. Absence of the MGMT protein as well as methylation of the MGMT promoter predict the sensitivity for temozolomide. Br J Cancer. 2010; 103(1): 29-35.
29. Qiu ZK, Shen D, Chen YS, Yang QY, Guo CC, Feng BH, et al. Enhanced MGMT expression contributes to temozolomide resistance in glioma stem-like cells. Chin J Cancer. 2014; 33(2): 115-122.
30. Chahal M, Abdulkarim B, Xu Y, Guiot MC, Easaw JC, Stifani N, et al. O6-Methylguanine-DNA methyltransferase is a novel negative effector of invasion in glioblastoma multiforme. Mol Cancer Ther. 2012; 11(11): 2440-2450.
31. Sen R, Baltimore D. Multiple nuclear factors interact with the immunoglobulin enhancer sequences. Cell. 1986; 46(5): 705-716.
32. Sharif O, Bolshakov VN, Raines S, Newham P, Perkins ND. Transcriptional profiling of the LPS induced NF-kappaB response in macrophages. BMC Immunol. 2007; 8: 1.
33. Li H, Lin X. Positive and negative signaling components involved in TNFalpha-induced NF-kappaB activation. Cytokine. 2008; 41(1): 1-8.
34. Wang Q, Jiang H, Li Y, Chen W, Li H, Peng K, et al. Targeting NF-kB signaling with polymeric hybrid micelles that co-deliver siRNA and dexamethasone for arthritis therapy. Biomaterials. 2017; 122: 10-22.
35. Greten FR, Karin M. The IKK/NF-kappaB activation pathway-a target for prevention and treatment of cancer. Cancer Lett. 2004; 206(2): 193-199.
36. Tang F, Wang H, Chen E, Bian E, Xu Y, Ji X, et al. LncRNA-ATB promotes TGF-β-induced glioma cells invasion through NF-κB and P38/MAPK pathway. J Cell Physiol. 2019; 234(12): 23302-23314.
37. Zhao P, Wang M, An J, Sun H, Li T, Li D. A positive feedback loop of miR-30a-5p-WWP1-NF-κB in the regulation of glioma development. Int J Biochem Cell Biol. 2019; 112: 39-49.

Cell J
Cell Journal(Yakhteh)
Homepage: https://www.celljournal.org/
Original Article
Vol 25, No 4, April 2023, Pages: 273-286

Effect of Deep Brain Stimulation in The Ventral Tegmental Area on Neuronal Activity in Local and Remote Brain Regions in Kindled Mice

Parisa Esmaeili Tazangi, M.Sc.[1#], Faisal Alosaimi, Ph.D.[2, 3#], Fatemeh Bakhtiarzadeh, M.Sc.[1], Amir Shojaei, Ph.D.[1], Ali Jahanshahi, Ph.D.[2*], Javad Mirnajafi-Zadeh, Ph.D.[1, 4*]

1. Department of Physiology, Faculty of Medical Sciences, Tarbiat Modares University, Tehran, Iran
2. Department of Neurosurgery, Maastricht University Medical Center, Maastricht, The Netherlands
3. Department of Physiology, Faculty of Medicine, King Abdulaziz University, Rabigh, Saudi Arabia
4. Institute for Brain Sciences and Cognition, Tarbiat Modares University, Tehran, Iran

Abstract

Objective: The mechanisms behind seizure suppression by deep brain stimulation (DBS) are not fully revealed, and the most optimal stimulus regimens and anatomical targets are yet to be determined. We investigated the modulatory effect of low-frequency DBS (L-DBS) in the ventral tegmental area (VTA) on neuronal activity in downstream and upstream brain areas in chemically kindled mice by assessing c-Fos immunoreactivity.

Materials and Methods: In this experimental study, 4-6 weeks old BL/6 male mice underwent stereotaxic implantation of a unilateral stimulating electrode in the VTA followed by pentylenetetrazole (PTZ) administration every other day until they showed stage 4 or 5 seizures following 3 consecutive PTZ injections. Animals were divided into control, sham-implanted, kindled, kindled-implanted, L-DBS, and kindled+L-DBS groups. In the L-DBS and kindled+L-DBS groups, four trains of L-DBS were delivered 5 min after the last PTZ injection. 48 hours after the last L-DBS, mice were transcardially perfused, and the brain was processed to evaluate c-Fos expression by immunohistochemistry.

Results: L-DBS in the VTA significantly decreased the c-Fos expressing cell numbers in several brain areas including the hippocampus, entorhinal cortex, VTA, substantia nigra pars compacta, and dorsal raphe nucleus but not in the amygdala and CA3 area of the ventral hippocampus compared to the sham group.

Conclusion: These data suggest that the possible anticonvulsant mechanism of DBS in VTA can be through restoring the seizure-induced cellular hyperactivity to normal.

Keywords: Deep Brain Stimulation, Epilepsy, Pentylenetetrazole, Ventral Tegmental Area

Citation: Esmaeili Tazangi P, Alosaimi F, Bakhtiarzadeh F, Shojaei A, Jahanshahi A, Mirnajafi-Zadeh J. Effect of deep brain stimulation in the ventral tegmental area on neuronal activity in local and remote brain regions in kindled mice. Cell J. 2023; 25(4): 273-286. doi: 10.22074/CELLJ.2023.557500.1058.

Introduction

Epilepsy is a prevalent neurological disorder that affects 1-2% of the population worldwide. It is characterized by unprovoked seizures caused by significant changes in the activities of different brain areas (1). Despite major progress in defining the mechanisms behind epileptic seizures, there is no safe and effective treatment for seizure suppression. About 20-30% of epileptic patients remain resistant to current pharmacological therapeutics and require surgical intervention if an epileptic focus can be identified (2).

Deep brain stimulation (DBS) has been used to reduce disease burden in several neurological disorders. Nevertheless, there is no consensus on the optimal stimulus paradigms and DBS target (3). Low-frequency DBS (L-DBS), is shown to be effective in suppressing seizure severity in animal models (4) and reducing seizure frequency in patients (5). However, there are lots of limitations in using DBS as a therapeutic manner in epilepsy patients including finding the best pattern of stimulation and the best brain target for inducing its therapeutic effects. In addition, the exact mechanism(s) underlying the anticonvulsant effects of L-DBS remains to be determined.

Different hypotheses including synaptic modulation and changes in different neurotransmitters or neuromodulators controlling neural hyperexcitability have been suggested as underlying mechanisms (6). The hyperexcitable state of epilepsy is thought to be due to an imbalanced excitatory (glutamatergic) and inhibitory (GABAergic) synaptic activity. However, neuromodulators such as dopamine (DA) can also affect this ratio by altering

Received: 10/July/2022, Revised: 07/January/2023, Accepted: 11/January/2023
# These authors equally contributed to this study.
*Corresponding Addresses: Department of Neurosurgery, Maastricht University Medical Center, Maastricht, The Netherlands
P.O.Box: 14115-111, Department of Physiology, Faculty of Medical Sciences, Tarbiat Modares University, Tehran, Iran
Emails: a.jahanshahi@maastrichtuniversity.nl, mirnajaf@modares.ac.ir

Royan Institute
Cell Journal (Yakhteh)

the glutamatergic and/or GABAergic activity (7, 8). A growing body of evidence suggests that epilepsy coincides with impaired DA-ergic neurotransmission in humans and laboratory animals (9, 10).

The mesolimbic DA-ergic projections are mainly from the DA-ergic neurons of the ventral tegmental area (VTA). It governs a range of non-motor behavioursbehaviours (11) as it widely projects both to limbic and neocortical areas (12). Given dense DA-ergic projections from the VTA to those brain areas that are involved in seizure propagation, such as the hippocampus (13), we sought to investigate the VTA as a potential target for DBS in a pentylenetetrazole (PTZ)-induced kindled mice. In support of this hypothesis, our recent studies have revealed that altered activity in the VTA DA-ergic neurons in the PTZ mouse model of epilepsy was associated with cognitive deficits (14). In addition, our recent studies show that applying DBS at low frequency in the VTA exerts anticonvulsant effects on PTZ-kindled seizures (15).

To address whether L-DBS in the VTA may change the activity of brain areas involved in seizure activity, we assessed c-Fos expression using a specific antibody, which is designed to measure chronic neuronal activity (16). c-Fos is a molecular marker for determining the neuronal activity in the central nervous system (17). The expression of this molecule increases following seizures (18).

Materials and Methods

42 male BL/6 mice aged 4-6 weeks were used in this study. The animal house had standard conditions (22-25°C, 12-h light/dark cycle). Animals had free access to food and water. The experimental procedures and the animals' handling were according to the Animal Ethics Committee's guidelines of the Faculty of Medical Sciences, Tarbiat Modares University (IR.Modares.52D/1178).

Experimental groups and design

Animals were randomly assigned into control, sham-implanted, kindled, kindled-implanted, L-DBS, and kindled+L-DBS (KL-DBS) groups. Animals in the Kindled group were administered with PTZ (37 mg/kg, i.p.) on alternating days until achieving three consecutive stages of 4 or 5 seizures (fully kindled). In the KL-DBS group, mice were implanted with unilateral stimulating electrodes in the VTA and received L-DBS after being fully kindled. In the L-DBS group, animals were handled similarly to the KL-DBS group but received only L-DBS (without PTZ administrations). In the sham-implanted group, animals were implanted with an electrode in the VTA and received saline. In the kindled-implanted group, animals were implanted with a stimulating electrode in the VTA and received PTZ. Animals were transcardially perfused at the end of experiments. Their brains were removed and processed for immunohistochemistry (Fig.1).

Electrode implantation

A mixture of ketamine/xylazine (100/10 mg/kg, 10/1 mg/ml) was injected intraperitoneally to anaesthetize the animals. Then, animals were fixed in a stereotaxic frame and their skull was exposed. Body temperature was maintained at 37ºC using a heating pad throughout the surgery. Two stainless Teflon-coated electrodes were twisted to make a bipolar stimulating electrode, which was isolated except at its tips. This bipolar electrode was implanted unilaterally in the right VTA (0.5 mm lateral, 3.5 mm posterior, and 4.5 mm ventral from bregma (19). Teflon was removed from one end of the electrodes that were connected to the pins of a plastic socket. The socket was fixed to the skull with dental acrylic as the head stage.

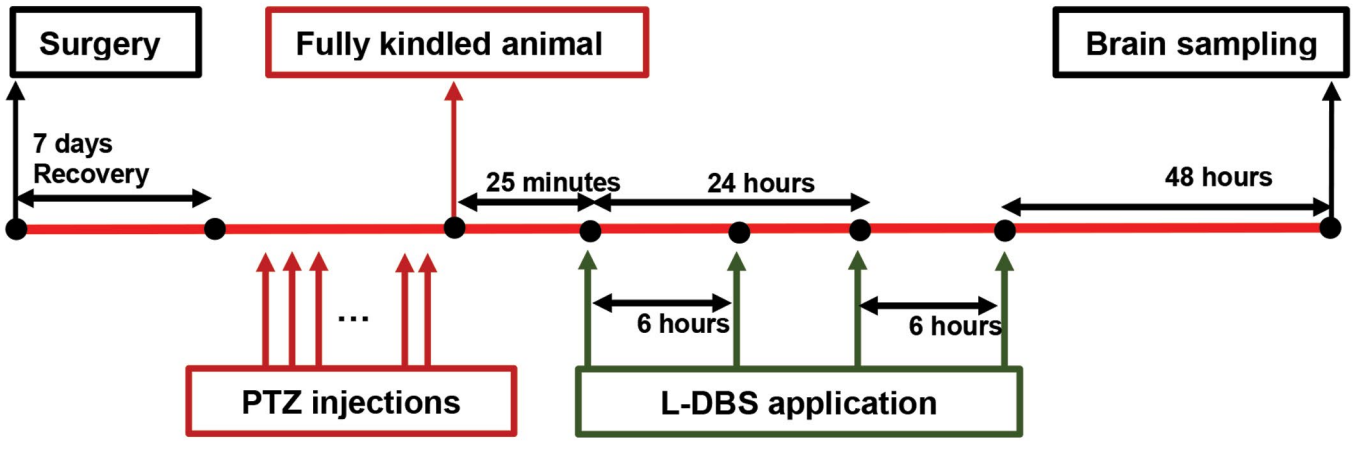

Fig.1: The timeline showing the experimental procedure. Please see the text for more explanation. PTZ; Pentylenetetrazol and L-DBS; Low frequency-deep brain stimulation.

Pentylenetetrazole (PTZ) kindling

After a recovery period of 10 days, mice received saline or PTZ. To induce the kindled seizure behaviours, subjects received sub-threshold dose of freshly prepared PTZ (37 mg/Kg, i.p.) at normal pH every other day while the animals were in their home cage (14). Bodyweight measured before each injection. Subjects in the sham group received PTZ vehicle (saline) and handled exactly similar to animals in the kindled group.

The mice's behaviour monitored for 20 minutes Immediately after PTZ injection and the convulsive seizures were scored follows stage 1: ear and facial contractions; stage 2: myoclonic jerks; stage 3: forelimb clonus; stage 4: tonic-clonic seizures and stage 5: generalized tonic-clonic seizure (20).

Low-frequency deep brain stimulation

L-DBS was applied using a digital stimulator and stimulus isolators (BIODAC ES1721, TRITA Health Technology CO., Tehran, Iran) for four sessions. The first stimulation session was administered 5 minutes after the last seizure behaviour observation in a fully kindled animal and the second session was applied 6 hours later. The third and fourth sessions were similarly applied on the next day (Fig.1). Each session lasted 20 minutes and consisted of 4 trains with 5 minutes intervals. 200 monophasic square wave pulses (with 0.1 ms pulse duration at 1 Hz) existed in each train. L-DBS parameters were designed based on our previous studies (21). L-DBS was applied through the bipolar electrode implanted in the VTA.

Tissue collection

48 hours after the last stimulation (or the equivalent time in animal groups that did not receive stimulation), mice were deeply anaesthetized with a ketamine/xylazine mixture (100/10 mg/kg, 10/1 mg/ml, i.p.) and were perfused with Tyrone's solution and Somogyi fixative solution [4% paraformaldehyde, picric acid, phosphate-buffered saline (PBS), glutaraldehyde] respectively (22). The removed brains were placed in fresh fixative solution (4% paraformaldehyde, 15% picric acid, and 0.05% glutaraldehyde in 0.1 M phosphate buffer (pH=7.6) at 4ºC for 2 hours. Then, brains were moved to 1% NaN_3 at 4ºC for long-term storage.

For preparing the brain slices, mice brains were embedded in 10% gelatin from porcine skin (Sigma-Aldrich, Zwijndrecht, The Netherlands), and then 30 µm coronal slices were prepared using a vibratome (Leica®, Wetzlar, Germany). Slices were immediately transferred into 1% NaN_3 and kept at 4ºC.

c-Fos Immunohistochemistry

Sections from 5 randomly selected mice per group were selected for immunohistochemistry. An indirect immunohistochemical (3,3′-Diaminobenzidine, DAB) staining method was used and amplification was employed using streptavidin and nickel-diaminobenzidine chromogen enhancement (23).

In brief, after overnight incubation of sections with polyclonal rabbit anti-c-Fos (K-25) (16); at first primary antibody (1:2000; Santa Cruz Biotechnology) and then biotinylated donkey anti-rabbit secondary antibody (1:800; Jackson Immunoresearch Laboratories) followed by avidin-biotin-peroxidase complex (1:800, Elite ABC-kit, Vestastatin, Burlingame, CA, USA) were applied. The stained brain slices were visualized by 3,3´-Diaminobenzidine (DAB) combined with $NiCl_2$ intensification. In the next step, the mounting and dehydrating of slices were done and samples were cover slipped with Pertex (Histolab Products ab, Goteborg, Sweden). All sections were stained in the same session and were kept in equal conditions to avoid variability.

For semi-quantitative analysis, photographs of the stained sections were taken from two sections (rostrocaudally) at 10x magnification through an Olympus DP70 digital camera connected to an Olympus AX 70 microscope (Olympus, Zoeterwoude, The Netherlands) and the Cell P software (Olympus Soft Imaging Solutions, Münster, Germany). Using ImageJ software [version 1.52; National Institutes of Health (NIH), Bethesda, USA], the number of c-Fos–positive cells was counted in the area of interest. The c-Fos immunopositive cells were counted manually, and the mean number of cells was corrected for surface area and expressed as cells/mm^2. If the staining intensity of the cell was significantly higher than the surrounding background, the cell was regarded as positive. The average value of two sections was used for statistical analysis in each subject.

In all cases, the delineation was based on standard anatomical landmarks for different brain areas and the anatomical descriptions of these regions according to the Mouse Brain Atlas (19).

Electrode trajectory verification

To verify the position of electrodes, the brain sections with the electrode trajectories were stained by hematoxylin-eosin and then sections were photographed under bright field microscopy (Fig.2).

Statistics

Data were presented as mean ± SEM values. A two-way ANOVA was used to compare the difference in kindling rate between the experimental groups. In addition, a one-way ANOVA was used to compare the parameters among different experimental groups. Bonferroni's post hoc test was run to compare the values between different experimental groups. All statistical analyses were conducted using GraphPad Prism 8 (GraphPad Software, Inc, USA). A $P<0.05$ was considered a significant difference.

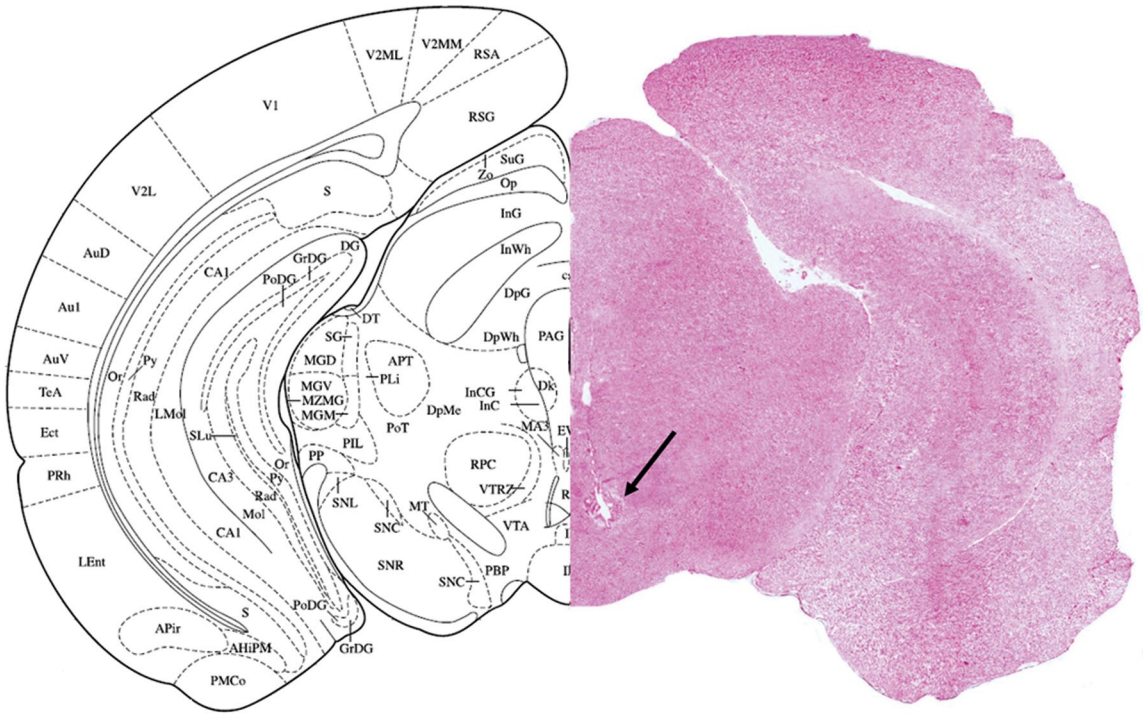

Fig.2. Verification of electrode placement in the ventral tegmental area (VTA). On the right side, a coronal histology section of the Nissl-stained is shown (40x). Arrow indicates the location of the electrode tip in the VTA. In the left, the corresponding slice of the stereotaxic atlas (-5.3 mm caudal to the Bregma) is showing.

Results

Repeated PTZ administration resulted in an increasingly tonic and clonic seizure. The number of PTZ injections in kindled and KL-DBS groups was 8.22 ± 0.72 and 8.38 ± 0.75, respectively and about 6 and 10 injections were required to induce full kindling (Fig.3). A two-way ANOVA showed that there was no significant difference in kindling rate between the two experimental groups ($F_{(1,80)}$=0.8674, P=0.3545). In addition, no significant difference was observed between control and sham-implanted groups in the expression of c-Fos. Therefore, data of these groups were merged and regarded as a sham group. Similarly, data of kindled and kindled-implanted groups were also merged and considered as a kindled group.

A one-way ANOVA and post-hoc Bonferroni test revealed that PTZ-induced kindling enhanced c-Fos expression in the inspected brain areas including CA1 ($F_{(3,19)}$=15.5, P=0.0018) and CA3 ($F_{(3,16)}$=7.41, P=0.0025) regions of the dorsal hippocampus, dorsal dentate gyrus (DG) ($F_{(3,19)}$=16.55, P=0.0009), CA1 ($F_{(3,16)}$=18.84, P=0.0001) and CA3 ($F_{(3,19)}$=16.08, P=0.0011) of ventral hippocampus, ventral DG ($F_{(3,19)}$=16.71, P=0.0008) (Fig.4) and basolateral amygdaloid nucleus (BLA) ($F_{(3,19)}$=15.47, P=0.0014), entorhinal cortex (EC) ($F_{(3,16)}$=34.63, P=0.00001), DRN ($F_{(3,19)}$=12.66, P=0.0054), VTA ($F_{(3,19)}$=12.12, P=0.007) and SNc ($F_{(3,19)}$=13.74, P=0.0033) (Fig.5).

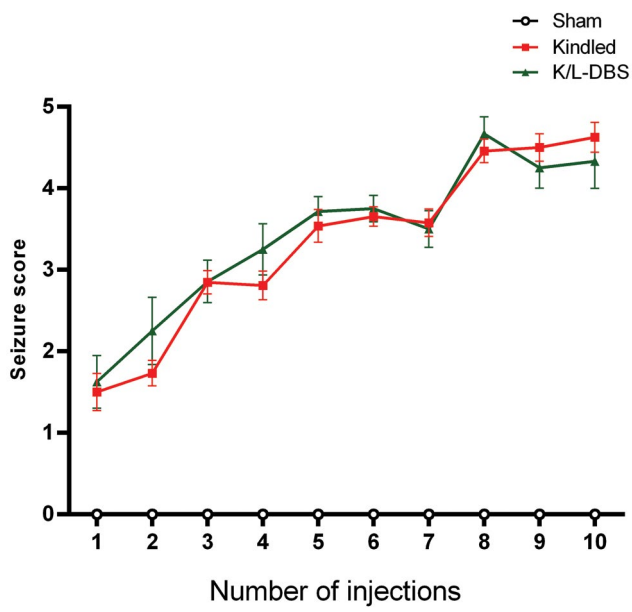

Fig.3: Pentylenetetrazole (PTZ) kindling procedure in experimental groups.

L-DBS in kindled animals (KL-DBS group) restored the observed increase in c-Fos expression in all the above-mentioned brain regions. A one-way ANOVA and post-hoc Bonferroni's test showed a significant difference between KL-DBS and kindled groups (P values being reported in Fig.5) except in the basolateral amygdala (Figs.4, 5).

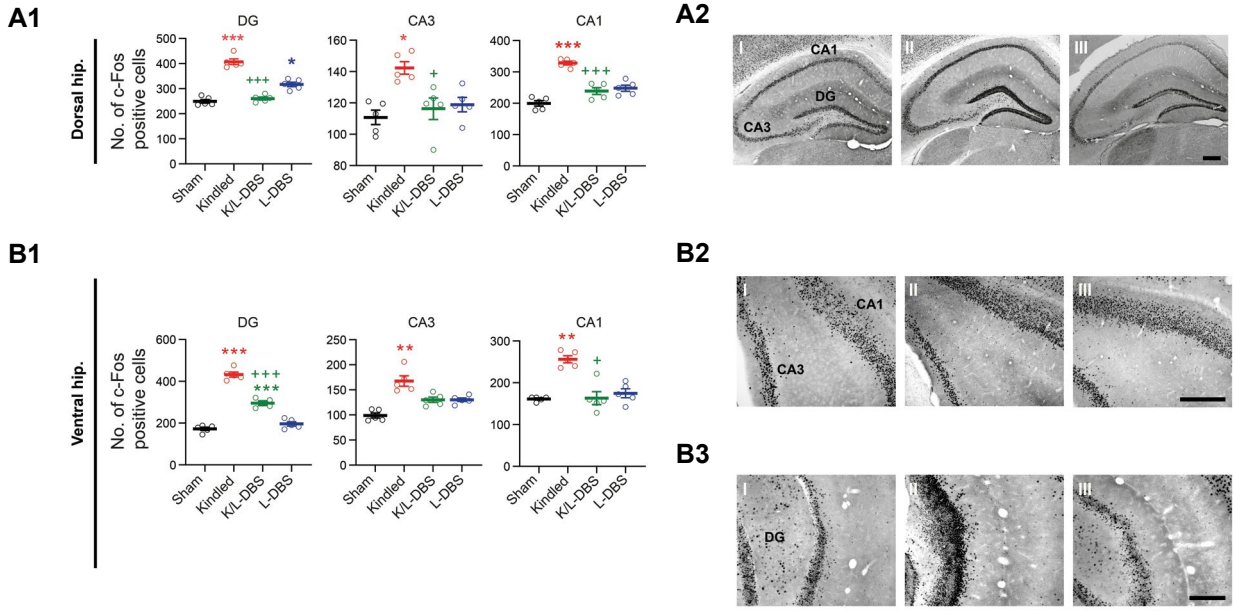

Fig.4: Effect of L-DBS on c-Fos neural activity. On the left, **A1.** The number of c-Fos positive cells is showing in the CA1, CA3, and DG of the dorsal hippocampus, **B1.** The CA1, CA3 and DG of the ventral hippocampus. Values are mean ± SEM, *; P<0.05, **; P<0.01, ***; P<0.001 compared to sham and +; P<0.05 and +++; P<0.001 compared to kindled group by one-way ANOVA. In right, **A2.** The distribution of c-Fos immunohistochemical staining of 30 -µm-thick sections of the above-mentioned areas is shown in the sham (I), kindled (II), and KL-DBS (III) groups for the dorsal hippocampus at the bregma level of -1.94 mm, **B2, B3.** The ventral hippocampus at the bregma level of -2.92 mm. The small dark dots represent c-Fos positive cells at 4x magnification power. L-DBS; Low frequency-deep brain stimulation, CA; Cornu ammunis, and DG; Dentate gyrus.

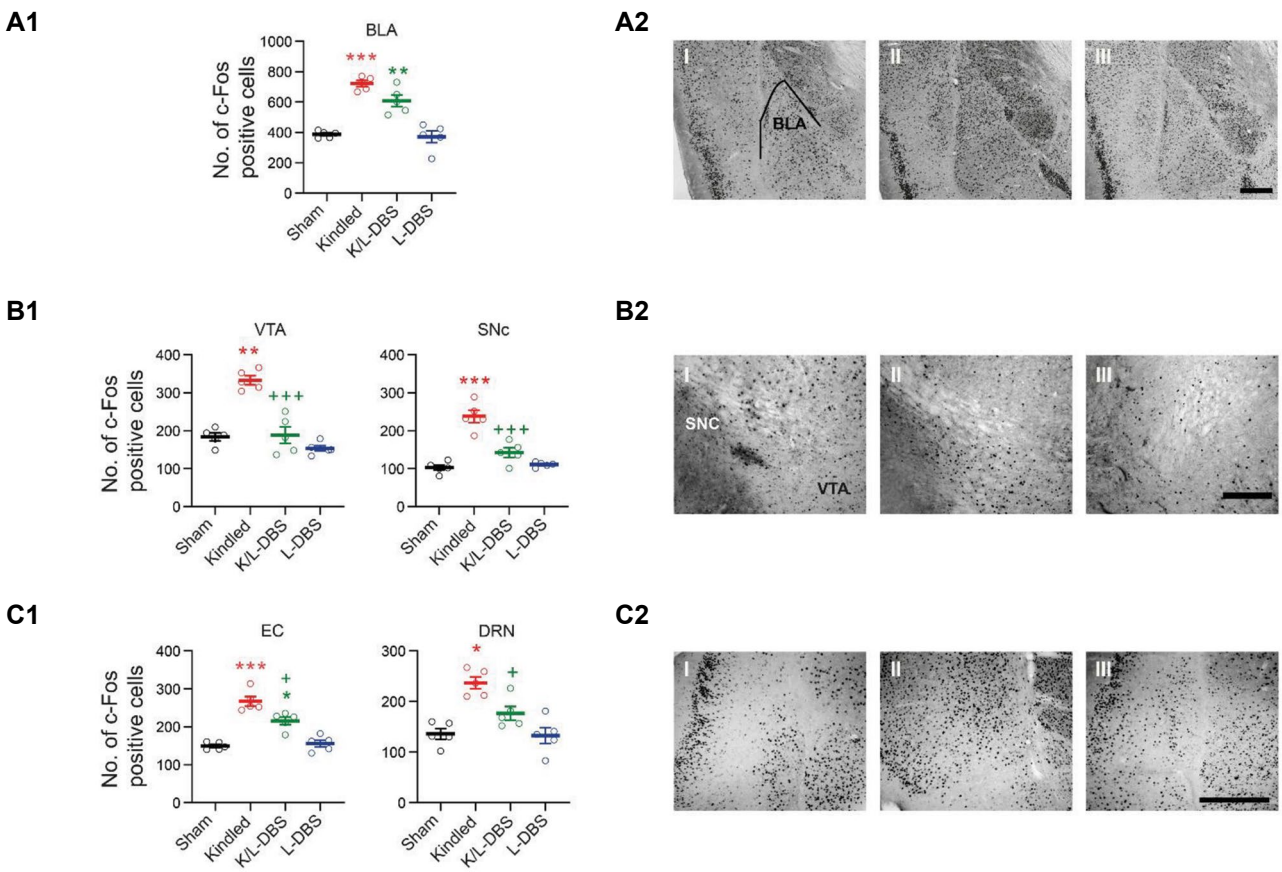

Fig.5: Effect of low frequency-deep brain stimulation (L-DBS) on c-Fos neural activity. On left, **A1.** The number of c-Fos positive cells is showing in the basolateral amygdala (BLA), **B1.** The ventral tegmental area (VTA) and substantia nigra pars compacta (SNc), **C1.** The entorhinal cortex (EC) and the dorsal raphe nucleus (DRN). Values are mean ± SEM, *; P<0.05, **; P<0.01, ***; P<0.001 compared to sham and +; P<0.05 and +++; P<0.001 compared to kindled group by one-way ANOVA. On right, **A2.** The distribution of c-Fos immunohistochemical staining of 30 -µm-thick sections of the above-mentioned areas is shown in the sham (I), kindled (II), and KL-DBS (III) groups for the BLA at the bregma level of -1.34 mm, **B2.** The VTA and the SNc at the bregma level of -3.16 mm, **C2.** The EC at the bregma level of -1.94 mm. The small dark dots represent c-Fos positive cells at 4x magnification power.

Discussion

Modulation of the DA-ergic system in managing epileptic seizures is gaining attention again. Unlike the nigrostriatal DA-ergic pathway, which primarily involves motor control, the mesolimbic DA-ergic pathway regulates non-motor functions. Herein we addressed whether the VTA could be targeted for seizure control. Our data suggest that VTA-DBS could reduce neuronal hyperactivity in different brain areas especially those involved in seizure generation and propagation and restore the kindling-induced increase in c-Fos expression (K-25, a chronic neuronal activity marker (16). To our knowledge, this is the first study that targets the VTA as a brain region for DBS in an animal model of epilepsy.

All regions of interest including the hippocampus, amygdala, entorhinal cortex, DRN, SNc and VTA showed a significant increase in neuronal activity (identified as a significant increase in c-Fos expression) in epileptic mice. Whereas, applying L-DBS in VTA restored the neuronal activity in all aforementioned areas to normal levels.

Altered DA neurotransmission has implications in a variety of brain disorders including epilepsy (9, 24). Furthermore, DA plays a key role in controlling cell excitability in different brain regions innervated by DA-ergic fibers, such as the prefrontal cortex and hippocampus (25). The VTA, as a major DA-ergic region, is made up of a heterogeneous population of DA (60%), GABA (35%), and glutamate (2-5%)-releasing neurons (26, 27). Two primary DA-ergic projections originate from the VTA, including mesocortical and mesolimbic pathways (12). We have recently shown that applying L-DBS in PTZ-kindled rats restores seizure-induced increase in firing of VTA DA-ergic neurons to the control level (21). VTA projects to the limbic areas that are involved in the generation and propagation of seizures. Therefore, it is an interesting area to investigate the mechanisms involved in neuromodulation in epilepsy.

DA-ergic neurons exert phasic burst activity accompanied by a transient and high-concentration DA release. Whilst, during the tonic pattern of activity, these neurons generate spikes at low frequency which results in tonic and low-concentration DA release (28). It has been suggested that encountering salient stimuli and reward is associated with a shift from a tonic firing pattern, an increase in D_2-like activity, to a burst firing mode, a rise in D_1-like activity (29). Moreover, D_2-like receptors exert an inhibitory and anticonvulsant effect while, D_1-like receptors involve an excitatory and proepileptic action (10, 25). The opposite action of D_1- and D_2-like receptors is thought to be due to a DA-glutamate interaction. This hypothesis has been supported both in epileptic and healthy animals (30, 31).

Based on this evidence, one may suggest that low-frequency DBS would enhance the tonic activity of DA neurons in the VTA in favour of D_2-like receptor activity. This is an important characteristic of VTA neurons, making it a suitable target for DBS compared to other brain areas.

The activity of the DA-ergic system increases in the epileptic brain (32, 33). An increase in the firing rate of DA-ergic neurons (21) and extracellular DA level during epilepsy have been reported (34). Therefore, a probable L-BDS-induced shift in the activity of the VTA DA-ergic neurons from phasic in kindled mice to a tonic in the K/L-BDS group could shift the excitation to inhibition ratio towards inhibition. Lower c-Fos expression following L-DBS in the VTA is in line with this hypothesis. However, electrophysiological recordings need to confirm this hypothesis.

The exact mechanism behind the effects of L-DBS is not clear. However, it has been hypothesized that L-DBS exerts excitatory effects at local neuronal element, and drive the neural pathways (35), unlike HFS which has been shown to induce ablative-like effects (6). Here we suggest that the observed DBS effects were probably caused by the modulatory effect of L-DBS on the pattern of DA-ergic cells activity. Based on this, the activity of DA-ergic cells in the VTA may be driven by the stimulation frequency of L-DBS. This would change the spontaneous activity of those neurons from phasic in epileptic mice to the tonic pattern that could shift the network from excitatory to inhibitory. We observed a significant increase in c-Fos expressing cells in the VTA in kindled mice, which was restored following L-DBS. VTA DA-ergic projections mainly innervate the ventral hippocampus (33). Nevertheless, we found that the effect of L-DBS was similar in both dorsal and ventral hippocampal areas.

The amygdala, the SNc (36), the DRN (37) and the hippocampus receive DA-ergic inputs from the VTA (38). L-DBS in the VTA would drive these projections towards a tonic firing mode. As a result of the tonic firing pattern, there will be an increase in the D_2-like dependent pathways which can reduce neuronal excitability (39). Our data showed that PTZ kindled mice exhibit high levels of c-Fos expression in the SNc, the DRN, the amygdala, the VTA, and the hippocampus. Subsequently, L-DBS restored those changes except in the amygdala. These changes in neuronal activity could be related to the different patterns of VTA projections or diverse distribution of DA-ergic receptors in different brain areas.

Herein we explained the outcomes based on the assumption that VTA-DBS would result in DA release in downstream areas following the tonic activity of DA-ergic neurons. However, other neurotransmitters are known to be involved in the complex VTA circuitry, which could play a role by sending long-range projections (38).

Owing to the preliminary nature of these results, this c-Fos mapping study would be a basis for further immunofluorescence assessment to unravel the cell types and a number of c-Fos expressing cells in the VTA. Moreover, additional research is needed to determine the mechanism of how L-DBS makes the VTA effective in reducing the activity of cells in different brain regions.

Conclusion

Given the current insights on the mechanism of DBS, we suggest that the firing of DA-ergic cells in the VTA is time-locked to the stimulation frequency. This would change the spontaneous activity of those neurons from phasic in epileptic mice to the tonic pattern that could shift the network from excitatory to inhibitory.

Acknowledgements

This research was supported by a grant (#957513) from National Institute for Medical Research Development (NIMAD) and a grant #IG-39709 from Tarbiat Modares University, Tehran, Iran. The authors declare no conflict of interest.

Authors' Contributions

P.E.T.; Participated in data collection and evaluation, drafting and statistical analysis. F.A.; Contributed to data collection, evaluation and analysis. F.B.; Contributed to histological experiments, preparing histological graphs and data analysis. A.S.; Participated in data evaluation, drafting and statistical analysis. A.J., J.M-Z.; Contributed to study design, interpretation of the data and the conclusion. All authors edited and approved the final version of this manuscript for submission, participated in the finalization of the manuscript and approved the final draft.

References

1. Fisher RS, van Emde Boas W, Blume W, Elger C, Genton P, Lee P, et al. Epileptic seizures and epilepsy: definitions proposed by the International League Against Epilepsy (ILAE) and the International Bureau for Epilepsy (IBE). Epilepsia. 2005; 46(4): 470-472.
2. Wiebe S, Blume WT, Girvin JP, Eliasziw M. Effectiveness and efficiency of surgery for temporal lobe epilepsy study group. a randomized, controlled trial of surgery for temporal-lobe epilepsy. N Engl J Med. 2001; 345(5): 311-318.
3. Sunderam S, Gluckman B, Reato D, Bikson M. Toward rational design of electrical stimulation strategies for epilepsy control. Epilepsy Behav. 2010; 17(1): 6-22.
4. Rashid S, Pho G, Czigler M, Werz MA, Durand DM. Low frequency stimulation of ventral hippocampal commissures reduces seizures in a rat model of chronic temporal lobe epilepsy. Epilepsia. 2012; 53(1): 147-156.
5. Koubeissi MZ, Kahriman E, Syed TU, Miller J, Durand DM. Low-frequency electrical stimulation of a fiber tract in temporal lobe epilepsy. Ann Neurol. 2013; 74(2): 223-231.
6. Jakobs M, Fomenko A, Lozano AM, Kiening KL. Cellular, molecular, and clinical mechanisms of action of deep brain stimulation-a systematic review on established indications and outlook on future developments. EMBO Mol Med. 2019; 11(4): e9575.
7. Gonzalez-Islas C, Hablitz JJ. Dopamine enhances EPSCs in layer II-III pyramidal neurons in rat prefrontal cortex. J Neurosci. 2003; 23(3): 867-875.
8. Slaght SJ, Paz T, Mahon S, Maurice N, Charpier S, Deniau JM. Functional organization of the circuits connecting the cerebral cortex and the basal ganglia: implications for the role of the basal ganglia in epilepsy. Epileptic Disord. 2002; 4 Suppl 3: S9-S22.
9. Bozzi Y, Dunleavy M, Henshall DC. Cell signaling underlying epileptic behavior. Front Behav Neurosci. 2011; 5: 45.
10. Starr MS. The role of dopamine in epilepsy. Synapse. 1996; 22(2): 159-194.
11. Waddington JL, Jenner P. D1: D2 dopamine receptor interactions: neuroscience and psychopharmacology (neuroscience perspectives). 1st ed. Academic Press; 1993.
12. Koob GF. Dopamine, addiction and reward. Semin Neurol. 1992; 4(2): 139-148.
13. Goto Y, Araki T, Kato M, Fukui M. Propagation of hippocampal seizure activity arising from the hippocampus: a local cerebral blood flow study. Brain Res. 1994; 634(2): 203-213.
14. Ahmadi M, Dufour JP, Seifritz E, Mirnajafi-Zadeh J, Saab BJ. The PTZ kindling mouse model of epilepsy exhibits exploratory drive deficits and aberrant activity amongst VTA dopamine neurons in both familiar and novel space. Behav Brain Res. 2017; 330: 1-7.
15. Rezaei M, Raoufy MR, Fathollahi Y, Shojaei A, Mirnajafi-Zadeh J. Tonic and phasic stimulations of ventral tegmental area have opposite effects on pentylenetetrazol kindled seizures in mice. Epilepsy Res. 2022; 189: 107073.
16. Budzikowski AS, Vahid-Ansari F, Leenen FH. Chronic activation of brain areas by high-sodium diet in Dahl salt-sensitive rats. Am J Physiol. 1998; 274(6): H2046-H2052.
17. Chung L. A brief introduction to the transduction of neural activity into Fos signal. Dev Reprod. 2015; 19(2): 61-67.
18. Malhi SM, Jawed H, Hanif F, Ashraf N, Zubair F, Siddiqui BS, et al. Modulation of c-Fos and BDNF protein expression in pentylenetetrazole-kindled mice following the treatment with novel antiepileptic compound HHL-6. Biomed Res Int. 2014; 2014: 876712.
19. Paxinos G, Franklin K. Paxinos and Franklin's the mouse brain in stereotaxic coordinates. 5th ed. Academic press; 2019.
20. Van Erum J, Van Dam D, De Deyn PP. PTZ-induced seizures in mice require a revised Racine scale. Epilepsy Behav. 2019; 95: 51-55.
21. Sadeghian A, Salari Z, Azizi H, Raoufy MR, Shojaei A, Kosarmadar N, et al. The role of dopamine D_2-like receptors in a "depotentiation-like effect" of deep brain stimulation in kindled rats. Brain Res. 2020; 1738: 146820.
22. Somogyi P, Takagi H. A note on the use of picric acid-paraformaldehyde-glutaraldehyde fixative for correlated light and electron microscopic immunocytochemistry. Neuroscience. 1982; 7(7): 1779-1783.
23. Tang Y, Liu L, Xu D, Zhang W, Zhang Y, Zhou J, et al. Interaction between astrocytic colony stimulating factor and its receptor on microglia mediates central sensitization and behavioral hypersensitivity in chronic post ischemic pain model. Brain Behav Immun. 2018; 68: 248-260.
24. Rasheed N, Alghasham A. Central dopaminergic system and its implications in stress-mediated neurological disorders and gastric ulcers: short review. Adv Pharmacol Sci. 2012; 2012: 182671.
25. Gangarossa G, Di Benedetto M, O'Sullivan GJ, Dunleavy M, Alcacer C, Bonito-Oliva A, et al. Convulsant doses of a dopamine D1 receptor agonist result in Erk-dependent increases in Zif268 and Arc/Arg3.1 expression in mouse dentate gyrus. PLoS One. 2011; 6(5): e19415.
26. Nair-Roberts RG, Chatelain-Badie SD, Benson E, White-Cooper H, Bolam JP, Ungless MA. Stereological estimates of dopaminergic, GABAergic and glutamatergic neurons in the ventral tegmental area, substantia nigra and retrorubral field in the rat. Neuroscience. 2008; 152(4): 1024-1031.
27. Taylor SR, Badurek S, Dileone RJ, Nashmi R, Minichiello L, Picciotto MR. GABAergic and glutamatergic efferents of the mouse ventral tegmental area. J Comp Neurol. 2014; 522(14): 3308-3334.
28. Ellwood IT, Patel T, Wadia V, Lee AT, Liptak AT, Bender KJ, et al. Tonic or phasic stimulation of dopaminergic projections to prefrontal cortex causes mice to maintain or deviate from previously learned behavioral strategies. J Neurosci. 2017; 37(35): 8315-8329.
29. Dreyer JK, Hounsgaard J. Mathematical model of dopamine autoreceptors and uptake inhibitors and their influence on tonic and phasic dopamine signaling. J Neurophysiol. 2013; 109(1): 171-182.
30. Gangarossa G, Di Benedetto M, O'Sullivan GJ, Dunleavy M, Alcacer C, Bonito-Oliva A, et al. Convulsant doses of a dopamine D1 receptor agonist result in Erk-dependent increases in Zif268 and Arc/Arg3.1 expression in mouse dentate gyrus. PLoS One. 2011; 6(5): e19415.
31. Tseng KY, O'Donnell P. Dopamine-glutamate interactions controlling prefrontal cortical pyramidal cell excitability involve multiple signaling mechanisms. J Neurosci. 2004; 24(22): 5131-5139.
32. Floresco SB, West AR, Ash B, Moore H, Grace AA. Afferent modulation of dopamine neuron firing differentially regulates tonic and phasic dopamine transmission. Nat Neurosci. 2003; 6(9): 968-973.
33. Lisman JE, Grace AA. The hippocampal-VTA loop: controlling the entry of information into long-term memory. Neuron. 2005; 46(5):

703-713.
34. Cifelli P, Grace AA. Pilocarpine-induced temporal lobe epilepsy in the rat is associated with increased dopamine neuron activity. Int J Neuropsychopharmacol. 2012; 15(7): 957-964.
35. Goodman JH, Berger RE, Tcheng TK. Preemptive low-frequency stimulation decreases the incidence of amygdala-kindled seizures. Epilepsia. 2005; 46(1): 1-7.
36. Ferreira JG, Del-Fava F, Hasue RH, Shammah-Lagnado SJ. Organization of ventral tegmental area projections to the ventral tegmental area-nigral complex in the rat. Neuroscience. 2008; 153(1): 196-213.
37. Kalén P, Skagerberg G, Lindvall O. Projections from the ventral tegmental area and mesencephalic raphe to the dorsal raphe nucleus in the rat. Evidence for a minor dopaminergic component. Exp Brain Res. 1988; 73(1): 69-77.
38. Fields HL, Hjelmstad GO, Margolis EB, Nicola SM. Ventral tegmental area neurons in learned appetitive behavior and positive reinforcement. Annu Rev Neurosci. 2007; 30: 289-316.
39. Cousineau J, Lescouzères L, Taupignon A, Delgado-Zabalza L, Valjent E, Baufreton J, et al. Dopamine D2-like receptors modulate intrinsic properties and synaptic transmission of parvalbumin interneurons in the mouse primary motor cortex. eNeuro. 2020; 7(3): ENEURO.0081-20.2020.